

MASTER'S THESIS

Surface roughness and its impact
on fatigue life

Bc. Tomáš Vrbata

Supervisors: Ing. Jan Papuga Ph.D. & Dr. Alaitz Zabala

FACULTY OF MECHANICAL
ENGINEERING

12105 – DEPARTMENT OF MECHANICS,
BIOMECHANICS AND MECHATRONICS



January 27, 2023

I. Personal and study details

Student's name: **Vrbata Tomáš** Personal ID number: **475007**
Faculty / Institute: **Faculty of Mechanical Engineering**
Department / Institute: **Department of Mechanics, Biomechanics and Mechatronics**
Study program: **Applied Sciences in Mechanical Engineering**
Specialisation: **Applied Mechanics**

II. Master's thesis details

Master's thesis title in English:

Surface roughness and its impact on fatigue life

Master's thesis title in Czech:

Drsnost povrchu a její dopad na únavovou životnost

Guidelines:

Perform: 1) Analysis of the effect of manufacturing parameters on surface roughness based on published papers. 2) Analyze suitability of various parameters describing the surface roughness. 3) Describe the technology of surface roughness measurements and the potential issues caused by the specific solutions. 4) Fatigue experiments with various manufacturing parameters (the scope of at least 5 S-N curves), including the analysis of the surface roughness. 5) Compare existing proposals on conversion of manufacturing parameters to output surface roughness based on these own experimental data items. 6) Based on literature review, compare various methods for fatigue life estimation based on a specific surface roughness 7) Results from item 6 compare also to your own outputs from item 4. 8) Describe your conclusions.

Bibliography / sources:

[1] Edoardo Capello, Residual stresses in turning: Part I: Influence of process parameters, Journal of Materials Processing Technology, Volume 160, Issue 2, 2005, Pages 221-228, ISSN 0924-0136
[2] Edoardo Capello, Residual stresses in turning: Part II. Influence of the machined material, Journal of Materials Processing Technology, Volume 172, Issue 3, 2006, Pages 319-326, ISSN 0924-0136.
[3] Tjarden Zielinski, Andrey Vovk, Oltmann Riemer, Bernhard Karpuschewski, Influence of local material loads on surface topography while machining steel 42CrMo4 and Inconel 718, Procedia CIRP 108, 2022, Pages 412-417

Name and workplace of master's thesis supervisor:

Ing. Jan Papuga, Ph.D. Division of strength and elasticity FME

Name and workplace of second master's thesis supervisor or consultant:

Date of master's thesis assignment: **30.10.2022** Deadline for master's thesis submission: **27.01.2023**

Assignment valid until: _____

Ing. Jan Papuga, Ph.D.
Supervisor's signature

prof. Ing. Michael Valášek, DrSc.
Head of department's signature

doc. Ing. Miroslav Španiel, CSc.
Dean's signature

III. Assignment receipt

The student acknowledges that the master's thesis is an individual work. The student must produce his thesis without the assistance of others, with the exception of provided consultations. Within the master's thesis, the author must state the names of consultants and include a list of references.

Date of assignment receipt

Student's signature

Annotation list

Author's name:	Bc. Tomáš Vrbata
Title of the thesis:	Surface roughness and its impact on fatigue life
Title of the thesis (Czech):	Drsnost povrchu a její dopad na únavovou životnost
Bibliographic data:	
	number of pages 104
	number of figures 70
	number of tables 22
Academic year:	2022/2023
Department:	Department of Mechanics, Biomechanics and Mechatronics
Field of study:	Applied Mechanics
Master's thesis Supervisors:	Ing. Jan Papuga Ph.D. & Dr. Alaitz Zabala
Keywords:	material fatigue, surface roughness, roughness parameter measurement, fatigue strength
Keywords (in Czech):	únava materiálu, drsnost povrchu, parametr drsnosti měření, únavová pevnost

Abstract

The thesis deals with surface roughness and its impact on fatigue life. The theoretical part contains essential knowledge of this topic. Subsequently, surface roughness measurements are performed and the effect of the methodology on the results is analyzed. Finally, the effect of surface roughness on fatigue life is investigated to determine whether different roughness parameters can be used to indicate fatigue life.

Abstrakt

Diplomová práce se zabývá drsností povrchu a jejím dopadem na únavovou životnost. V teoretické části jsou sepsány základní znalosti problematiky. Následně je provedeno měření drsnosti povrchu a analýza vlivu metodiky na výsledky. Na závěr je zkoumán vliv drsnosti na únavovou životnost s cílem zjistit, zda lze použít různé parametry drsnosti k indikaci únavové životnosti.

Declaration

I declare that this thesis is my own work supervised by Ing. Jan Papuga, Ph.D. and Dr. Alaitz Zabala (Mondragon Unibertsitatea). All sources used during the elaboration of this thesis are listed as references.

In Prague

Acknowledgment

I would like to express my deepest gratitude to my supervisors Ing. Jan Papuga, Ph.D., and Dr. Alaitz Zabala for their guidance during the work on my thesis. I would also like to thank Iñigo Llavori, Ph.D., for his advice during my stay at Mondragon University. I also thank Bc. Petr Kolovratník for his help with fatigue testing. I would like to extend my sincere thanks to Prof. Aleksander Karolczuk for providing his experimental data on the A22 series. The thanks should also go to Ing. Kirill Loshkarev for permission to use his data from the previously prepared analysis. I am also thankful to Ing. Jiří Čapek, Ph.D. for the information on residual stresses.

Contents

I List of Figures

II List of Tables

III List of Variables

1	Introduction	1
1.1	Motivation and background	1
1.2	Scope of the thesis	1
1.3	Thesis layout	2
2	Theoretical background	4
2.1	Introduction to Fatigue	4
2.2	S-N curves	5
2.2.1	Other influences affecting fatigue life	7
2.3	Roughness characterization	8
2.3.1	Measuring instruments	9
2.3.2	Measurement post-processing	13
2.3.3	2D profile parameters	15
2.3.4	3D profile parameters	18
2.4	Effect of machining parameters on surface roughness	20
2.4.1	Machining	20
2.4.2	Turning parameters and conditions	20
2.4.3	Formulas	22
2.5	Effect of surface roughness on fatigue endurance	24
2.5.1	Surface finish factor	24
3	Systematic Analysis of The States of The Art	31
3.1	Motivation	31
3.2	Methodology	31
3.3	Results	33
3.3.1	General overview	33
3.3.2	3D Areal profilometry	34
3.3.3	2D profilometry	35
3.4	Critical analysis	38
4	Sensitivity Analysis	39
4.1	Motivation	39
4.2	Methodology	39

4.3	Results	41
4.4	Conclusion	49
5	Fatigue strength correction due to roughness	51
5.1	Methodology	51
5.1.1	Description of used data sets	53
5.2	Results	58
5.2.1	Simplified model	59
5.2.2	Logarithmic model	60
5.2.3	Comparison of models	61
5.3	Conclusion	63
6	Experimental Testing	64
6.1	Material and Methods	64
6.1.1	Material and sample geometry	64
6.1.2	Manufacturing setup	65
6.1.3	Roughness characterization	65
6.1.4	Residual stresses testing	69
6.1.5	Fatigue setup	69
6.2	Results and discussion	69
6.2.1	Roughness results	69
6.2.2	Residual stresses results	73
6.2.3	Fatigue results	74
7	Effect of machining on surface roughness	76
7.1	Methodology	76
7.2	Results	76
7.3	Discussion	79
8	Correlation between roughness and fatigue	81
8.1	Methodology	81
8.2	Results	82
8.2.1	Comparison of results with results from Section 5	87
8.3	Conclusion	88
9	Conclusion	91
	Appendix A	94
	References	98

List of Figures

2	Harmonic loading [11].	4
3	Wöhler diagram [70].	5
4	Effect of stylus tip radius [8].	10
5	Principle of interferometer [18].	11
6	Focus variation [40].	12
7	Confocal microscopy [47].	13
8	Surface profile [15].	15
9	Root mean square deviation [1].	16
10	Skewness and Kurtosis ([77].	17
11	Schematic description of the functional parameters [57].	20
12	Turning parameters [74].	21
13	Surface finish factor given by Johnson [48]. AA = arithmetic average (Ra).	25
14	Surface finish factor given by Italian UNI 7670 standard [24].	25
15	Surface finish factor given by Juvinall [49].	26
16	Surface roughness reduction factor ([68]).	26
17	Search criteria at Engineeringvillage.com.	32
18	General overview.	33
19	3D Areal measuring technology.	34
20	3D Areal profilometry - Methodology description.	34
21	Areal parameters.	35
22	Measurement from which the 2D parameters where computed.	36
23	Extraction of 2D parameters from 3D areal measurements.	36
24	2D parameters.	37
25	$R_a = 0.8 \mu\text{m}$: 2D and axonometric pseudo-color views of the surface obtained by different technologies. (a) Interferometry (b) Confocal (c) Focus variation.	42
26	$R_a = 1.6 \mu\text{m}$: 2D and axonometric pseudo-color view of the surface obtained by different technologies. (a) Interferometry (b) Confocal (c) Focus variation.	42
27	2D surface profiles obtained by different technologies. (a) $R_a = 0.8 \mu\text{m}$, (a) $R_a = 1.6 \mu\text{m}$	43
28	Comparison of areal parameters obtained by different technology for two measured samples with different surface roughness. Values show the percentage difference to interferometry.	43
29	$R_a = 0.8 \mu\text{m}$: 2D and axonometric pseudo-color view of the surface obtained by objectives with different magnification. (a) 5x (b) 10x (c) 20x.	44

30	$R_a = 1.6 \mu\text{m}$: 2D and axonometric pseudo-color views of the surface obtained by objectives with different magnification. (a) 5x (b) 10x (c) 20x.	44
31	2D surface profiles obtained by objectives with different magnification. (a) $R_a = 0.8 \mu\text{m}$, (a) $R_a = 1.6 \mu\text{m}$	45
32	Comparison of areal parameters obtained by objectives with different magnification. for two measured samples with different surface roughness. Values show the percentage difference to 20x magnification.	46
33	2D and axonometric pseudo-color view of the uncropped evaluation area (a) $R_a = 0.8 \mu\text{m}$ (b) $R_a = 1.6 \mu\text{m}$	46
34	Comparison of areal parameters obtained by cropping the size of evaluation area for two measured samples with different surface roughness. Values show the percentage difference to the uncropped area.	47
35	2D pseudo-color view of the surface acquired by interferometer and marked positions of evaluation profiles in measured areas. (a) $R_a = 0.8 \mu\text{m}$, (a) $R_a = 1.6 \mu\text{m}$	48
36	Comparison of 2D parameters obtained by areal measurement as a percentage difference to the values obtained from contact measurement.	48
37	Comparison of areal parameters obtained by different post-processing approaches.	49
38	APG data set.	53
39	ITN data set.	54
40	LAL data set.	54
41	LDD data set.	55
42	LHA data set.	56
43	LHB data set.	56
44	LHC data set.	56
45	SCC data set.	57
46	SSC data set.	58
47	ZWW data set.	58
48	Model comparison in terms of accuracy of methods.	62
49	Comparison of the model in terms of accuracy of estimation of methods for data set.	62
50	Specimen drawing.	64
51	Areal measurement setup.	67
52	The final surface topography after post-processing.	68
53	Linear measurement setup.	68
54	Surface defect observed by visual inspection. (a) Step defect on A35_2 (b) Inhomogenous defect on A36_3.	70
55	2D roughness parameters obtained by contact stylus profilometer.	71

56	Areal roughness parameters obtained by non-contact 3D areal profilometer.	71
57	The effect of the central step on areal parameters. Uncropped = step is located within the evaluation area, cropped = step is not located in the evaluation area.	72
58	Average values of 2D parameters calculated from external measurements.	73
59	S-N curves obtained from measured data.	75
60	Comparison of trends for series A35-A37 from the measurement conducted in the current project	77
61	Comparison of trends for all series from data from all measurements. .	78
62	Comparison of roughness estimation errors from machining parameters according to (a) series, (b) method. THE = ideal roughness, COE = correction factor between ideal and actual roughness.	79
63	Scatter graph showing the dependence of the fatigue strength on the roughness parameter R_a	82
64	Comparison of trends of roughness parameters and fatigue strength for series A35-A37 from the measurement conducted in the current project. (a) 2D parameters (b) areal parameters.	83
65	Scatter graph showing the dependence of the fatigue strength on the 2D roughness parameters.	84
66	Scatter graph showing the dependence of the fatigue strength on the 2D roughness parameters. (a) S_a and S_q parameters, (b) S_z parameter . .	84
67	Comparison of average errors for the simplified and logarithmic models for each method.	86
68	Comparison of average errors for the simplified and logarithmic models for each series.	87
69	Comparison of the simplified model when applied to FABEST and external data.	88
70	Comparison of the simplified model when applied to FABEST and external data.	88

List of Tables

1	Comparison of the abundance of equivalent parameters.	37
2	Effect of optical measuring technology.	40
3	Effect of magnification.	40
4	Effect of evaluation area.	40
5	Overview of selected data sets. "T" = tensile loading, "RB" = rotating bending loading.	59
6	Average errors of each method and of each series for the simplified model.	60
7	Average errors of each method and each series for the logarithmic model.	61
8	Material properties.	64
9	Chemical composition (wt. %).	64
10	Machining setup for series A25-A29 ; *(Decocut 1040 during roughing).	65
11	Machining setup for series A35-A37 ; *(Decocut 1040 during roughing).	65
12	Visual inspection of measured samples.	70
13	Results of residual stresses measurement. The table is taken from my colleague Bc. Petr Kolovratník.	73
14	Average errors of each method and of each series for the simplified model.	85
A1	Table of computed areal parameters obtained by different technology for two measured samples with different surface roughness.	94
A2	Table of computed areal parameters obtained by objectives with different magnification for two measured samples with different surface roughness.	94
A3	Table of computed areal parameters obtained by cropping the size of evaluation area for two measured samples with different surface roughness.	95
A4	Table of computed areal parameters obtained by different post-processing approaches for two measured samples with different surface roughness.	95
A5	Table of computed 2D parameters obtained by areal measurement for two measured samples with different surface roughness.	95
A6	2D roughness parameters calculated from 2D measurement that was conducted in the current project.	96
A7	Areal roughness parameters calculated from 3D areal measurement that was conducted in the current project.	97
A8	Average errors of each method and of each series for the logarithmic model.	97

List of Variables

a_p	[mm]	Depth of cut
b	[MPa]	Fatigue strength exponent of the Basquin S-N curve model
C	[-]	Coefficient of the power law S-N curve model
F	[mm/rev]	Feed rate
K_t	[-]	Stress concentration factor
l	[mm]	Notch width
ln	[mm]	Evaluation length
lr	[mm]	Sampling length of the roughness profile
lw	[mm]	Sampling length of the waviness profile
N	[-]	Fatigue life (cycles to failure)
R	[-]	Stress ratio
R_a	[μm]	Arithmetic mean deviation
R_c	[μm]	Mean height of the profile
R_{ku}	[-]	Kurtosis
R_m	[MPa]	Ultimate tensile strength (UTS)
R_{mr}	[-]	Relative material ratio
R_n	[mm]	Nose radius of the cutting tool
R_p	[μm]	Maximum profile peak height
R_q	[μm]	Root mean square deviation
R_{sk}	[-]	Skewness
R_{sm}	[μm]	Mean width of the profile elements
R_t	[μm]	Total height of the profile
R_v	[μm]	Maximum profile valley depth
R_z	[μm]	Average maximum height of the profile
S_a	[μm]	Arithmetic mean deviation
S_{al}	[-]	Autocorrelation length
S_{ku}	[-]	Kurtosis
S_p	[μm]	Maximum peak height
S_q	[μm]	Root mean square deviation
S_s	[RPM]	Spindle speed
S_{sk}	[-]	Skewness
S_{tr}	[-]	Texture aspect ratio
S_v	[μm]	Maximum valley depth
S_z	[μm]	Maximum height
t	[mm]	Notch depth
V_c	[m/min]	Cutting speed

V_{vv}	$[\mu\text{m}^3/\mu\text{m}^2]$	Pit void volume
w	$[-]$	Exponent of the power law S-N curve model
λ_c	$[\text{mm}]$	C filter wavelength
λ_f	$[\text{mm}]$	F filter wavelength
λ_s	$[\text{mm}]$	S filter wavelength
σ_a	$[\text{MPa}]$	Stress amplitude
σ'_f	$[\text{MPa}]$	Coefficient of the Basquin S-N curve model
σ_{FS}	$[\text{MPa}]$	Fatigue strength corresponding to a certain fatigue life
σ_{FSac}	$[\text{MPa}]$	Actual fatigue strength
σ_{FSt}	$[\text{MPa}]$	Theoretical fatigue strength
σ_{FSr}	$[\text{MPa}]$	Fatigue strength of the reference
σ_m	$[\text{MPa}]$	Mean stress
σ_{max}	$[\text{MPa}]$	Maximum stress
σ_{min}	$[\text{MPa}]$	Minimum stress
ρ	$[\text{mm}]$	Notch root radius

1 Introduction

1.1 Motivation and background

Technical development is constantly moving forward. It is driven by competition and increasing customer demands. New technologies mean new possibilities in product design, thus it is possible to produce smaller, faster, cheaper machines and components while not setting aside the requirements for their life cycle. Material fatigue is influenced by several different factors which include surface quality itself. To properly understand what surface roughness is and what effects it can have on fatigue, we need to characterize it as best as we can. Not so long ago, mankind was able to measure surface roughness in two dimensions, even though every surface in the world is three-dimensional. With the development of modern technology, primarily microscopy, a new possibility of surface characterization has opened up, in particular, a three-dimensional one. It is a relatively new approach to surface roughness analysis, and there are not yet well-established procedures, especially in connection with material fatigue, where two-dimensional surface characterization has been the predominant approach to date. This provides an opportunity to push the boundaries of what is currently possible and to gain a better understanding of the effect of surface roughness on fatigue. To do so, it is essential to understand the current approach to this problem to find opportunities for improvement. One possibility appears to be the use of surface parameters as indicators of fatigue life in terms of surface quality.

1.2 Scope of the thesis

The main goal of the present thesis is to analyze surface roughness and its impact on fatigue life. To meet the main goal, the study comprises the following specific objectives:

1. Analyzing the effect of manufacturing parameters on surface roughness based on published papers.
2. Analyzing the suitability of various parameters describing the surface roughness.
3. Describing the technology of surface roughness measurements and the potential issues caused by the specific solutions.
4. Performing fatigue experiments with various manufacturing parameters, including the analysis of the surface roughness.
5. Comparison of existing proposals on the conversion of manufacturing parameters to output surface roughness based on these own experimental data items.

6. Based on the literature review, comparing various methods for fatigue life estimation based on specific surface roughness.
7. Results of item 6 compared with the outputs of item 5.
8. Describing the conclusions.

The focus of this thesis is limited to conventional subtractive manufacturing processes. Additive processes are not included because of a completely different microstructure, different distributions of residual stresses, and often much higher porosity, which can cause the surface roughness effect to be marginal.

1.3 Thesis layout

The current thesis comprises nine chapters, including the introduction and the conclusion. For the reader's easy orientation, a brief content of each chapter is given.

Section 2

Section two is devoted to the theoretical background needed to elaborate the experimental part of this thesis.

Section 3

Section three focuses on reviewing the state of the art on how the scientific community reports on the measurement of surface roughness in fatigue life analysis. The aim was to investigate how surface roughness is measured, what parameters are used to characterize surface roughness, and how detailed the measurement is reported.

Section 4

Section four focuses on the sensitivity analysis of the areal parameters that were indicated as potential indicators of fatigue performance. How their values differ when using different 3D areal measurement technologies, objectives with different magnification, evaluation area size, and different post-processing procedures.

Section 5

Section five focuses on verifying the precision of different fatigue life estimation methods based on specific roughness values in external data sets that were obtained from journal articles.

Section 6

Section six focuses on the experimental testing of the in-house samples. First, their surface roughness and residual stresses were measured, and then their fatigue life was determined.

Section 7

Section seven focuses on the analysis of the effect of manufacturing parameters on surface roughness. First, the correlation between the machining parameters and the individual roughness parameters is analyzed, and then the accuracy of different methods of roughness estimation based on the machining parameters is verified.

Section 8

Section eight builds on the results obtained in Section 6 and focuses on the analysis of the effect of surface roughness on fatigue life. First, the correlation between individual roughness parameters and fatigue life is analyzed and then the precision of different fatigue life estimation methods based on specific roughness values is verified on the same experimental data.

2 Theoretical background

2.1 Introduction to Fatigue

Fatigue of materials is a phenomenon in which the structure fails due to the initialization and propagation of cracks through the component when exposed to cyclic loads. Characteristically, the degradation process occurs when the material is subjected to stress ranges lower than the static strength of the material [11]. Approximately 90% of all operational failures of mechanical structures are caused by fatigue. There are several domains of fatigue, including, for example, low-cycle fatigue, high-cycle fatigue, thermal fatigue, or corrosion fatigue [39].

Cyclic loading

Cyclic loads acting on machine components can be divided according to the character of the time course into stochastic and deterministic. In the time domain, stochastic loads are completely random, while deterministic loads have a regular form and can be described mathematically. The real load on the components is usually a combination of both waveforms. The area of interest of this thesis is focused only on deterministic loading and more precisely on harmonic loading with uniaxial stresses. This type of loading can be described by the mean stress (σ_m) and the stress amplitude (σ_a). The maximum stress (σ_{max}), the minimum stress (σ_{min}) and the stress ratio (R) can also be used to describe it [11]. The relationships between them are very simple:

$$\sigma_a = \frac{\sigma_{max} - \sigma_{min}}{2} \quad (1)$$

$$\sigma_m = \frac{\sigma_{max} + \sigma_{min}}{2} \quad (2)$$

$$R = \frac{\sigma_{min}}{\sigma_{max}} \quad (3)$$

For $R = -1$, the cyclic loading is fully reversed. The harmonic loading with sinusoidal waveform with constant stress amplitude and mean stress is shown in Figure 2. In this work, fully reversed cyclic loading will be used.

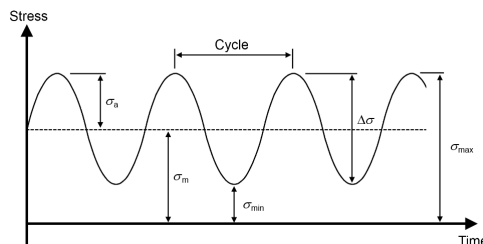


Figure 2: Harmonic loading [11].

2.2 S-N curves

S-N (Stress - life) curves, also known as Wöhler curves after August Wöhler (1819-1914), are commonly used to represent experimental data from a series of fatigue tests conducted to characterize the fatigue life of materials. The course of the S-N curves can be influenced by many factors such as the stress ratio, temperature, corrosion, surface finish, and residual stresses. It is important to indicate under what conditions the curve was obtained.

The S-N curve describes the relationship between the magnitude of cyclic stress and the number of cycles to failure. Wöhler is shown in Figure 3. The vertical axis of the diagram represents the magnitude of the cyclic loading of, for example, the material, component, or notch. It is most often related to the amplitude of the cyclic load σ_a . In this work, the vertical axis will be related to this metric because all the experimental data used in this work are reported in this metric. In certain S-N diagrams given in the literature, it is possible to find that the vertical axis is related to a different metric, for example, the maximum stress of the cyclic load and also certain publications, mainly of older date of publication, such as [58], use other units such as ksi (kilopounds per square inch). The vertical axis is usually not strictly a logarithmic or linear scale. In this work, a linear scale will be used but the theoretical description in this chapter will work with the axis in a logarithmic scale.

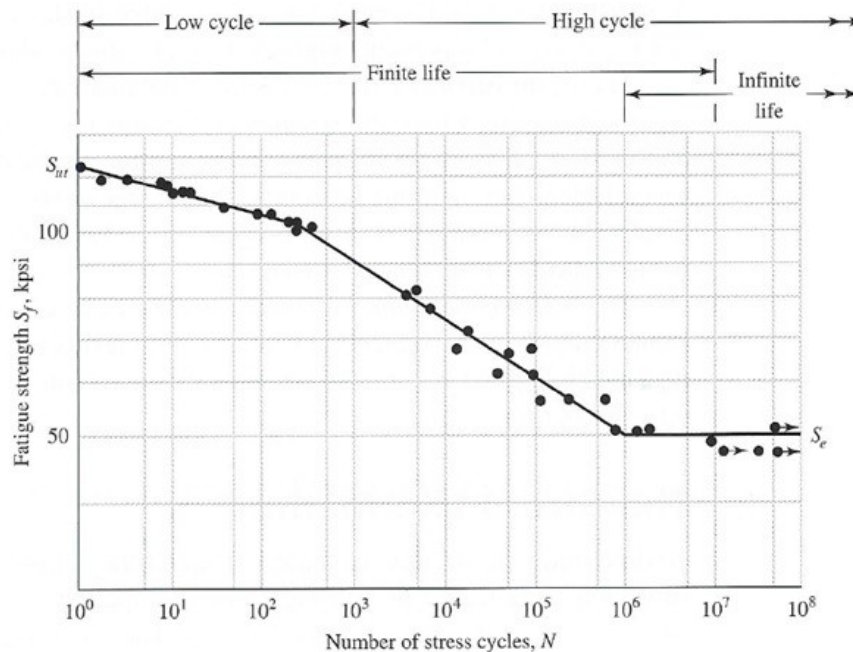


Figure 3: Wöhler diagram [70].

The horizontal axis is related to fatigue life, usually as the number of cycles N [-] until a certain end criterion has been met, for example, total failure of the sample or a drop in natural frequency of a certain value/percentage due to loss of stiffness

caused by crack growth. The horizontal axis is on a logarithmic scale because the experimental values of N are usually distributed over several orders of magnitude; for this reason, using a linear scale would be highly confusing and would severely complicate the reading of the data from the graph. Another advantage of using $\log_{10}(N)$ is that the experimental data show a linear trend between the magnitude of stress and the life of fatigue.

The Wöhler diagram can be divided into 4 parts on the horizontal axis. The leftmost, in the lowest life domain, where failure occurs approximately in the range of units to tens of cycles of loading, is the quasi-static region, where the S-N curve has an almost horizontal slope. In this region, it is not possible to speak of a classical fatigue process because the stress levels are so high and the fracture surface propagates so rapidly that it has the characteristics of a static fracture in places and the fractured surface usually shows signs of ductile fracturing as opposed to brittle, which is typical for fatigue. The curve then bends and starts to trend downward, where the two most important and best-described parts of the curve are located, the low-cycle fatigue region (LCF) and the high-cycle fatigue region (HCF). The mutual boundary of the regions is not clearly visible on the curve, and its exact boundary is not strictly defined. It is generally accepted that the LCF lies between the lifetimes of the 10^2 to 10^4 (10^5) cycles. The stress level is still very high in this region, so cyclic plastic deformation dominates. In the HCF, the stresses are already significantly lower and no plastic deformation occurs here and the fatigue fracture is characterized by a pure transcrystalline fracture. As the stress level is further reduced, the S-N curve becomes almost horizontal again. This region is called giga-cycle fatigue. This region starts from approximately 10^9 cycles and is characterized by fractures initiating at inhomogeneities within the material and further crack growth continues to the surface, this type of fracture is called fish-eye [61] [56].

A mathematical description of the S-N curves is introduced to estimate the life-time value for certain load values from the experimental data. The most widely used mathematical model is called the power-law model:

$$N \cdot \sigma_a^w = C \quad (4)$$

where N is the number of cycles to break, σ_a is the stress amplitude, and w and C are empirically determined constants.

The power-law model is the simplest and often sufficient one that describes the slat branch of the log-log curve and is applicable over the range of stress amplitude from the yield strength to the fatigue limit. Another model that describes the slat branch of the log-log curve was proposed in 1910 by Basquin when he expressed the experimental

data measured by Wöhler et al. using the following exponential equation [52]:

$$\sigma_a = \sigma'_f (2N)^b \quad (5)$$

where b and σ'_f are empirically determined constants [65] [70].

Endurance Limit

Certain materials (for example, steel or titanium) have a stress level (the lower asymptote in the S-N curve) below which the material does not fail and can theoretically be loaded for an infinite number of cycles, and the structure is said to have an infinite life. It is important to remember that this is not an absolute value for 100 % of the cases. The value is determined statistically from experiments. Many non-ferrous metals and alloys, such as aluminum or magnesium, do not have this limit, and their curve in the S-N diagram is in continuous decline. For these materials, an infinite life is sometimes defined at a stress level at which the material reaches $2 \cdot 10^7 - 1 \cdot 10^8$ cycles [70].

2.2.1 Other influences affecting fatigue life

Size factor

Most metals in the solid state have a regular arrangement of atoms called a crystal structure, which we describe using a crystal lattice. Ideally, it would be regular without any defects, but in reality there are all kinds of defects, from point defects to various impurities. These result in an increased probability of crack initiation, leading to a reduced fatigue limit. As the size of the component increases, the probability of more defects increases. A size factor has been introduced that reduces fatigue endurance and is given as a function of the size of the component. It is used for components with a diameter greater than 8 mm (this size is given by the size of the experimental specimens for which the fatigue life was measured). For smaller diameters, this factor is not used [7].

Heat treatment factor

Different heat treatment conditions give different microstructures of the material. The effect of microstructure on fatigue endurance is related not only to mechanical properties (hardness, residual stresses, tensile strength) but also to grain size, where grain size has an impact on the yield strength of steels. For notched parts, heat treatment can increase the fatigue limit up to 100% [65].

Residual stresses factor

The occurrence of residual stresses has a major impact on fatigue. Tensile residual stresses can have a negative effect on fatigue life, while compressive residual stresses can improve fatigue properties because they prevent crack propagation. Residual stresses are referred to as the stress distribution in the component/material when no external load is applied. At a given time, both types of residual stress are present in the body because they must satisfy stress balance, i.e. the sum of the stresses must be zero. The occurrence of residual stresses in the material is the result of previous processes, including heat treatment and production processes. For the latter, cold work is a typical process that results in plastic deformation of the material, the other common process is machining, during which the chip breakage is preceded by plastic deformation, leaving residual stresses that can be very pronounced in a thin layer below the surface [68] [31] [32]. In grinding, compressive residual stresses can reach more than 900 MPa [65].

2.3 Roughness characterization

Roughness and waviness have been part of quality control for more than 100 years. Traditionally, surface profile acquisition is done using a 2D measuring instrument to obtain roughness/waviness characterization. Until about 20 years ago, this was the only way to measure surface roughness. Mádl et al. [60] in their 2000 textbook stated that the technology at that time did not allow evaluation of roughness over the entire surface (three-dimensional), but only in a section perpendicular to the underlying surface, the profile. 2D surface measurements continue to be still important for industrial profile definition and are still used for applications where processes are well defined, for example, technical drawings. 2D measurement system still has many benefits:

1. Small, portable, and relatively cheap solution
2. Simple to operate and implement
3. High flexibility
4. Well-established standards and worldwide traceability

The advantages listed above are mainly economic rather than functional and do not lead to better surface characterization [23].

With the development of new technologies, materials, and processes, as well as a better understanding of friction, surface finishes, etc., surface quality becomes increasingly important. For this reason, 2D characterization is no longer sufficient and it is now accepted that a surface cannot be adequately described without three-dimensional information. 3D measurements, mainly using optical measuring instruments, provide

extremely useful information about surface characterization, such as protrusions or depressions. The 3D areal roughness measurement has many reasons why it is better than 2D:

1. Every surface in nature is three-dimensional, so 2D profile measurement cannot fully describe surface characterization.
2. Three-dimensional surface measurement allows the calculation of extra functional parameters, such as void volume or debris volume.
3. No physical contact with the measured component [23].

2.3.1 Measuring instruments

There are many different measurement instruments for surface characterization. Instruments can be classified by measurement dimension: 2D or 3D. The former can only be used to obtain 2D roughness parameters, while the latter can be used to obtain both 2D and areal roughness parameters. The other and most common way is to classify the instruments into three types by the principle of operation: contact (stylus), non-contact (optical), and scanning probe microscopy. Each type has its advantages and disadvantages and is projected for different types of applications. The main parameters of the instrument include vertical resolution and range, lateral resolution and range, and probe size/geometry.

Stylus Method

By this method, 2D and 3D areal measurements can be obtained, but the vast majority of instruments are made only for 2D measurements. During measurement with the contact-type instrument, the stylus tip is in contact with the measured surface and moves along the evaluation length. The instrument detector electrically detects the vertical movement of the stylus. The signal is amplified, converted digitally, and recorded. To achieve the best possible resolution of the tester, the radius of the stylus tip must be as small as possible and as hard as possible to minimize wear. The radius of the stylus tip is usually smaller than 10 μm and is made of diamond or sapphire.

2D measurement of roughness with a contact-type instrument is the most widely used method to characterize surface roughness in the industry. Positives include ease of use or reliability of measurement due to contact between instrument and sample. For example, in dirty environments (oil, etc.), where the non-contact measurement may be affected/impeded by surface contamination. However, it has many disadvantages, such as gradual wear and tear of the stylus during use. Over time, the tip will become flat or rounded. Logically, a different tip shape will produce a different wave profile. Furthermore, styluses are made of very hard material, which can leave scratches on the

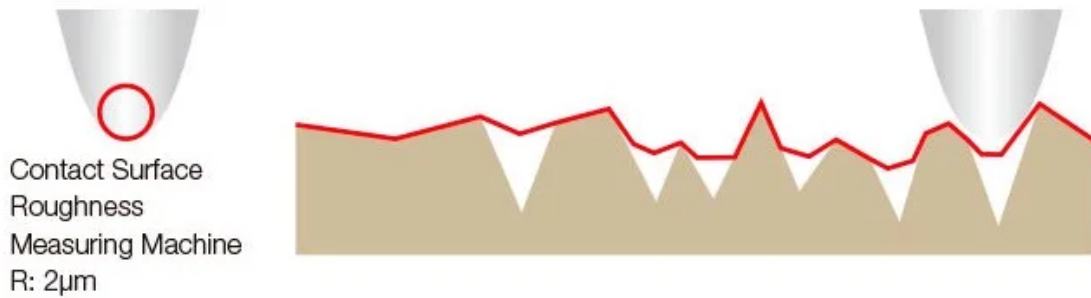


Figure 4: Effect of stylus tip radius [8].

surface of the measured sample. The biggest disadvantage of contact measurement is that it cannot detect the correct shape of the grooves (valleys, scratches) if their width is smaller than the radius of the tip, and then the valleys are rounded, as can be seen in Figure 4 [4].

Interferometry

The interferometer is an optical instrument that works on the principle of light interference. The instrument compares the distances of two objects, the reference and the tested one. The interferometer consists of a light source, a beamsplitter, a detector (CCS image sensor), a reference surface, and a tested surface. The beamsplitter splits the beam from the light source to reference and test beams, which then reflect off the surfaces into the detector, creating an interference pattern that varies with the amplitude and phase of these beams. The optical paths from the reference mirror to the detector and from the tested surface to the detector are the same. However, due to the topography of the profile, these optical paths are not the same, creating an interference pattern on the detector. The resulting pattern is then translated into peaks and valleys. A basic schematic of the interferometer is shown in Figure 5.

One of the advantages of interferometry is its high sensitivity to surface topography and very high vertical resolution which can go down to 0.1 nm. Furthermore, interferometers can cover a large area with a high lateral resolution. The only limitation is the resolution of the detector (number of pixels) and the optical diffraction. However, this method also has limitations. It has limited use on certain objects with good reflection, and measurement may also not be possible on spiky or bumpy samples. Furthermore, the method has a high sensitivity to vibrations, so the instrument must be placed on shock-absorbing tables [18] [9].

Focus Variation

The technique provides topographic and color information about a surface based on the combination of the optical system with a small depth of focus and vertical scanning. The main part of a microscope capable of focus variation is precision optics

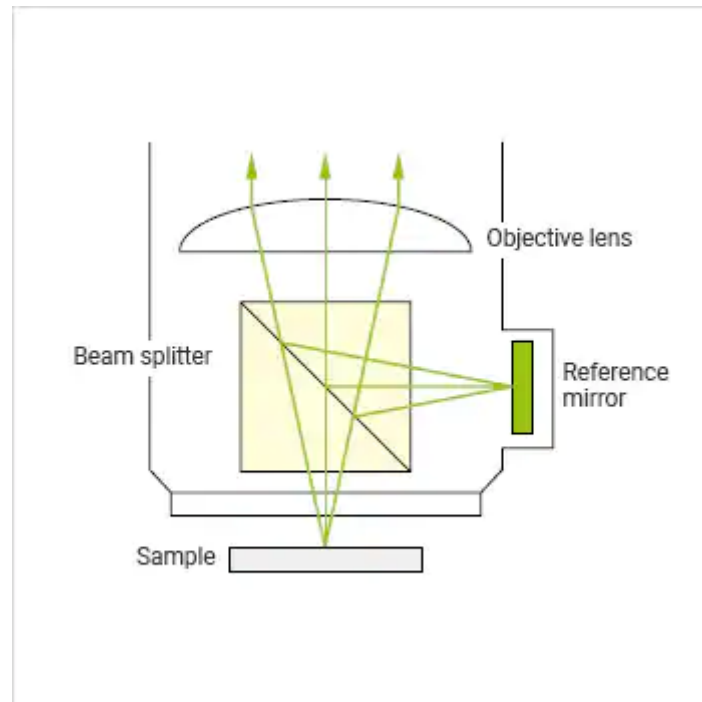


Figure 5: Principle of interferometer [18].

with various lens systems that can be equipped with different objectives with different magnifications and resolutions. In addition, it consists of a light source emitting white light that is directed through a mirror into the microscope's optical system and focused onto the specimen by an objective lens. According to the surface properties of the object to be scanned, part of the light is reflected into the optical system and incidents on the light-sensitive sensor. Only a small area of the surface is scanned sharply due to the small depth of field. To scan the entire surface at full depth of field, the whole optical system moves vertically along the optical axis and captures the surface at each vertical step until the entire surface is sharply scanned. A basic schematic of the focus variation is shown in Figure 6. The software then processes the recorded data to create a 3D surface profile at the full depth of field and true color. The vertical and the lateral resolutions depend on the optics used and the first one can go as low as 10 nm. The vertical scanning range depends on the range of movement of the objective and usually varies between 3.2 and 22 mm [67].

The advantages of the technique include, that, unlike other optical methods, it is not limited by coaxial illumination, can also be used with various illumination sources (such as ring light), and can measure slopes exceeding 80° . The method is very flexible and can be used on a wide range of surfaces, from smooth to rough, glossy to matte, and homogeneous to compound material. The drawback is that it is not suitable for measuring very smooth surfaces because the vertical resolution is only 10 nm [40].

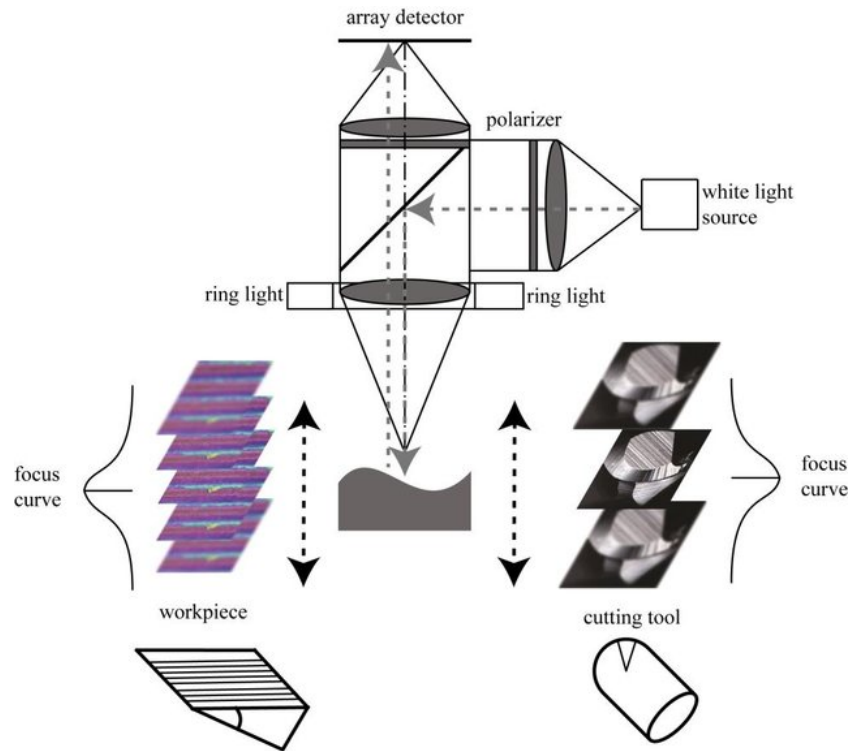


Figure 6: Focus variation [40].

Confocal Microscopy

The technique of confocal microscopy was invented by Martin Minsky in 1955. Its principle is based, unlike previous methods, on illuminating a single point on a surface at a time through a pinhole that is situated in a conjugate plane (confocal) with a scanning point on the specimen. This eliminates unwanted scattered light that would illuminate the entire surface at the same time and reduce image quality. The light reflected by the sample surface passes through the lenses and is directed through another pinhole into the photodetector. The only light that is reflected exactly from the focal point will pass through the pinhole into the photodetector. By eliminating scattered and out-of-focus lights, the strongest possible in-focus light is achieved. As the above description suggests, the name confocal refers to the fact that both illuminating and back-projecting pinholes have a focus on the sample surface. A basic schematic of confocal microscopy is shown in Figure 7.

The confocal profilometer is a non-contact technique based on confocal microscopy. During measurement, the sample surface is vertically scanned step by step, so that every point on the surface passes through the focus. When measuring the 3D surface topography, every illuminated point is scanned in the vertical direction, and then the illuminated point is moved horizontally and the whole process is repeated until the entire surface is scanned. The scan time of the entire surface can be reduced by using a series of pinholes that scan the surface simultaneously. Confocal microscopy provides the highest lateral resolution of all methods presented here, reaching $0.1 \mu\text{m}$. However,

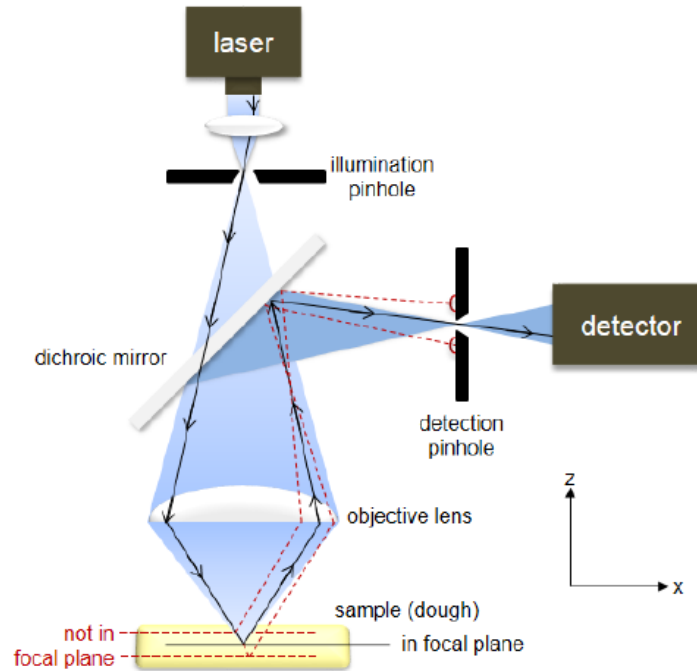


Figure 7: Confocal microscopy [47].

this technique is limited by the requirement of minimum reflectivity of the sample and maximum slope of the measured sample, which is given by the numerical apparatus of the objective. In addition, high spikes and sharp valleys can occur in the data when scanning a steep slope because the instrument loses focus and rapidly searches for a new one before moving into a new vertical position [3] [13] [76].

2.3.2 Measurement post-processing

Measurement post-processing must be used to extract the desired surface quality information, which is usually achieved by using filters. The first filter used is usually the λ_s filter, which filters out short wavelengths, such as noise. Then the form removal operator (filter) is used to remove the form, leaving only the primary profile. When using the filter with the cut-off λ_c , the roughness and waviness surface are obtained. *"In 3D characterization, a filtered surface is referred to as scale limited surface rather than a surface with limited bandwidth."* [76] For this reason, different filters are used for 3D characterization: S, L, and F filters. The first is used to filter out the information at the smallest scale, such as noise, and is similar to λ_s , The L filter is equivalent to the λ_c filter and the F filter removes nominal form. The SL and SF surfaces are defined in ISO 25178-2 [44] as two scale limited surfaces. The SF is referred to as the primary surface and the SL is referred to as the roughness surface. [76]

The most commonly used filter in metrology is the Gaussian filter, which belongs to the category of linear filters. It works on the principle where it replaces each point on a profile or surface by a weighted average of points in its neighborhood and thus

obtains a mean line (2D) or mean surface (3D), and these serve as a reference for the subsequent calculation of topographic parameters [76].

Actual profile

The profile is created by the intersection of the surface of the workpiece and the plane normal to the surface and in a direction where the surface roughness values are the highest and are usually perpendicular to the direction of surface machining/finishing.

Measured profile

Is the profile that was obtained by 2D scanning of the actual profile. Surface defects, such as cracks and scratches, should not be included in the record.

Primary Profile

The primary profile (P profile) is the result of applying an electronic low-pass filter with cut-off wavelength λ_s to a measured profile. Using the λ_s filter removes the shortest wavelengths that are not considered relevant for roughness measurements and can be called white noise. These profiles are evaluated within the evaluation length ln .

Roughness Profile

The roughness profile (R profile) is the result of applying an electronic low-pass filter with cut-off wavelength λ_c to the primary profile. Using the λ_c filter removes longer wavelengths that are not already considered as roughness but as waviness. These profiles are evaluated within the evaluation length ln , which usually consists of five sampling lengths lr , which correspond to the cut-off wavelength λ_c .

Waviness Profile

The waviness profile (W profile) is the result of the application of an electronic low-pass filter with cut-off wavelength λ_c and a high-pass filter with cut-off wavelength λ_f on the primary profile. The W profile is evaluated within the evaluation length ln consisting of several sampling lengths lw that correspond to the cut-off wavelength λ_w [2].

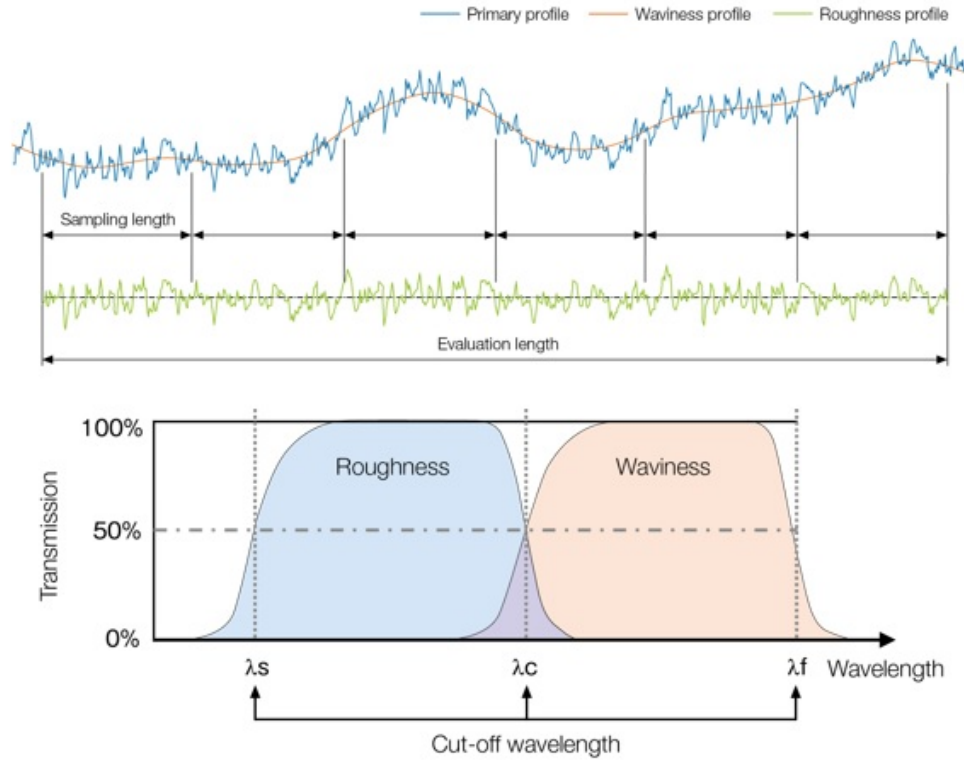


Figure 8: Surface profile [15].

2.3.3 2D profile parameters

The most used 2D surface roughness parameters are described in this section. For more detailed information or a description of more parameters, the reader is referred to ISO 4287:97 [45].

Arithmetic mean deviation (R_a)

The arithmetic mean deviation (R_a) [μm] indicates the average of the absolute value of the trace above and below the center line.

$$R_a = \frac{1}{l_n} \int_0^{l_n} |z(x)| dx \quad (6)$$

This definition implies that it is not possible to determine whether the prevailing deviations are peaks or valleys. Furthermore, the value of R_a is not significantly affected by isolated extremes, which may, however, be significant in terms of fatigue. The most common R_a values for machining range from 0.2 to 1.6 μm (the lower the value, the smoother the surface) [6].

Maximum profile peak height (R_p)

Represents the maximum profile peak height of a profile along the sampling length.

Maximum profile valley depth (R_v)

Represents the maximum profile valley depth of a profile along the sampling length.

Average maximum height of the profile (R_z)

This parameter is calculated as the average of the sum of the maximum peak to valley height of each sampling length. This parameter was first defined in the German DIN standard; therefore, in some publications, this parameter may be defined as $R_z(\text{DIN})$ [17].

Total height of the profile (R_t)

This parameter represents the total height of the profile as the vertical distance between the highest peak of the profile and the lowest valley of the profile along the length of evaluation.

Mean height of the profile (R_c)

Represents the mean height of the profile along the sampling length.

$$R_c = \frac{1}{m} \sum_{i=1}^m R_{ti} \quad (7)$$

where m is the number of sampling lengths.

Root mean square deviation (R_q)

The root mean square deviation of the profile R_q [μm] is the quadratic mean of the coordinates $z(x)$ throughout the sampling length. It is one of the most widely used parameters because it gives stable values as it is not significantly influenced by scratches and enables easy statistical processing [14].

$$R_q = \sqrt{\frac{1}{l_n} \int_0^{l_n} z^2(x) dx} \quad (8)$$

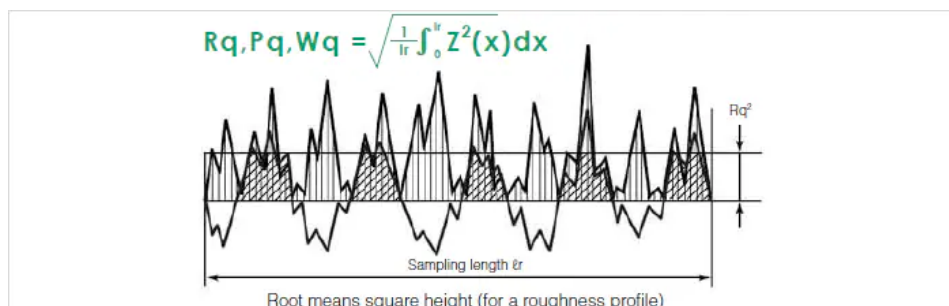


Figure 9: Root mean square deviation [1].

Skewness (R_{sk})

The quotient of the mean cube value of $Z(x)$ and the cube of R_q within a sampling length and represents the profile asymmetry against the mean line. A negative value indicates a predominance of sharp valleys and rounded peaks, whereas a positive value indicates a predominance of sharp peaks and rounded valleys. $R_{sk} = 0$ represents symmetry against the mean line. See Figure 11 a) [77].

$$R_{sk} = \frac{1}{R_q^3} \left[\frac{1}{l_n} \int_0^{l_n} z^3(x) dx \right] \quad (9)$$

Kurtosis (R_{ku})

The quotient of the mean quadratic value of $Z(x)$ and the fourth power of R_q within a sampling length. R_{ku} indicates the presence of high peaks and deep valleys for $R_{ku} > 3$, while $R_{ku} < 3$ means an even height distribution and $R_{ku} = 3$ when the surface peaks are normally distributed. See Figure 11 b) [77].

$$R_{ku} = \frac{1}{R_q^4} \left[\frac{1}{l_n} \int_0^{l_n} z^4(x) dx \right] \quad (10)$$

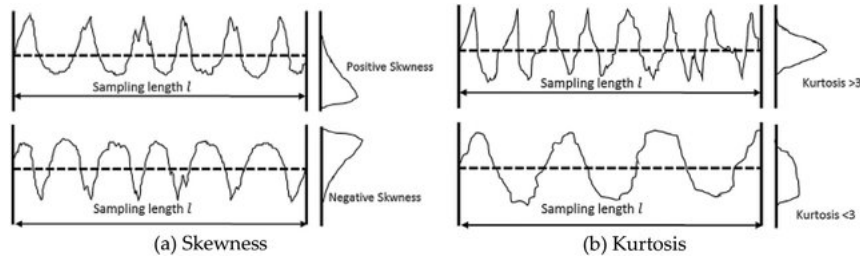


Figure 10: Skewness and Kurtosis ([77]).

Mean width of the profile elements (R_{sm})

R_{sm} is the horizontal parameter that expresses the average value of the width of the profile elements within the sampling length. Distance is measured on the mean line of the profile. When measuring a 2D profile according to ISO 4287, which is a periodic profile, the value of the cut-off wavelength λ_c is governed by the value of R_{sm} , for a non-periodic profile it is judged by the value of R_a (R_z).

$$R_{sm} = \frac{1}{m} \sum_{i=1}^m X_{si} \quad (11)$$

where m is the number of sampling lengths and X_{xi} is the length of a single profile element.

2.3.4 3D profile parameters

The most used areal surface roughness parameters are described in this section. For more detailed information or a description of more parameters, the reader is referred to ISO 25178:2012 [44].

The arithmetic mean deviation (S_a)

The arithmetic mean deviation (S_a) [μm] indicates the average of the absolute values of the trace above and below the mean surface within the evaluation area. The parameter is equivalent to the 2D parameter R_a .

$$S_a = \frac{1}{A} \iint_A z(x, y) dx dy \quad (12)$$

where A is area [μm^2] of the evaluation area.

Maximum valley depth (S_v)

Represents the maximum valley depth of a surface in the evaluation area. The parameter is equivalent to the 2D parameter R_v .

Maximum peak height (S_p)

Represents the maximum peak height of a surface in the evaluation area. The parameter is equivalent to the 2D parameter R_p .

Maximum height (S_z)

Is equal to the sum of maximum peak height S_p and maximum valley depth S_v . Although it is often used in practice, its disadvantage is that it is strongly affected by scratches, contamination, or measurement noise such as spikes; hence, it is not representative of the evaluated surface.

Root mean square deviation (S_q)

The root mean square deviation of the surface S_q [μm] is the quadratic mean of the $z(x,y)$ coordinates in the evaluation area. The parameter is equivalent to the 2D parameter R_q .

$$S_q = \sqrt{\frac{1}{A} \iint_A z^2(x, y) dx dy} \quad (13)$$

where A is area [μm^2] of the evaluation area.

Skewness (S_{sk})

The quotient of the mean cube value of $Z(x,y)$ and the cube of S_q within an evaluation area and represents the profile asymmetry against the mean line. The parameter is a three-dimensional extension of a 2D parameter R_{sk} .

$$S_{sk} = \frac{1}{S_q^3} \left[\frac{1}{A} \int_0^A z^3(x,y) dx dy \right] \quad (14)$$

Kurtosis (S_{ku})

The quotient of the mean quadratic value of $Z(x,y)$ and the fourth power of R_q within an evaluation area. The parameter is a three-dimensional extension of a 2D parameter R_{ku} .

$$S_{ku} = \frac{1}{R_q^4} \left[\frac{1}{A} \int_0^A z^4(x,y) dx dy \right] \quad (15)$$

Autocorrelation length (S_{al})

S_{al} is one of the spatial parameters that describe the texture of the surface as periodicity. This set of parameters originates from the concept of an autocorrelation function. The autocorrelation length is used to describe the horizontal distance of the autocorrelation function with the fastest decay to a specific value.

Texture aspect ratio (S_{tr})

Describes the texture pattern of a surface and is defined as the ratio of the distance between the autocorrelation function with the fastest decay to a specific value and the autocorrelation function with the slowest decay to a specific value. The value can be between 0 and 1. A value of about 1 is achieved by an isotropic surface that has the same characteristics in all directions, the opposite limit value indicates an anisotropic material that has a single-oriented (periodic) structure.

Pit void volume (V_{vv})

Functional parameters are calculated from the Abbott-Firestone curve (material ratio curve). It represents the percentage of material traversed at a given depth. The pit void volume of the scale limited surface is void volume located in the valley zone of the Abbott-Firestone curve between 80 % and 100 % of the material ratio [76].

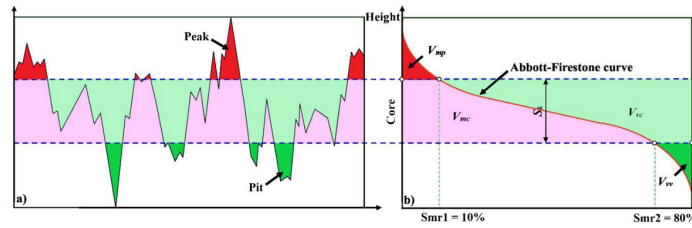


Figure 11: Schematic description of the functional parameters [57].

2.4 Effect of machining parameters on surface roughness

2.4.1 Machining

“The material removal processes are a family of shaping operations in which excess material is removed from a starting workpart so that what remains is the desired final geometry. The most important branch of the family is conventional machining, in which a sharp cutting tool is used to mechanically cut the material to achieve the desired geometry. The three main machining processes are turning, drilling, and milling.” [41]

The surface layer of components is the result of a manufacturing process, primarily a finishing process, which may be, for example, machining, grinding, or polishing. Very often, the final surface is achieved by turning, for example, in the manufacture of shafts or various pins and studs. This process is very complex, and the result is influenced by many factors: the properties of the material to be machined, cutting parameters, vibration, cooling, etc. During machining, elastic-plastic deformation and heat change the material properties of the surface layer, which then differs in its properties from the rest of the material [41].

2.4.2 Turning parameters and conditions

The factors affecting surface roughness originating from the machining operation can be divided into three groups: 1) geometric, 2) work material, and 3) vibration and machine tools. The first group includes the type of machining operation (turning, milling, etc.), cutting tool geometry (nose radius), and feed rate. The result of these factors alone is so-called theoretical roughness, which is no longer affected, compared to the actual roughness, among other things, by vibration. The second group includes factors related to the work material and its interaction with the tool. All material removal processes produce waste material, the chip, which in most cases adversely affects the surface quality, for example, by the ingress of cracks due to non-continuous chip formation when machining brittle materials. The last group includes machine vibration, poor tool fit, thus resulting in vibration and backlash in the feed mechanism [41].

This thesis will not address the effect of vibration and work material factors due to the external fabrication of the test specimens. Only the effect of factors that have been

clearly defined (cutting speed, feed rate, nose radius, and cut height) will be treated.

Feed rate

The feed rate in turning is the distance along the axis of the workpiece that the cutting tool traverses per one revolution of the workpiece. The feed rate is selected according to the type of tool, the desired surface quality, and the properties of the material being machined. If surface quality is one of the main parameters in part production, it is necessary to focus on the appropriate choice of feed rate [5]. Research by various authors [80] [26] [66] indicates that the feed rate has the greatest influence on the resulting surface quality of all the machining parameters. For the smoothest surface possible, it is essential to choose the lowest value of this parameter. In this paper, it will be denoted as F [mm/rev].

Cutting speed

Cutting speed can be defined as the relative speed between the surface of the workpiece and the cutting tool. In turning, it is achieved by rotating the workpiece in the lathe. Its correct choice is very important in machining because it determines other machining parameters such as cutting temperature, tool life, energy consumption, and, of course, the achieved surface quality of the workpiece. According to different authors, the effect of speed on roughness varies. Different publications [41] [34] [51] [79] report that the R_a roughness value decreases with increasing speed. Other authors [26] [35] state that the best surface quality is achieved at medium-range cutting speeds. On the other hand, according to [62] [43], the speed does not have a negligible effect on the surface quality. In this document, it will be denoted as V_c [m/min].

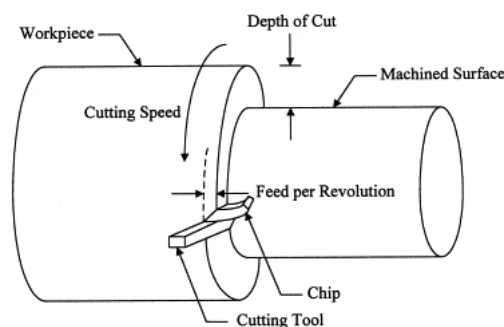


Figure 12: Turning parameters [74].

Depth of cut

Depth of cut a_p is the thickness of the material that is removed from the workpiece during a cut. The size of the chip is proportional to the depth of cut and affects the resulting cutting force. The higher value of the cutting force is associated with a decrease in the machining performance and the occurrence of vibrations. The higher

depth of cut values also increases the risk of mechanical damage to the cutting tool, which can result in breakage. The selection of the appropriate depth of cut value is influenced by the following requirements: productivity, cut quality, type of machining operation, workpiece characteristics, and machine/tool limitations [16]. According to different authors [50][26][62], the depth of the cut has a similar or even a lower influence on the roughness than the cutting speed. In this document, it will be denoted as a_p [mm].

Nose radius

Another parameter that affects roughness is the nose radius of the cutting tool. The use of a radius as opposed to a sharp end has, among other things, design reasons, its use reduces the risk of sudden breakage of the tool tip, and is easier and cheaper to manufacture. However, it increases the cutting force and generates more heat [12]. Its size has a direct impact on the resulting surface texture, according to several authors [30] [63], and increasing the radius has a positive effect on reducing surface roughness. However, the nose radius size is limited by the shape of the tool and the vibrations [29]. In this document, it will be indicated as R_n [mm].

2.4.3 Formulas

There are two possible ways to determine the relationship between surface roughness and machining parameters during machining. The first possibility is the analytical approach, in which a mathematical description of the machining process is made, in particular the surface profile that is generated by the cutting tool activity. The second option is the construction of an empirical model based on experimental data. This option is discussed by many authors in their research, who investigate the influence of individual parameters.

Analytical approach

Analytically calculated surface roughness is the ideal/geometric one. For the sharp tool, the parameter R_{tg} is calculated from the feed rate and the angles of the tools κ_{re} and κ'_{re} .

$$R_{tg} = \frac{F}{\cot\kappa_{re} + \cot\kappa'_{re}} \quad (16)$$

The average geometric roughness R_{ag} is 1/4 of R_{tg} due to the triangular contact between the tool and the workpiece.

For a tool with the nose radius, R_{ag} is independent of the tool angles but depends on the nose radius and is calculated as:

$$R_{ag} = \frac{F^2}{32R_n} \quad (17)$$

where R_{ag} is the geometric mean roughness, F is the feed rate and R_n is the nose radius. The following equation shows that a smoother surface is achieved by choosing a lower feed rate and a larger nose radius [72].

Under normal conditions, the ideal roughness cannot be achieved due to other influences. Groover [41] proposed a ratio between actual and ideal roughness, which includes the effect of material and cutting speed:

$$R_a = r_{ai} \cdot R_{ag} \quad (18)$$

where R_a is the estimated value of the actual roughness; r_{ai} is the ratio between the actual and the ideal surface. For this case, the ratio is plotted on the graph against the cutting speed and is given by different curves that represent different material types.

Empirical approach

Hadi and Ahmed [42] proposed a different empirical formula in their work, where they carried out an experiment on high-carbon steel (HCR40) to obtain a regression coefficient for the proposed exponential formula. Spindle speed, feed rate, and depth of cut were chosen as machining variables. From the ANOVA test, they concluded that the lowest roughness value was achieved with the lowest feed rate value and a higher spindle speed smoothed the surface. From the data regression, they obtained the following mathematical model:

$$R_a = 1113.5S_s^{-0.78}F^{0.3}a_p^{0.18} \quad (19)$$

Özdemir et al. [80] conducted a similar study, aiming to analyze the effect of cutting parameters on surface roughness and cutting forces in the machining of a high-hardness structural steel alloy (42CrMo4). The set of different cutting speeds, feed rates, depths of cut, and cutting tool nose radius were used as machining variables. From the results of the ANOVA analysis, they concluded that the feed rate followed by the nose radius had the greatest effect on the roughness. The authors proposed a complicated mathematical model from measured data using RSM (response surface methodology):

$$\begin{aligned} R_a = & 0.259923 - 0.00600782V_c + 15.0441F - 0.481891a_p + 0.787321R_n + \\ & + 6.93077 \cdot 10^{-6}V_c^2 + 40.964F^2 + 0.468282a_p^2 - 0.0143909V_c \cdot F + 0.00320303V_c \cdot a_p + \\ & + 0.00160064V_c \cdot R_n + 1.8188F \cdot a_p - 14.5249F \cdot R_n - 0.95457a_p \cdot R_n \quad (20) \end{aligned}$$

Patel and Gandhi [63] studied the effect of cutting parameters (cutting speed, feed rate, and nose radius) on surface roughness during the machining of hardened

steel alloy (AISI D2). They concluded that roughness decreased with (a) decreasing feed rate, (b) increasing cutting speed, and (c) increasing nose radius. The authors proposed a mathematical model based on the linear relationship found between the input variables and the surface roughness:

$$R_a = 4.1135 - 0.7439\ln(V_c) + 0.3177\ln(F) - 0.3846\ln(R_n) \quad (21)$$

Kittali et al. [50] study was the last publication from which the proposal on the relationship between machining and surface quality was taken. The study dealt with optimizing the machining parameters to minimize the surface roughness of the steel alloy (EN1A). Cutting speed, feed rate, and depth of cut were chosen as turning variables, and R_a as the search parameter. One of the conclusions of the study is that the feed rate has the largest impact on surface quality. The following mathematical relationship is proposed:

$$R_a = 2.55 - 0.000433V_c + 7.53F + 0.142a_p \quad (22)$$

2.5 Effect of surface roughness on fatigue endurance

The fatigue cracks mostly initiate on a free surface of a material; thus, surface quality has a non-negligible effect on fatigue strength. Therefore, according to Murakami [58], the following factors must be taken into account during the evaluation of fatigue strength: a) surface roughness as a stress raiser, b) residual stresses in a surface layer induced by machining, c) hardening and softening in a surface layer due to plastic deformation, and d) change or transformation of the microstructure due to plastic deformation. These factors, which depend on the manufacturing techniques used in the production of components, such as grinding and polishing, act together and affect fatigue life in a complex way.

2.5.1 Surface finish factor

The surface finish factor c_{sf} is one of the fatigue life modifiers, others are the size factor of the component, heat treatment, working temperature, or loading factor. These factors modify the fatigue limit compared to a reference laboratory sample on which the S-N curve and the fatigue limit are experimentally determined. Testing information should be given for the curve, which is usually made for cylindrical polished specimens of 10 mm diameter without grooves.

The value of the surface finish factor is calculated empirically and is usually reported in graphs in the literature. It can be directly related to the roughness value, where the fatigue surface factor is plotted against the material's ultimate tensile strength (UTS) and a roughness parameter. In this format, the graphs for calculating the surface finish

factor are given by Johnson [48] (see Figure 13) and by Italian standard, UNI 7670 [24]. The other possibility is that the surface finish factor is related to the different surface finish methods such as machining, grinding, and forging, as used in [49].

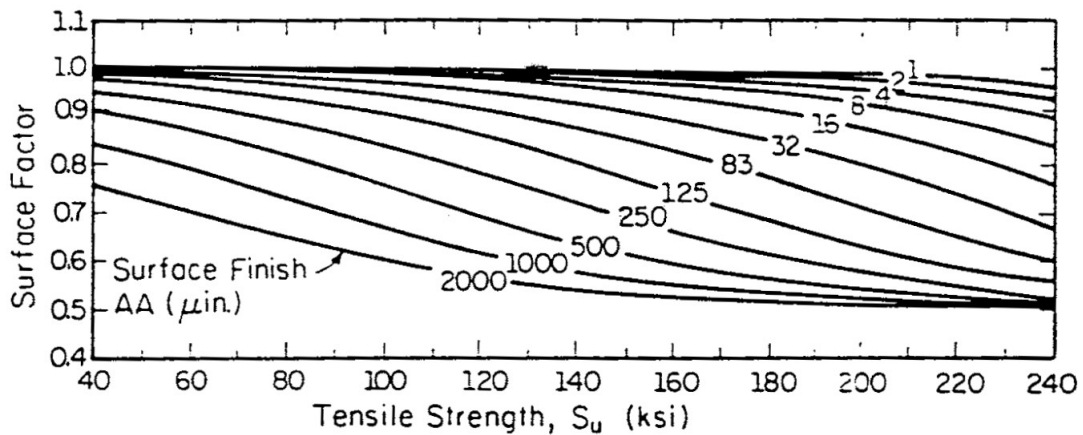


Figure 13: Surface finish factor given by Johnson [48]. AA = arithmetic average (Ra).

UNI 7670

The Italian standard deals with design instructions for mechanisms of lifting appliances, where the surface finish factor for shafts is given in the form of a diagram (see Figure 14) [24].

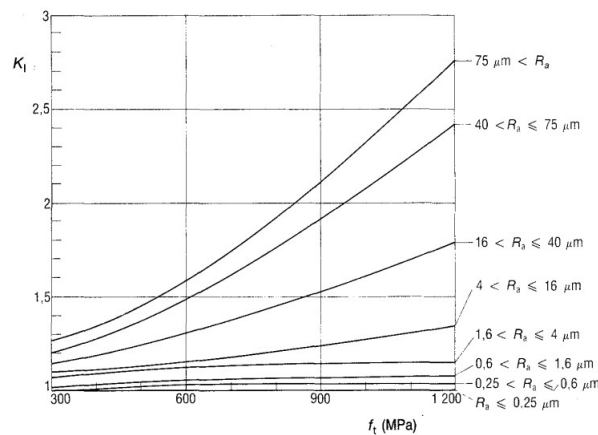


Figure 14: Surface finish factor given by Italian UNI 7670 standard [24].

Juvinall

In his book, the author presents a diagram (see Figure 15) where the surface finish factor depends on UTS and surface finish technique [49].

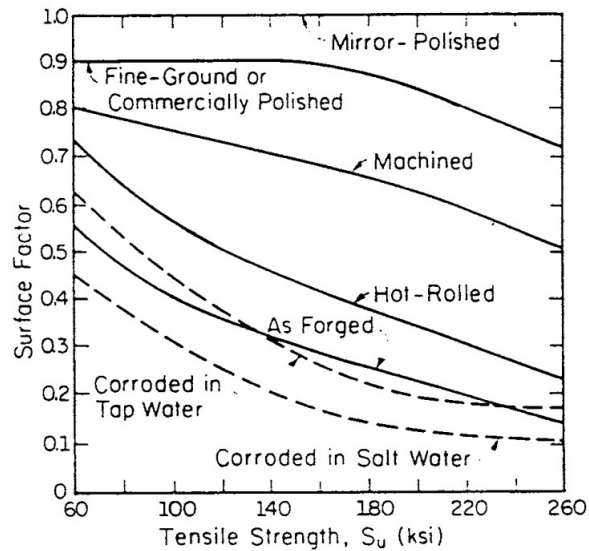


Figure 15: Surface finish factor given by Juvinall [49].

Jaap Schijve

Jaap Schijve states in his book *Fatigue of Structures and Materials* [68] that the effect of roughness on a fatigue limit has already been investigated by many experiments on different materials. As an illustration (see Figure 16), he presents a graph obtained by experimental tests in which the surface roughness reduction factor γ depends on the ultimate tensile strength and the roughness parameter R_a . To unify the forms of the surface finish factor, c_{sf} is calculated as follows: $c_{sf} = \gamma$.

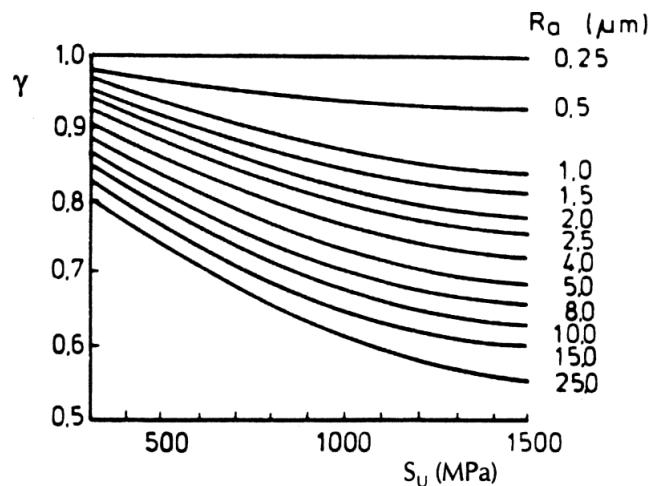


Figure 16: Surface roughness reduction factor ([68]).

Shigley

Shigley et al. [70] do not report the surface factor as a function of roughness and ultimate tensile strength (UTS), but more generally as a function of the finishing technology used and UTS. The resulting relationship was obtained by regression analysis

of the measured data:

$$k_a = a \cdot R_m^b \quad (23)$$

R_m is ultimate tensile strength and a and b are coefficients obtained from the regression analysis. $a = 4.51$, $b = -0.265$ for machined surface. To unify the forms of the surface finish factor, c_{sf} is calculated as follows: $c_{sf} = k_a$.

Stress concentration factor - Arola and Ramulu

The evaluation of the effect of surface defects on the strength of components is most often addressed by calculating the stress concentration factor (Kt). To address the case of a single notch on a plain surface, the stress concentration factor can be calculated as the result of combining the notch depth and the notch root radius:

$$K_t = 1 + 2\sqrt{\frac{t}{\rho}} \quad (24)$$

where t is the notch depth and ρ is the notch root radius. This approach can be applied to surface topography as a case of repeated notches. Since the depth of notches is rarely measured in the case of a real surface, Neuber proposed a semi-empirical relation that uses a commonly measured roughness parameter:

$$K_{t1} = 1 + n\sqrt{\lambda\frac{R_z}{\rho}} \quad (25)$$

where R_z is the 10-point surface height and n represents the stress state ($n = 1$ for shear and $n = 2$ for tension) and λ represents the ratio between the depth of the notch and the distance of the pitch between adjacent notches. However, its value is usually chosen as 1 because it is difficult to determine in practice [28].

Arola and Ramulu [27] further explored this approach and modified the previous equation and used more roughness parameters to redefine it. Finally, the authors point out that they validated this equation for the case of the effect of surface texture on the strength of the material under static and dynamic loads but did not use it to estimate the fatigue strength.

$$K_{t2} = 1 + 2\frac{R_a R_y}{R_z \rho} \quad (26)$$

where R_a is the arithmetic mean deviation, $R_y(=R_t)$ is peak to valley height and R_z and ρ have the same meaning as in the previous equations. The question of how to correctly determine ρ , which is very important in the calculation of the factor, arises. Quan et al. [64] proposed a new method to calculate the notch root radius:

$$\rho = \frac{t}{2} + \frac{l^2}{8t} \quad (27)$$

where t is the notch depth, and l is the notch width and are calculated as:

$$t = R_v \quad (28)$$

$$l = R_{sm} \cdot (1 - R_{mr}) \quad (29)$$

where R_v is the maximum depth of the valley of the profile, R_{sm} is the mean width of the elements of the profile, and R_{mr} is the average support ratio of a unit. However, this proposal does not seem ideal because R_{sm} can vary widely between measurements. On the other hand, Chen et al. [33] proposed not to consider ρ in Eq. 26.

Yang et al. [73] suggested that Eq. 26 can be modified by replacing the linear (two-dimensional) parameters with areal parameters because they better represent the actual surface and suggested this modification:

$$K_{t3} = 1 + 2 \frac{S_a S_p + S_v}{S_z \rho} \quad (30)$$

where S_a , S_p , S_v , and S_z are the arithmetical average height, the maximum peak height, the maximum valley depth, and the maximum height of the scale-limited surface [44].

EN 13445-2009

It is the European standard for pressure vessels. The standard specifies a surface quality factor as a function of tensile strength and surface roughness for non-welded components. f_s is a correlation factor that expresses the relationship between the reference (polished) specimen and the specimen under test. f_s is defined as:

$$f_s = F_s^{0.1 \cdot \ln N - 0.465} \quad (31)$$

$$F_s = 1 - 0.056(\ln R_z)^{0.64} \cdot \ln R_m + 0.289(\ln R_z)^{0.53} \quad (32)$$

where N is the fatigue life, R_m [MPa] is the ultimate tensile strength. For $N \geq 2 \cdot 10^6$ $f_s = F_s$ ([21] taken from [37]). To unify the forms of the surface finish factor, c_{sf} is calculated as follows: $c_{sf} = f_s$.

ASME BPVC

It is the American standard for boilers and pressure vessels that provides various fatigue curves for the design of pressure components. The effect of surface roughness is incorporated into the fatigue strength factor K_r , which is valid for the low and high-cycle

fatigue regions. K_r is defined as:

$$K_r = \frac{1}{-0.16998 \log R_a + 0.94546} \quad (33)$$

for $R_a < 0.5; 6.4$ μm ([22] taken from [37]). To unify the form of the surface finish factor, c_{sf} is calculated as follows: $c_{sf} = 1/K_r$.

KHKS0220

KHKS is a Japanese design code for ultra-high pressure gas equipment in which a surface finish factor is specified for high-cycle fatigue. Its use is limited to high-strength steel with ultimate tensile strength greater than 800 MPa. The factor expresses the ratio between the reference (polished) specimen and the specimen with a specific surface finish quality and is calculated as:

$$K_t = 0.912R_z^{0.0829} \quad (34)$$

for $R_z \geq 3.2$ μm ([20] taken from [37]). In order to unify the surface finish factor forms, c_{sf} is calculated as follows: $c_{sf} = 1/K_t$.

FKM

In the FKM-Guideline of Analytical Strength Assessment of Components in Mechanical Engineering, a roughness factor K_r is given that expresses the effect of surface roughness on fatigue strength.

$$K_r = 1 - a_r \log R_z \log \frac{2 \cdot R_m}{R_{m,N,min}} \quad (35)$$

where a_r is constant and $R_{m,N,min}$ is minimum tensile strength. For steel $a_r = 0.22$ and $R_{m,N,min} = 400$ MPa [19]. To unify the forms of the surface finish factor, c_{sf} is calculated as follows: $c_{sf} = K_r$.

\sqrt{area}_R Parameter

In his book, Murakami [58] approaches surface roughness as a series of surface notches that interfere with each other. From the fatigue tests performed, he determined that fatigue life is affected by the notch depth and the notch pitch, which is the effect of interference between the notches. He quantified its influence in terms of a single representative parameter, which he called \sqrt{area}_R , and further approached the effect of surface roughness as a crack problem rather than a notch problem. This parameter is the evolution of the \sqrt{area} method, which is given for a single circumferential notch, where \sqrt{area} is given as:

$$\sqrt{area} \cong \sqrt{10} \cdot a \quad (36)$$

where a [μm] is the notch depth. This equation is further modified to describe roughness as a series of notches:

$$\sqrt{area}_R/2b \cong 2.97(a/2b) - 3.51(a/2b)^2 - 9.74(a/2b)^3 \text{ for } a/2b < 0.195 \quad (37)$$

$$\sqrt{area}_R/2b \cong 0.38 \text{ for } a/2b > 0.195 \quad (38)$$

where a [μm] is the notch depth and $2b$ [μm] is the pitch size between the notches. The maximum height of the roughness R_y (R_t) was used as the variable a . However, Itoga et al. suggested the use of R_a , as it appeared to them, to be a more representative parameter [46]. After obtaining the equivalent defect size (\sqrt{area}_R), it is possible to calculate the fatigue limit σ_w at which the component has a theoretically unlimited lifetime [59].

$$\sigma_w = \frac{C(HV + 120)}{\sqrt{area}_R^{\frac{1}{6}}} \quad (39)$$

where HV is Vickers hardness and C is the constant for the defect, $C = 1.43$ for a surface defect.

3 Systematic Analysis of The States of The Art

3.1 Motivation

The main objective was to determine how the scientific community performs roughness measurements and how they report about it in their published papers. Since this whole work is focused on the effect of surface roughness on material fatigue, the selection was focused on publications focusing on fatigue. The International Journal of Fatigue was chosen for the selection of articles because it is the most important journal focused on material fatigue. Before working on the actual experimental part that focused on the effect of roughness on fatigue, it was beneficial to find out how the scientific community approaches this problem and, more specifically, how they measure surface roughness. While gaining theoretical knowledge regarding the measurements, it was noted that there has been a great development in 3D areal measurement in recent years and this gives the opportunity to gain much more qualitative information about the topographical characteristics of the surface. Therefore, it was decided to carry out extensive research of scientific articles. It aimed to do statistics on how the publications report about a method of measurement, the parameters used, and overall, how they report in detail on the measurement itself.

3.2 Methodology

The Engineering Village scientific publication search engine, which is available through the university, was chosen to search for scientific articles. Searches can be conducted using several keywords. The search was limited to articles published in the International Journal of Fatigue, which is ranked in the first quartile of its impact factor among journals in materials science, engineering, and mechanics of materials [10], and the search was further limited to articles published in the last 10 years, primarily because if the selected articles were older than, for example, 20 years, there would be a high probability that they used, now obsolete, instrumentations or methodologies. Only in recent years, there has been a strong development of optical roughness measurement methods). A series of searches were then carried out using keywords such as "fatigue", "surface roughness", and "measurement". Words related to additive manufacturing were excluded because of the concern that the vast majority of samples produced by additive manufacturing were measured by CT. These searches found only approximately 50-130 articles, which did not meet the original expectations of the number of articles. For this reason, it was decided to take the opposite approach to the search, where only the journal, the last 10 years, and any mention of "rough" was defined. The search defined by these parameters yielded 210 articles, which could be

considered sufficient. In Figure 17, one of the previous search criteria is shown on the left, and on the right the final search performed at the Engineering village site.



Figure 17: Search criteria at Engineeringvillage.com.

To make the evaluation of the articles comprehensive, it was necessary to define the questions concerning the roughness measurements, to which answers were sought. The following questions were selected:

- Percentage of works using 2D and 3D roughness characterization
- 2D - Standard specified
- 2D - Use of 2D parameters
- 2D - 2D parameters computed from 3D areal measurements
- 3D - Standard specified
- 3D - Use of 3D parameters
- 3D - Used measuring technology
- 3D - Quality of reporting (area, vertical/lateral resolution, post-processing, filtering, etc.).

To record the searched data from the articles, an Excel spreadsheet was created in which the information from each article about the roughness measurements was written.

- General information about the articles: reference, year of publication.
- 3D areal measurement: measurement technique, standard, the area measured, vertical and lateral resolution, magnification, and number of measurements.
- 2D profile measurements: if it was measured at all, a standard used, and a number of measurements.
- Areal parameters: Parameters used, post-processing.
- 2D parameters: measurement from which the 2D parameters were computed, parameters used, the evaluation length, and the number of measurements per sample.

3.3 Results

After going through all the articles, the collected data were evaluated to make statistics. The data was processed so that the required questions could be answered. In all cases, the results were displayed as the percentage of articles in which the parameter of interest was present to those, in which it was expected to be present; for example, the percentage of occurrence of the interferometry was not reflected in the total number of articles, but only in the number of articles in which the 3D areal measurements were used.

3.3.1 General overview

First, a general overview of the collected data is shown followed by more detailed statistics for each category: 3D areal measurements and its parameters, 2D profile measurements and its parameters, and finally, a comparison of definitionally equivalent parameters.

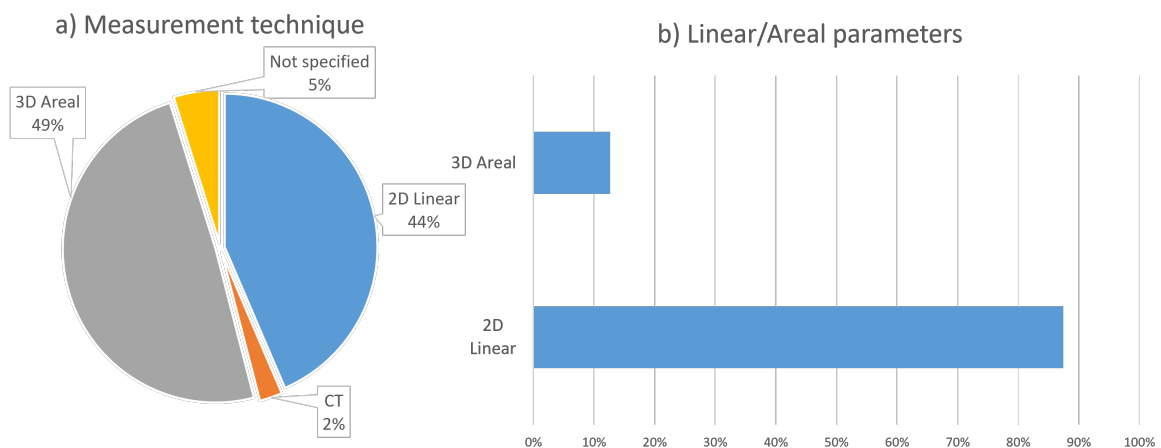


Figure 18: General overview.

In Figure 18a) is shown that 49 % of all measurements were made by 3D areal profilometry, which involved several different techniques. Followed by 44 % by 2D (stylus) profilometry. 5 % of the measurements were not specified if they were performed by 2D profilometry or by 3D areal profilometry. 2 % (3) measurements were performed by CT scan, this technique was used to obtain the surface roughness of additively printed samples. The results (roughness parameters, etc.) of the CT scans were excluded from further statistics because it uses a different method to obtain parameters.

Figure 18b) shows how many articles reported in the 2D or areal parameters. Only 13 % of the articles reported in the areal parameters, although almost half of the measurements were made using 3D areal profilometry. This indicates the extended practice of measuring in 3D and computing parameters in 2D. Only 6 % (7) articles were reported in both the areal and 2D parameters.

3.3.2 3D Areal profilometry

3D areal profilometry can be performed by different methods; three of them are based on optical technology and are described in detail in Section 2.3.1. These three techniques together represented 72 % of all 3D areal measurements, as shown in Figure 19.

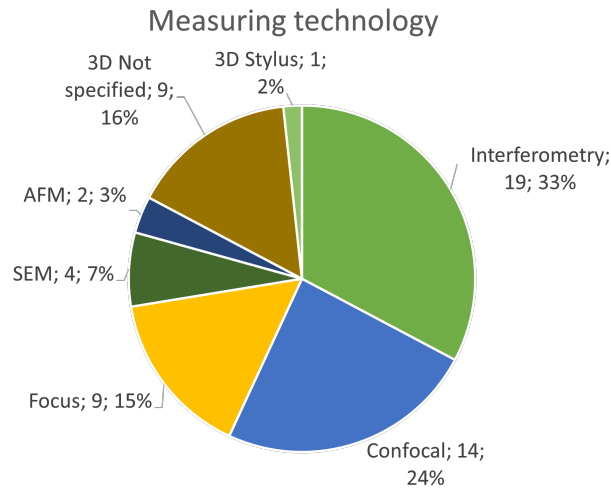


Figure 19: 3D Areal measuring technology.

Interferometry was used in 33 % of the measurements for surface acquisition and was the most widely used method, followed by confocal and focus variation. In 4 (7 %) cases, SEM (scanning electron microscope) was used, which is usually used for qualitative analysis of the surfaces. Finally, atomic force microscopy was used in 2 (3 %) cases, followed by the 3D stylus profilometer which was used only once (2 %).

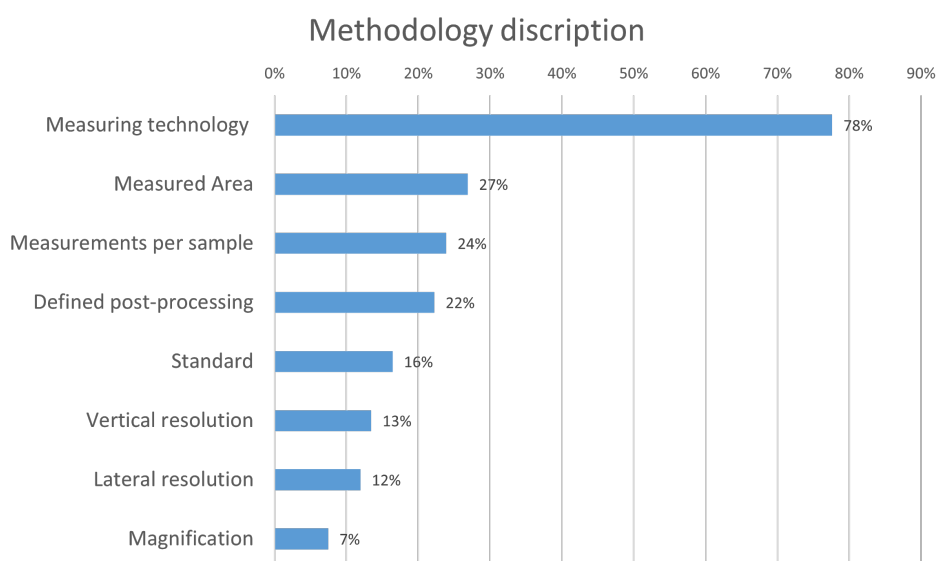


Figure 20: 3D Areal profilometry - Methodology description.

Figure 20 shows what percentage of articles used 3D areal measurement and re-

ported on the technology used and the other information related to obtaining surface topography. 78 % reported the technology used, while the remaining articles only mentioned that they used 3D areal profilometers or an optical microscope, but did not specify further the exact technology used. Only 27 % of the articles reported on the size of the measured area and 25 % on the number of measurements per sample. 22 % specified post-processing: software used, filters used. 16 % reported on the standard, 13 % on vertical resolution, followed by lateral resolution, and magnification of the objective.

As stated above, only 13 % of the articles worked with areal parameters, although almost half of them used 3D areal measurement technology. Figure 21 shows the percentage use of the areal parameters. The most widely used areal parameter was S_a , the arithmetical average height of the area, which was used in 87 % cases, the second most widely used parameter was S_q , followed by S_v and S_z , which were used in 1/3 of the work. Skewness and kurtosis were used in 27 % and 20 %, respectively. The remaining seven parameters were used only once.

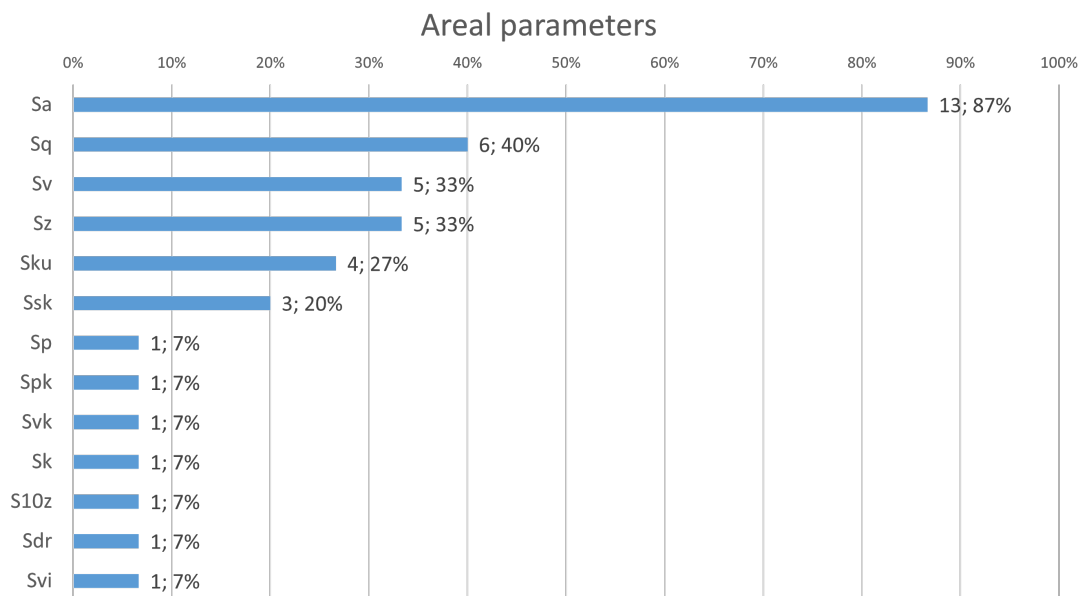


Figure 21: Areal parameters.

3.3.3 2D profilometry

For the 2D parameters, the calculation process was analyzed. Unlike areal parameters, 2D parameters can be calculated from profiles measured, using stylus measurement or from profiles extracted from areal measurements acquired by optical technologies. In the first case, the parameters were calculated by the instrument (contact profilometer) from the measured profile according to the selected standard, while in the second case, the evaluation profile can be selected at any location from the acquired area in the post-processing software. As shown in Figure 22 almost half of the 2D parameters

were obtained from the 2D profile measurement, 45 % were extracted from the 3D areal measurement during post-processing, and for the remaining cases, it was not specified how they were calculated.

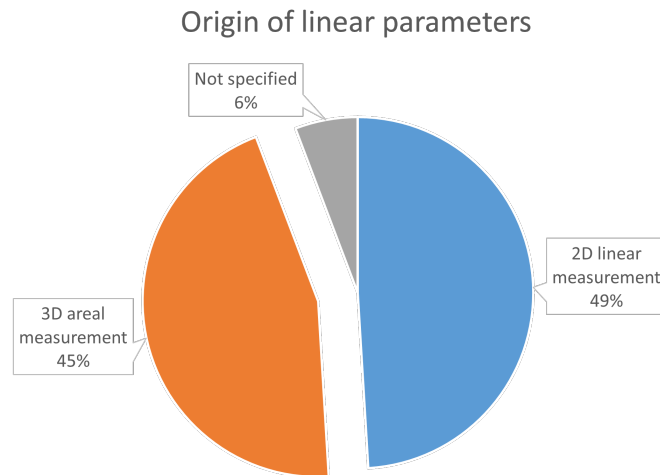


Figure 22: Measurement from which the 2D parameters were computed.

2D parameters calculated from the 3D areal measurements were checked for post-processing information. The condition of mentioning post-processing was met when the software used was mentioned in the text or when they wrote about using the form removal operator. The results are shown in Figure 22. This information is provided in only 21 % of the articles. 19 % defined the evaluation length of the profile from which the parameters were calculated. The fewest papers reported on the cut-off wavelength λ_c , which filters out higher wavelengths (waviness) from roughness.

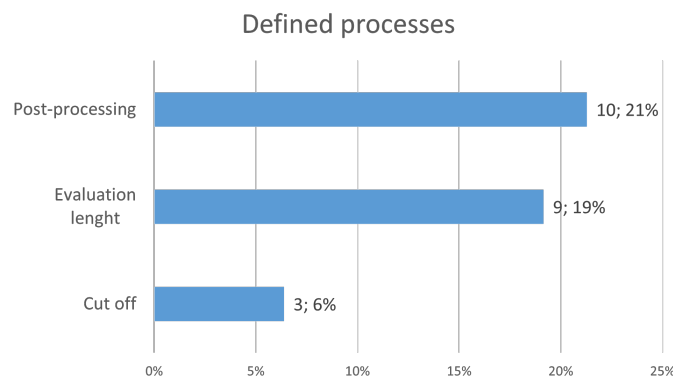


Figure 23: Extraction of 2D parameters from 3D areal measurements.

2D parameters were used most frequently to describe surface roughness, and their percentages are shown in Figure 24. The most commonly used parameter was the arithmetic mean deviation of the profile (R_a), which was calculated in 91 % of the articles. The second parameter that was used the most was R_z but its use was less than half that of R_a . Other parameters were used in less than one-fifth of the articles.

The mean spacing of adjacent peaks (Msap), which is not part of the ISO 4287 standard, was used three times. It is similar to R_{sm} but it does not evaluate the mean spacing on the mean line of the profile, but it evaluates the average horizontal distance of the profile peaks within the evaluation length [38].

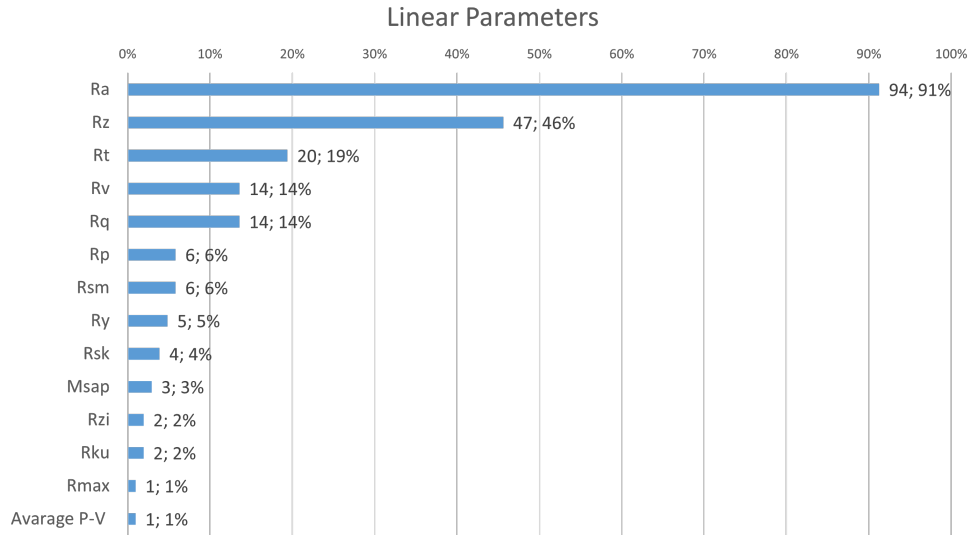


Figure 24: 2D parameters.

Finally, a comparison of the parameters equivalent by definition was made. R_a and S_a , the arithmetic mean deviation of the profile and the area, respectively, were the most commonly used. For the 2D parameters, R_z was then the parameter most frequently represented, and the other parameters were only sparse. On the contrary, the areal parameters had a higher representation of the other parameters. For example, the skewness and kurtosis parameters were represented at values around 25 %, but for the 2D ones, they were only low units of percent.

Table 1: Comparison of the abundance of equivalent parameters.

	2D	Areal	
R_a	91%	87%	R_a
R_z	46%	27%	S_z
R_t	19%	7%	S_t
R_v	14%	33%	S_v
R_q	14%	40%	S_q
R_p	6%	7%	S_p
R_{sk}	4%	20%	S_{sk}
R_{ku}	2%	27%	S_{ku}

3.4 Critical analysis

The most visible result of the State of the art was the complete domination in the use of 2D parameters over the areal even though almost half of the measurements were done by 3D areal profilometry. Therefore, almost half of the 2D parameters were calculated from the 3D areal measurements, which may affect the final value. First, when acquiring the 2D parameter through the 2D stylus measurement, the whole procedure is standardized, starting at the radius and angle of the tip followed by the cutoff value λ_c depending on the R_{sm} or R_a/R_z if the surface is periodic or non-periodic, continuing, for example, with the size of the sampling length. In contrast, when acquiring the surface topography, for example, by interferometry, objectives with different magnifications can be used, which goes hand in hand with different lateral and vertical resolutions that can affect the smoothness of the obtained surface. In the case of selecting a 2D profile from any location of the surface measurement, it is necessary to take into account the curvature of the surface in the y direction caused by the shape of the object to be measured, for example, a cylindrical surface, it is necessary to remove the form correctly, otherwise, the extracted profile off the intersection of the workpiece surface and a plane normal to the surface will be skewed with respect to the actual roughness.

The use of 2D parameters has several advantages in the industry, as stated in Section 2.3, but 2D characterization cannot fully characterize a three-dimensional surface. Therefore, areal roughness characterization should be preferred over linear, especially when the topography of the surface is scanned using the 3D areal method.

R_a was the most widely used parameter in this review and is also the most widely used surface roughness parameter in the industry. It is used, among other things, to prescribe the surface quality on functional surfaces of components. The parameter is not significantly affected by individual defects and gives stable values. As stated by [75] in their critical analysis of R_a as an indicator of fatigue, R_a is a useful parameter for quality control of a well-defined manufacturing process, but its definition is too general to describe surface topography and its attributes that have the greatest influence on fatigue strength, such as the tip radius of notches and their mutual distance. As evidence of the inadequacy of R_a as an indicator of fatigue strength, they simulated two sine wave surfaces with the same $R_a = 0.8\mu\text{m}$ value but different wavelengths, $10\mu\text{m}$ and $50\mu\text{m}$, respectively. Both waves had the same R_a values and also R_z , R_t , and R_v values, but different tip radius and notch spacing. Using FEM, they calculated the stress concentration factor K_t for both notches and their values were different from each other. Where its higher value is associated with a shorter fatigue life.

4 Sensitivity Analysis

4.1 Motivation

When using 3D areal technology for roughness characterization, no standard specifies how to take surface measurements. There is an ISO 25178 standard [44] that only defines the calculation of areal parameters and filtering and the instruments used, but no longer defines how to proceed with measurement. It is not defined how large the acquired area should be, the evaluation area, and what magnification of the objectives should be used. In contrast, for linear measurement, the ISO standard defines the measurement instrument used, the sampling length, and the evaluation length. This chapter aims to see how the resulting parameters vary as the acquisition variables change. Four different measurements were chosen to discover the effect of the measurement technology used, the effect of objectives magnification, the effect of the measurement area, and lastly, the effect of post-processing.

4.2 Methodology

In total, 4 series of experiments were prepared, each of which aimed to determine the sensitivity of the areal or 2D parameters to acquisition variables. All experiments were performed on the SensoFar NeoX profilometer, an optical profilometer that allows the use of three different non-contact methods: white light interferometry, confocal microscopy, and focus variation. A turned surface standards (Flexbarcomposite pocket set no. 16008) with roughness $R_a = 0.8 \mu\text{m}$ and $R_a = 1.6 \mu\text{m}$ were chosen for the measurements due to its high surface quality without any defects that could affect the results of the sensitivity analysis. These two roughness values were chosen because the results of the external roughness measurements of the samples, which are used in the rest of this thesis, are approximately in this roughness range.

A set of areal parameters defined in ISO 25178 [44], which may be a potential indicator of fatigue, were selected for this analysis. In total, 8 parameters were selected: S_a , S_q , S_{sk} , S_{ku} , S_z , S_{al} , S_{tr} and V_{vv} . These parameters were chosen from an article by Zabala et al. [75] in which they identified them as possible indicators of fatigue performance. For S_{sk} and S_{tr} the trend change was examined, for the former the change from negative to positive and vice versa and for the latter the change from isotropic to anisotropic and vice versa. They are only mentioned in the results if one of the above-described phenomena has occurred. To evaluate the remaining parameters, in each experiment, one measurement was set as the reference and the others were calculated as the percentage change from the reference.

Effect of optical measuring technology

The analysis of the effect of optical measuring technology was investigated using 3 different 3D areal measurement technologies at the same magnification and in the same measured area. The values of the experiment settings are shown in Table 2.

Table 2: Effect of optical measuring technology.

Technology	Magnification	Area [μm^2]
Interferometry		
Confocal	20x	877x660
Focus variation		

Effect of magnification

The analysis of the effect of magnification was investigated using 3 objectives with different magnifications under confocal microscopy and the same evaluation area. The values of the experiment settings are shown in Table 3. First, colocalization was carried out so that the acquired areas were equal and then they were cropped to the same size as that obtained with the 20x magnification objective so that the evaluation area was the same for all measurements.

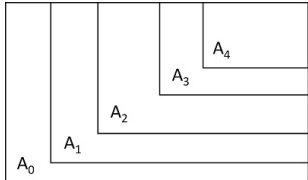
Table 3: Effect of magnification.

Technology	Magnification	Area [μm^2]
	5x	3508x2640
Confocal	10x	1754x1320
	20x	877x660

Effect of evaluation area

The analysis of the effect of the evaluation area was investigated using five different evaluation areas, the initial acquired area and the remaining four that were cropped from the initial area (A_0), where $A_1 = \frac{3}{4}A_0$, $A_2 = \frac{2}{4}A_0$, $A_3 = \frac{1}{4}A_0$, $A_4 = \frac{1}{8}A_0$. The values of the experiment settings are shown in Table 4.

Table 4: Effect of evaluation area.

Technology	Magnification	Area [μm^2]	Scheme
Interferometry	20x	2850x1650	
		2424x1455	
		1980x1188	
		1400x840	
		990x594	

Effect of post-processing on areal and linear roughness parameters

Different post-processing approaches were applied to the surface obtained by objective with 20x magnification by interferometry and their effect on roughness parameters was analyzed. For the areal parameters, the effect of form, noise, and waviness (λ_c) was studied, while for the 2D parameters, the effect of cut-off λ_c after form removal and the effect of the length of the evaluation length were studied. For the former, the evolution area from the previous experiment was used, and for the latter, a 7x1 FOV (field of view) area was imaged to make it at least 4 mm long.

4.3 Results

For S_{sk} and S_{tr} the trend change was examined, for the former, the change from negative to positive and vice versa and for the latter the change from isotropic to anisotropic and vice versa. They are only mentioned in the results if one of the above-described phenomena has occurred. To evaluate the remaining parameters, in each experiment, one measurement was set as the reference, and the others were calculated as the percentage change from the reference. The measured values are attached in Appendix A.

Effect of optical measuring technology

The effect of optical measuring technology was analyzed by acquiring the same area with different technologies: interferometry, confocal, and focus variation. As shown in Figure 25 for $R_a = 0.8 \mu\text{m}$, the quality of the surface obtained by interferometry and confocal was almost similar, except for a small defect in the lower left corner, which was detected as a valley spike by interferometry, compared to a peak spike by confocal. The quality of the surface obtained by the focus variation was much worse than that of the first two. The surface consisted of many spikes that invalidated the detection of micro-irregularities. This type of defect could be caused by the glossy surface of the samples, which caused reflections that subsequently caused problems for the software when composing individual images from different scanning planes into a 3D surface model.

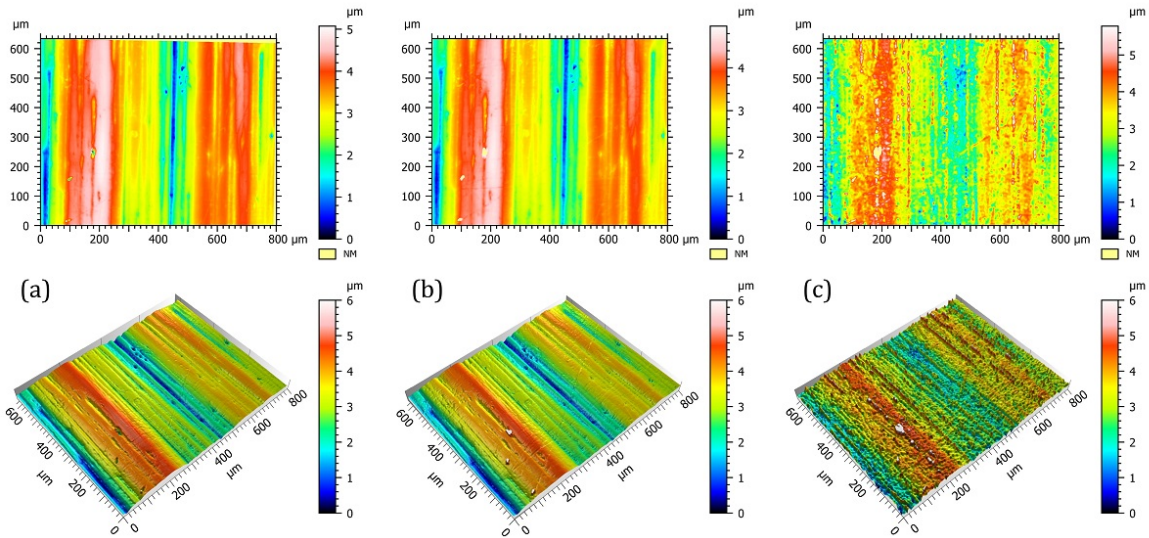


Figure 25: $R_a = 0.8 \mu\text{m}$: 2D and axonometric pseudo-color views of the surface obtained by different technologies. (a) Interferometry (b) Confocal (c) Focus variation.

A similar surface quality obtained by different technologies can be observed in Figure 26 for $R_a = 1.6 \mu\text{m}$, where the surface obtained by the focus variation had a much worse quality again than the other two.

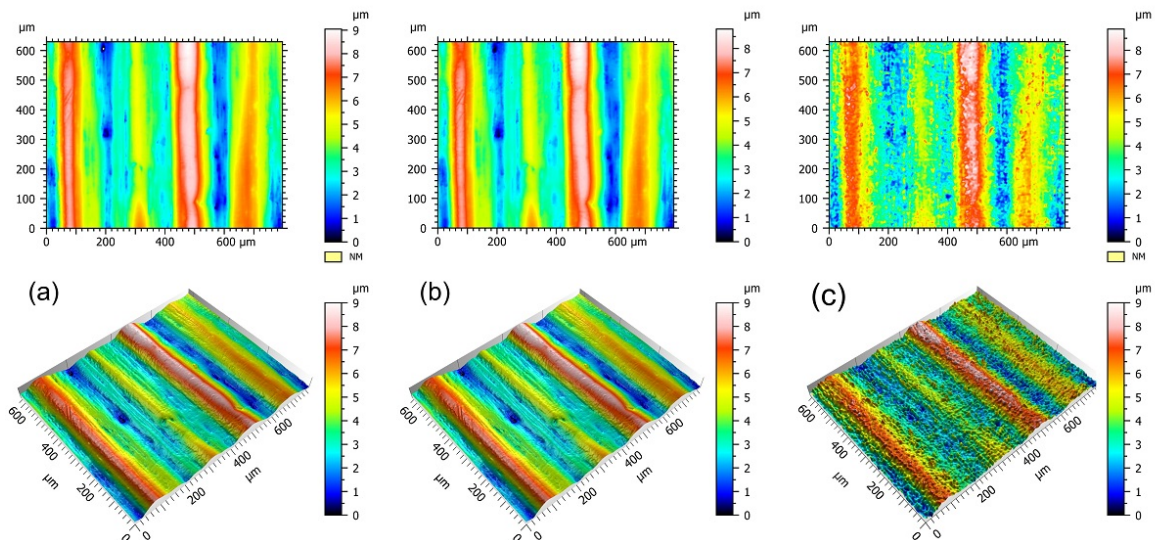


Figure 26: $R_a = 1.6 \mu\text{m}$: 2D and axonometric pseudo-color view of the surface obtained by different technologies. (a) Interferometry (b) Confocal (c) Focus variation.

A more detailed comparison is shown in Figure 27, where 2D profiles of surfaces are shown at the same location. (a) Shows the profiles of $R_a = 0.8 \mu\text{m}$ and (b) shows the profiles of $R_a = 1.6 \mu\text{m}$. The profile obtained by confocal was smoother compared to that obtained by interferometry, which may be due to the different principles of the two technologies. The focus variation was able to capture large irregularities (waviness) as it followed the curves of the other two, but it contained many spikes, which greatly affected the result and failed to adequately display the roughness.

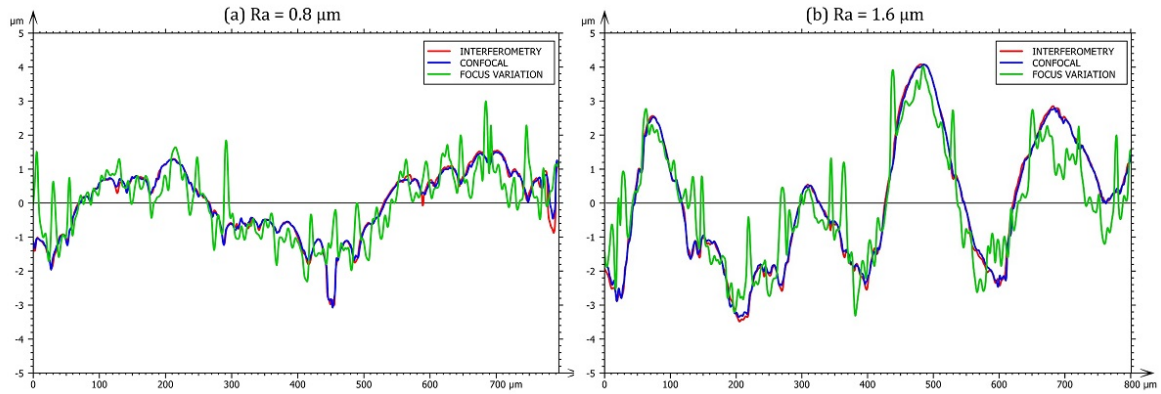


Figure 27: 2D surface profiles obtained by different technologies. (a) $R_a = 0.8 \mu\text{m}$, (a) $R_a = 1.6 \mu\text{m}$.

The Figure 28 shows the areal parameters as a percentage change to the measurement made by interferometry. The graphs further confirm that confocal and interferometry captured the surface almost with a similar quality, as the differences in parameters were not more than 6 %. Such a small difference may be due to measurement inaccuracy and could be declared insignificant. In contrast, the results of the focus variation differed more, most often around 10 %, but there were also much larger deviations; for example, the value of V_{vv} for the first sample differed by -29 % and the value of S_{sk} was positive in contrast to the other values, indicated the predominance of sharp peaks (the negative value indicates the predominance of sharp valleys). On the other hand, the values of S_a and S_q were lower for the focus variation than for interferometry, indicating a better surface quality, which was completely opposite to the trend shown in the previous figure with the profiles.

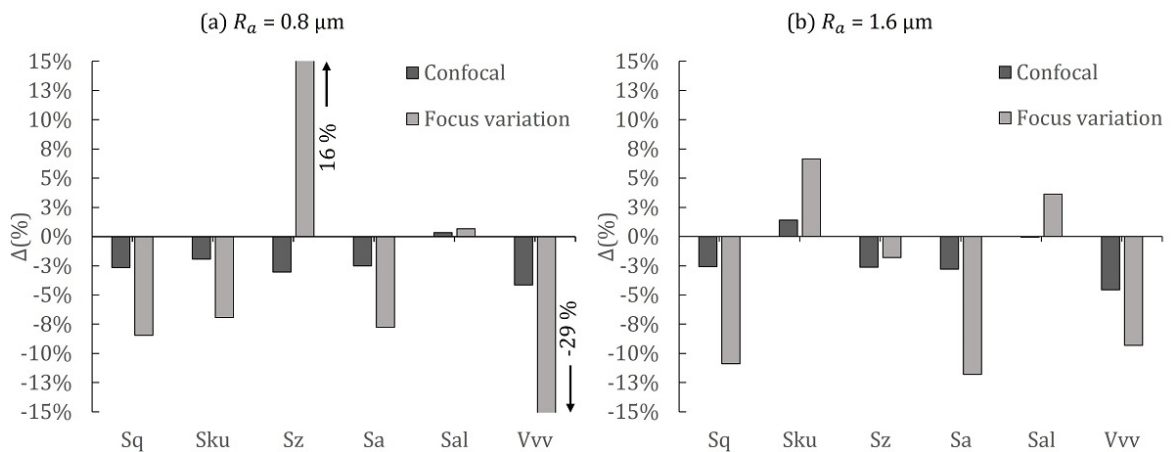


Figure 28: Comparison of areal parameters obtained by different technology for two measured samples with different surface roughness. Values show the percentage difference to interferometry.

Effect of magnification

The effect of objective magnification was analyzed by acquiring the area using objectives with magnifications of 5x, 10x, and 20x. The evaluation areas were cropped to the size of the area obtained by the objective with 20x magnification. As shown in Figure 29 and Figure 30 for $R_a = 0.8 \mu\text{m}$ and $R_a = 1.6 \mu\text{m}$, respectively, a decrease in surface roughness (surface smoothing) was observed, which was caused by increasing longitudinal resolution and decreasing measurement noise.

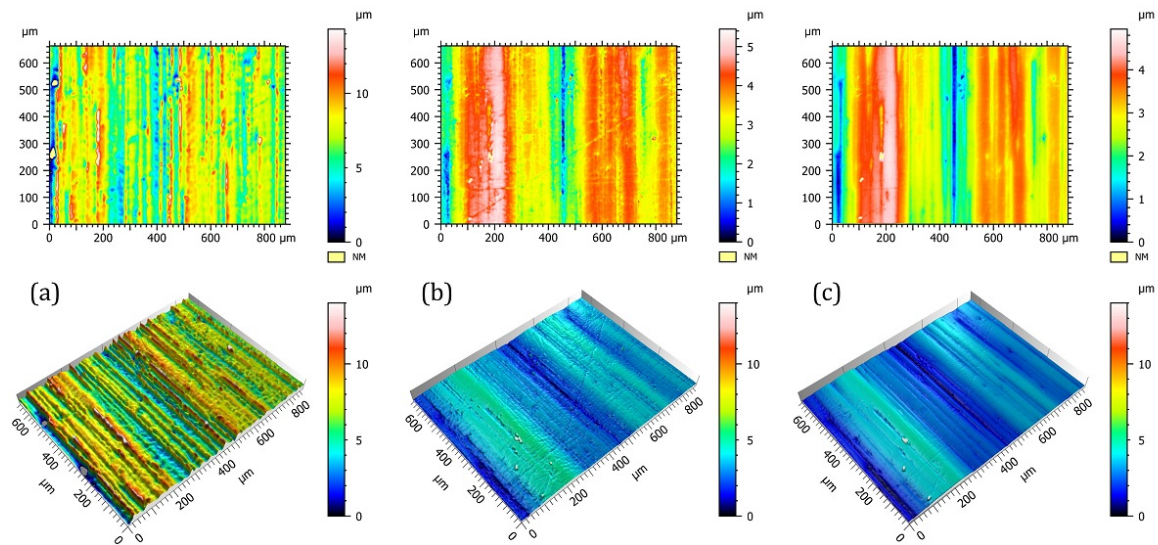


Figure 29: $R_a = 0.8 \mu\text{m}$: 2D and axonometric pseudo-color view of the surface obtained by objectives with different magnification. (a) 5x (b) 10x (c) 20x.

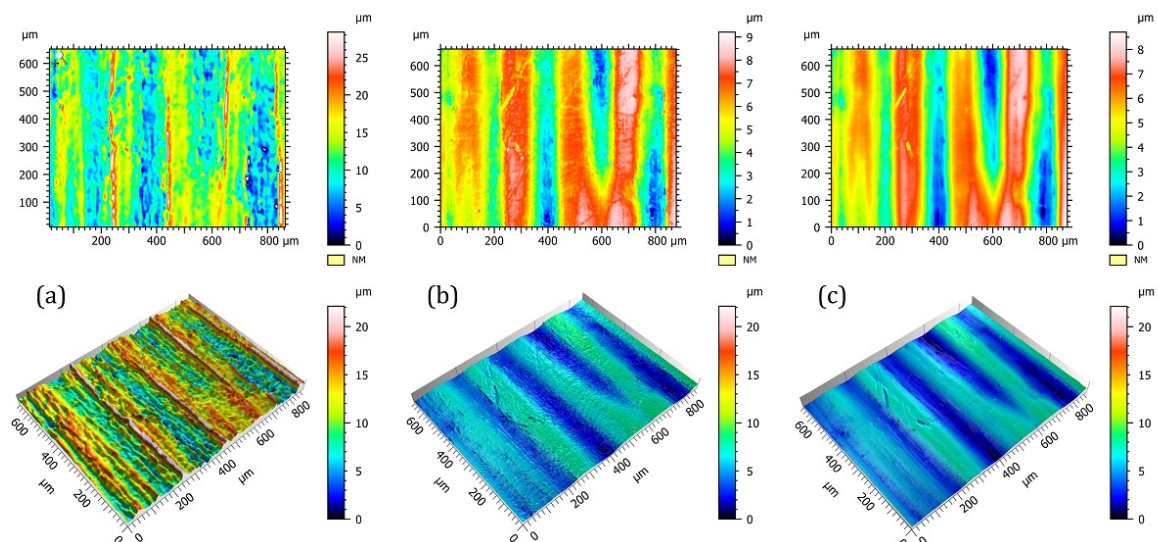


Figure 30: $R_a = 1.6 \mu\text{m}$: 2D and axonometric pseudo-color views of the surface obtained by objectives with different magnification. (a) 5x (b) 10x (c) 20x.

A more detailed comparison is shown in Figure 27, where 2D surface profiles are shown at the same location. (a) Shows the profiles for the surface with $R_a = 0.8 \mu\text{m}$

and (b) shows the profiles for the surface with $R_a = 1.6 \mu\text{m}$. The curves only further confirmed what was seen in the previous figures, that the curve obtained with the highest magnification is the smoothest. The curve showing the profile obtained at 10x magnification showed larger fluctuations from the imaginary mean curve, indicating a less accurate measurement. The curve obtained at the lowest magnification slightly followed the waviness profile but contained many significant spikes that had an absolute effect on the evaluated parameters. For the profile of the rougher surface, it was observed that the highest spikes occurred when the other two curves had the highest waviness.

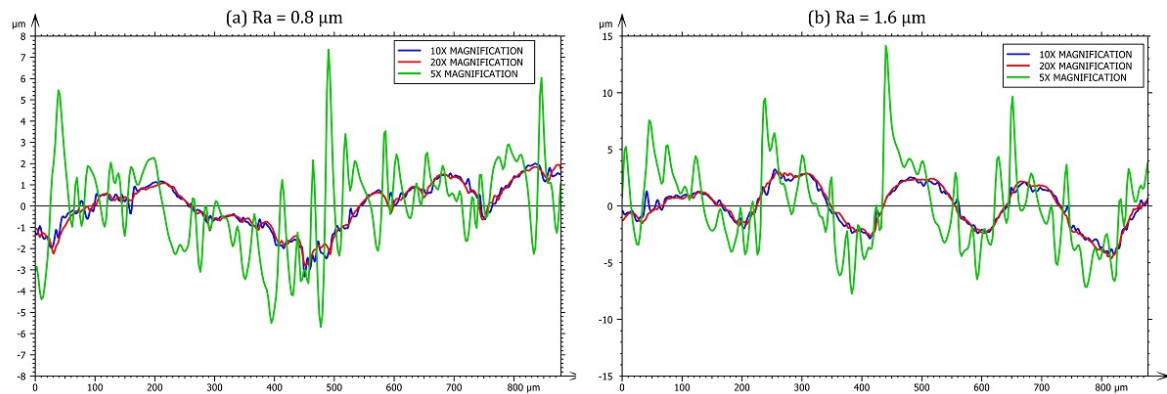


Figure 31: 2D surface profiles obtained by objectives with different magnification. (a) $R_a = 0.8 \mu\text{m}$, (a) $R_a = 1.6 \mu\text{m}$.

The Figure 28 shows the areal parameters as a percentage change to the measurement made by the objective with a magnification of 20x. At 10x magnification, the direct dependence between the parameters S_q , S_a , and the magnification could not be determined because for the first surface, the values increased but for the second surface the values decreased. Furthermore, there was no direct dependence for S_{al} , where the opposite trend occurred. For 5x magnification, the differences ranged from tens to hundreds of percent. Except for S_{al} , which decreased, all other parameters increased and differed so significantly that the measurements by 5x could be considered non-meaningful in practical use, for example, the values of S_a were $1.49 \mu\text{m}$ and $3.08 \mu\text{m}$, respectively, while for the reference measurement, values were $0.66 \mu\text{m}$ and $1.49 \mu\text{m}$, respectively.

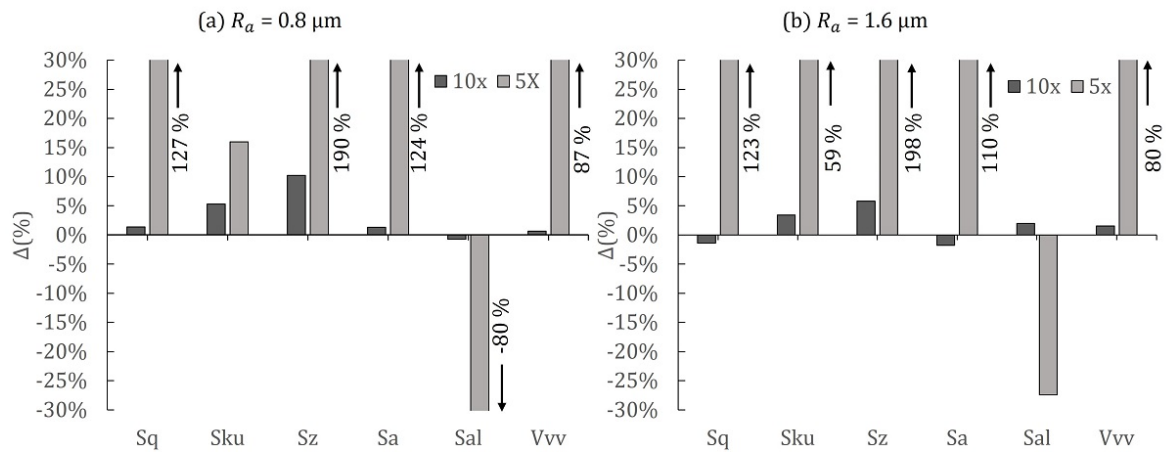


Figure 32: Comparison of areal parameters obtained by objectives with different magnification. for two measured samples with different surface roughness. Values show the percentage difference to 20x magnification.

Effect of evaluation area

The effect of the size of the evaluation area was studied on the area of 2850 x 1650 μm^2 , which was gradually cropped down while maintaining the aspect ratio.

Pseudo-color 2D and axonometric views of the uncropped evaluation area are shown in Figure 33. The surface on the left, $R_a = 0.8 \mu\text{m}$, contained a significant wave on its left side, which could increase the values of some of the reference parameters.

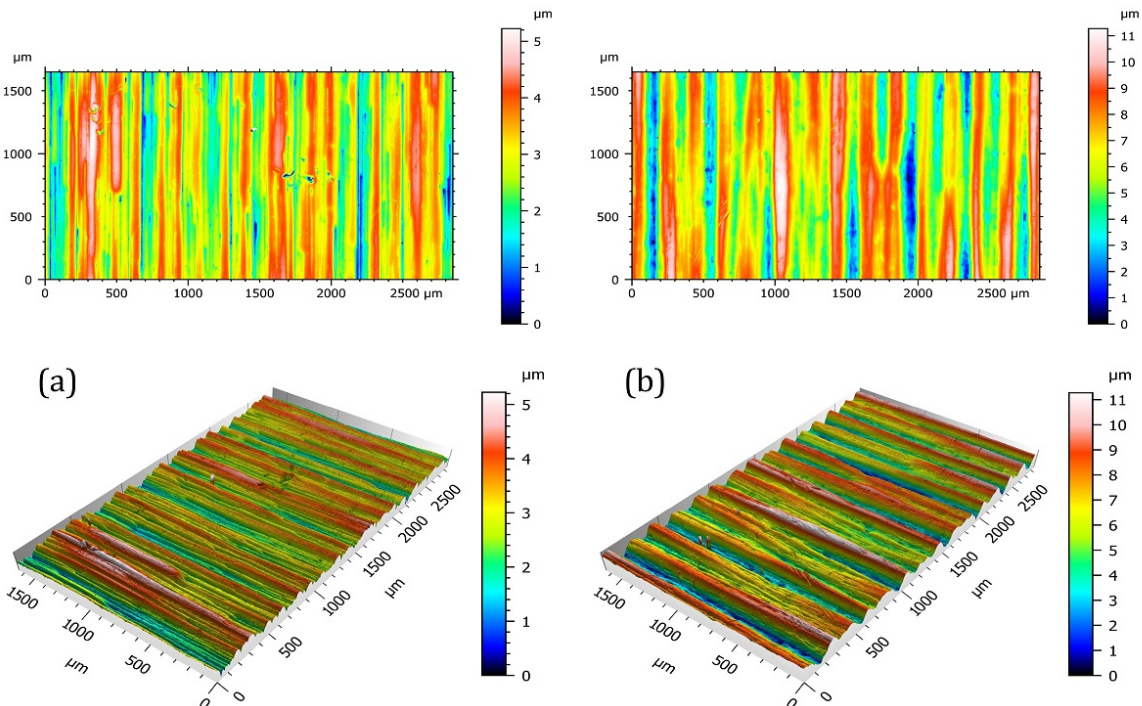


Figure 33: 2D and axonometric pseudo-color view of the uncropped evaluation area (a) $R_a = 0.8 \mu\text{m}$ (b) $R_a = 1.6 \mu\text{m}$.

Furthermore, the surface contained several defects on its right part, caused by mechanical damage, which may have affected the value of S_{tr} or V_{vv} . The surface on the right, $R_a = 0.8 \mu\text{m}$, contained a higher peak in the middle part, which could also affect the average value of certain parameters such as S_a or S_q

The results are shown in Figure 34, where the values are shown as a percentage difference from the uncropped area. All parameters, except S_{ku} and S_{al} decreased as the evaluation area decreased. For the first surface, v_{vv} showed a decreasing trend, which was also expected for the other parameters, because as the area decreased, the amount of topographic data decreased and thus the precision of the output decreased. Regarding the sensitivity of the parameters, the S_{sk} , S_{tr} , S_{al} and V_{vv} were the most affected.

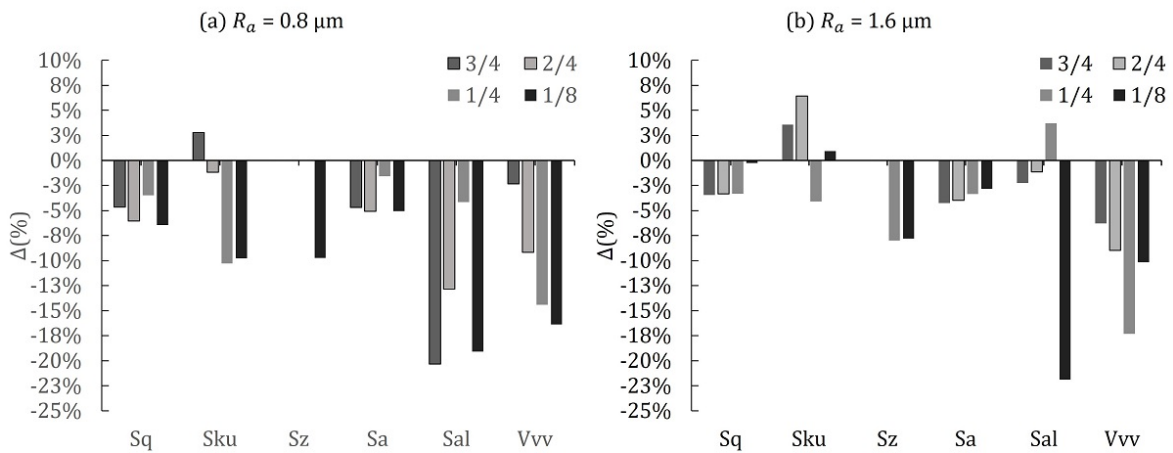


Figure 34: Comparison of areal parameters obtained by cropping the size of evaluation area for two measured samples with different surface roughness. Values show the percentage difference to the uncropped area.

Calculation of 2D parameters from 3D areal measurement

The effect of extracting 2D parameters from 3D areal measurements was tested on an area 4.8 mm long to comply with the ISO 4287 standard, as the resulting values were compared with those obtained using the contact stylus profilometer in which the ISO4287 standard was followed. Three measurements were taken on each surface, and their average value was used as a reference value in this experiment. Three different approaches were chosen to calculate the parameters: (a) form removal operation, evaluation length $ln = 4 \text{ mm}$ and $\lambda_c = 0.8 \text{ mm}$ (following the standard indications); (b) form removal operation, evaluation length $ln = 4 \text{ mm}$ and λ_c was not used; (c) form removal operation, evaluation length $ln = 2 \text{ mm}$ and $\lambda_c = 0.8 \text{ mm}$. The positions of the evaluation profiles are shown in Figure 35.

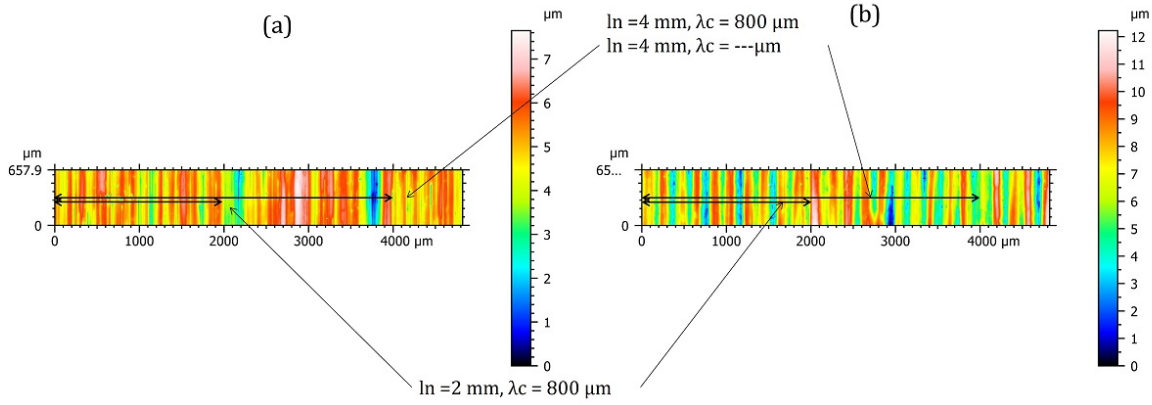


Figure 35: 2D pseudo-color view of the surface acquired by interferometer and marked positions of evaluation profiles in measured areas. (a) $R_a = 0.8 \mu\text{m}$, (a) $R_a = 1.6 \mu\text{m}$.

As shown in Figure 36, the results for the two surfaces are different. For the smoother surface, the parameters obtained by procedure (a) were most similar to those obtained by contact measurement, but for the other surface, the most similar parameters were obtained by procedure (b). Certain parameters for the first surface had opposite values to those for the second surface.

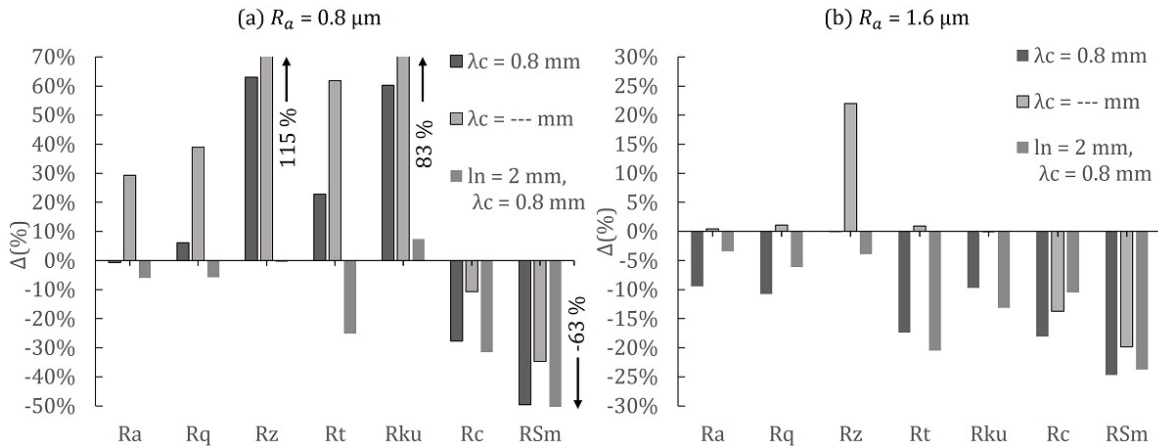


Figure 36: Comparison of 2D parameters obtained by areal measurement as a percentage difference to the values obtained from contact measurement.

Effect of post-processing

The last experiment aimed to analyze the effect of post-processing in the calculation of area parameters, that is, how the form removal operator, noise filter, and cut-off λ_c affected the result. As the reference measurement was chosen the one that contained the primary profile, that means that only the form removal operator and noise filter were applied.

In this case, a different display of the results had to be chosen, where the results are shown in two graphs, the first shows the comparison of the reference results with those where λ_c was used, and the second shows the result of the process where the form

removal operator was not used. Previous comparison graphs by the measured surface would not be appropriate here, as the final values differed by hundreds of percent.

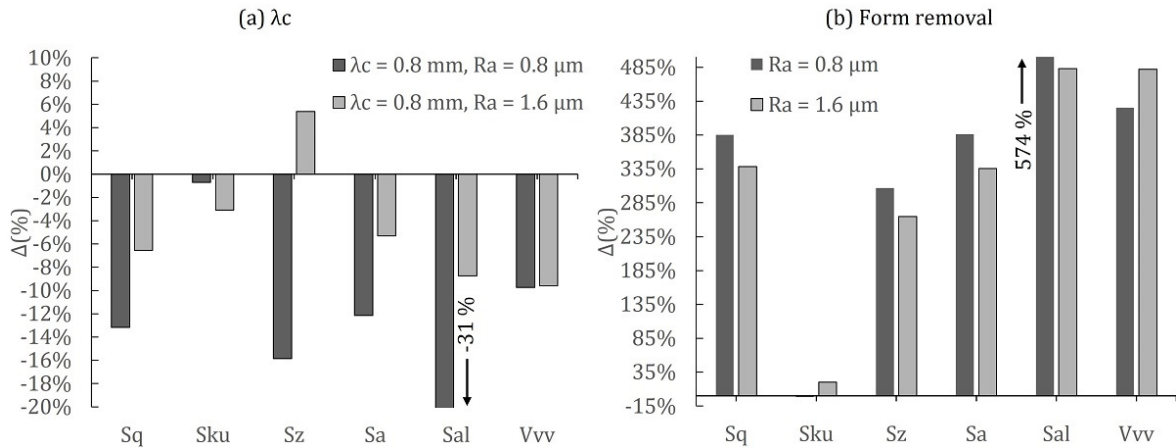


Figure 37: Comparison of areal parameters obtained by different post-processing approaches.

As shown in Figure 37 (a), the use of the cut-off λ_c had a more pronounced effect, where the change ranged from units percent to low tens of percent. Most parameters decreased, which may have been caused by double filtering, first by the form removal operator and then by applying the cut-off λ_c itself. As shown in Figure 37 (b), the evaluation of the surface roughness with the form resulted in a significant influence on the resulting values, where they differed up to several times, where, for example, S_a was 3-4 times larger compared to the case where the form is correctly removed. The result of noise filtering is not shown in graphs because it changed the resulting values only by hundredths to tenths of a percent and its effect can be said to be negligible.

4.4 Conclusion

The aim of this chapter was to investigate how sensitive the roughness parameters are to different methods of 3D areal measurement.

The first experiment focused on how different 3D areal technologies affect the areal roughness parameters. The three technologies most frequently encountered in the previous chapter were selected and a sensitivity analysis was performed on them. The results showed that the surface quality and the areal parameters obtained with interferometry and confocal measurements were hardly different, and both are suitable for usage in the measurement of metal surfaces. However, spikes in the surface obtained using the focus variation were observed, most likely caused by the difficulty of the scanning technology for glossy surfaces. When measuring the smoother surface, the value of the parameter S_{sk} was positive, but all other measurements were negative. The only advantage of this technology can be considered to be the speed of scanning.

The second experiment focused on how objectives with different magnifications affect the areal roughness parameters. The three objectives available on the profilometer, 5x, 10x, and 20x, were selected. The results showed that the surface quality obtained with 20x and 10x magnification did not differ significantly, the differences in parameters did not exceed 10 % and the values of 10x magnification increased compared to 20x magnification, which may indicate higher noise and lower measurement quality. The results obtained using the 5x magnification can be considered unusable, as the results of the measurement did not reflect the topography of the actual surface. The topographic model contained many spikes that occupied a large part of the surface. Therefore it could not be filtered out and it affected all parameters by tens to hundreds of percent.

The third experiment focused on the effect of the size of the evaluation area, where the original evaluation area was cropped several times. The results showed that the size of the evaluation area did not have a significant effect on the average parameters S_a and S_q , but the other parameters were more affected. The largest changes were observed for the parameters S_{al} and V_{vv} .

The experiment aimed at determining the influence of post-processing on 2D parameters showed inconclusive results. For the smoother surface, the lowest differences of R_a and R_q were measured for the evaluation length of 4 mm and $\lambda_C = 0.8$ mm, followed by the measurement with the evaluation length equal to 2 mm. However, for a rougher surface, the most similar results to contact measurement were observed for the case without λ_C and an evaluation length of 4 mm.

The last experiment aimed to determine the effect of different post-processing approaches. The results showed that the application of noise removal had almost no effect. The application of λ_c already had a visible effect and it separated the rough surface from the primary surface. The experiment also showed the absolute necessity of proper form removal, which elsewhere affected the resulting values several times and made them unusable.

5 Fatigue strength correction due to roughness

5.1 Methodology

This chapter aims to investigate the precision of different methods for estimating the reduced fatigue life based on the specific roughness of the surface. The methods are listed in Subsection 2.5. The analysis was performed on data sets obtained from the literature review. Only data sets in which the final surface quality was achieved by machining (turning, milling, or grinding), or polishing were analyzed. In the existing literature, the results of the fatigue tests were searched in the form of S-N diagrams, from which it was possible to read the results of individual samples and then enter their values into the in-house FinLiv.Q repository of experimental fatigue results. This chapter builds on the work of Ing. Kirill Loshkarev in the previous project SGS17/175/OHK2/3T/12, which had to be modified, starting from the correct data used to the modification of the calculations.

For the case where the experimental data are plotted in the S-N diagram, the S-N curves for each series were then calculated using the power law-type regression model. Based on the experimental data, a range of lifetimes was chosen in which the regression curve sufficiently interpolated the data, so if the experimental data ended in $2 \cdot 10^5$ cycles, for example, it would be very inaccurate to calculate with the value of the fatigue strength in $2 \cdot 10^6$ cycles. In each data set, a reference curve with the lowest possible roughness was selected, to which the surface finish factor was then applied, and thus a theoretical fatigue strength was calculated taking into account surface roughness. A dual approach to calculating this value was chosen by using a simplified and logarithmic model. As an evaluation criterion for the methods used, the relative error of the theoretical fatigue strength was calculated with respect to the actual fatigue strength.

Simplified model

Only the value of the surface finish factor and the reference and actual fatigue strength values on a certain number of cycles are used to calculate the theoretical value of the fatigue strength after considering the effect of surface roughness. The calculation is as follows:

$$\sigma_{FSt} = \sigma_{FSr} \cdot c_{sf} \quad (40)$$

Where σ_{FSt} is the theoretical fatigue strength, σ_{FSr} is the fatigue strength of the reference series, and c_{sf} is the surface finish factor. The relative error of this estimate was then calculated:

$$x_r = \frac{\sigma_{FSac} - \sigma_{FSt}}{\sigma_{FSac}} \quad (41)$$

Where x_r is the relative error and σ_{FSac} is the actual fatigue strength.

If $\sigma_{FSac} < \sigma_{FSt}$, the estimated fatigue strength is lower than the actual fatigue strength and is a safe (conservative) estimate. In the opposite case, it is an unsafe (non-conservative) estimate. Finally, the average of relative errors and its standard deviation from all strength levels was calculated. The same correction, the value of the surface finish factor, is applied to the fatigue strength at any fatigue life (within the valid range of the regression) and therefore the whole curve is shifted against the direction of the vertical axis.

Logarithmic model

The logarithmic model is more complex, but at the same time takes into account the slope of the slant branch of the reference S-N curve. The calculation uses the endpoints of this curve; one endpoint is the fatigue strength at the highest number of cycles where the regression model is still valid, and the other endpoint is the UTS and the corresponding number of cycles. This model, unlike the simplified one where the whole curve is shifted, works on the change in slope of the slant branch of the S-N curve, where the strength limit is still at the same lifetime for any roughness, but the fatigue limit is reduced. Using these two points, it is possible to calculate any point on the curve, i.e. the stress level at the required number of cycles.

$$\sigma_{FS} = 10^{\log \sigma_F + \log \frac{R_m}{\sigma_F} \cdot \frac{\log \frac{N_F}{N_x}}{\log \frac{N_F}{N_{Rm}}}} \quad (42)$$

Where σ_{FS} is the stress level for the selected number of cycles, N_x is the selected number of cycles, R_m is the ultimate tensile strength, N_{Rm} the number of cycles for R_m , σ_F is the stress level for the maximum number of cycles and N_F is the maximum number of cycles.

This curve description is then used to determine the size of the surface finish factor for the different fatigue life, it is scaled to match the desired number of cycles. First, its value is calculated according to the chosen method, and this value is defined for σ_F . Then its value is calculated for the desired number of cycles:

$$c_{sfx} = 10^{\log c_{sf} \cdot \frac{\log \frac{N_x}{N_{Rm}}}{\log \frac{N_F}{N_{Rm}}}} \quad (43)$$

Where c_{sfx} is the surface finish factor in a given number of cycles, c_{sf} is the surface finish factor in the maximum number of cycles N_F .

The equation shows that the value of the surface finish factor for R_m is 1. The procedure for calculating the relative error is identical to the simplified method.

5.1.1 Description of used data sets

This subsection provides descriptions of data sets selected from the available literature. Their description includes the type of fatigue loading, the number of series and the corresponding number of S-N curves, the material, and the surface finish technique for all series.

APG [25]

In this paper, the results of fully reversed plane bending are presented in a graph. The data set is made up of four S-N curves with different roughness values. The material used for these tests was Al7050 aluminum alloy. The reference S-N curve was obtained from polished samples where the value of R_a was $0.02\ \mu\text{m}$. The final surface quality of the remaining series was achieved by milling, where the roughness values were: $R_a = 1.02\ \mu\text{m}$, $R_a = 9.27\ \mu\text{m}$ and $R_a = 7.1\ \mu\text{m}$. It should be noted here that the series with the highest roughness had a better fatigue life than the series with a lower roughness of $R_a = 7.1\ \mu\text{m}$. This example clearly shows the limitations of 2D parameters. The authors also reported the values of the parameter S_a , where its values were $4.2\ \mu\text{m}$ and $5.5\ \mu\text{m}$, respectively, and these values are consistent with the result of the fatigue tests.

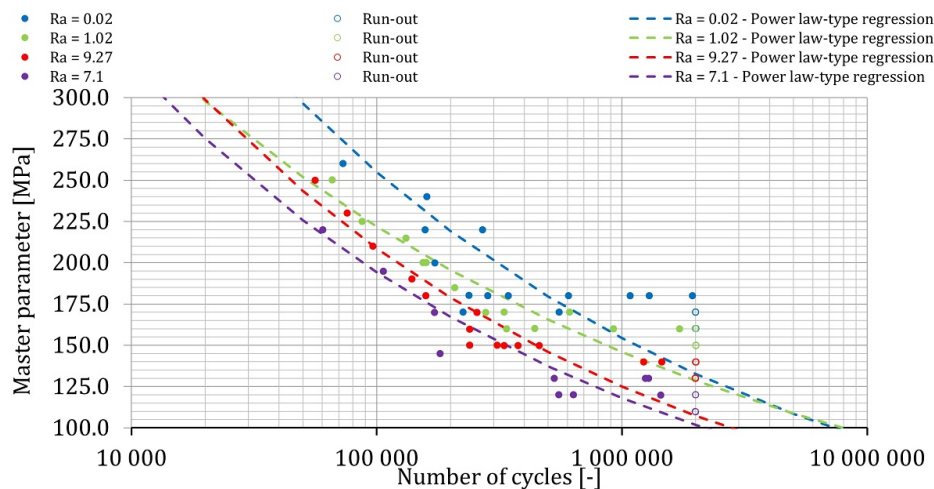


Figure 38: APG data set.

ITN [46]

In this paper, the results of the rotating bending fatigue testing are presented in a graph. The data set is made up of four S-N curves with different roughness values. The material used for these tests was Ni-Cr-Mo steel (JIS SNCM439). The reference S-N curve was obtained from buff polished samples where the value of R_a was $0.092\ \mu\text{m}$. The final surface quality of the remaining series was achieved by polishing with emery paper, where the roughness values were: $R_a = 1.386\ \mu\text{m}$, $R_a = 2.142\ \mu\text{m}$

and $R_a = 3.154 \mu\text{m}$. In the fatigue testing results, the position of crack initiation was distinguished into surface and subsurface, and only the specimens in which the crack started on the surface of the specimen were selected for the calculation of the S-N curves because only these cases should respond to the surface roughness effect.

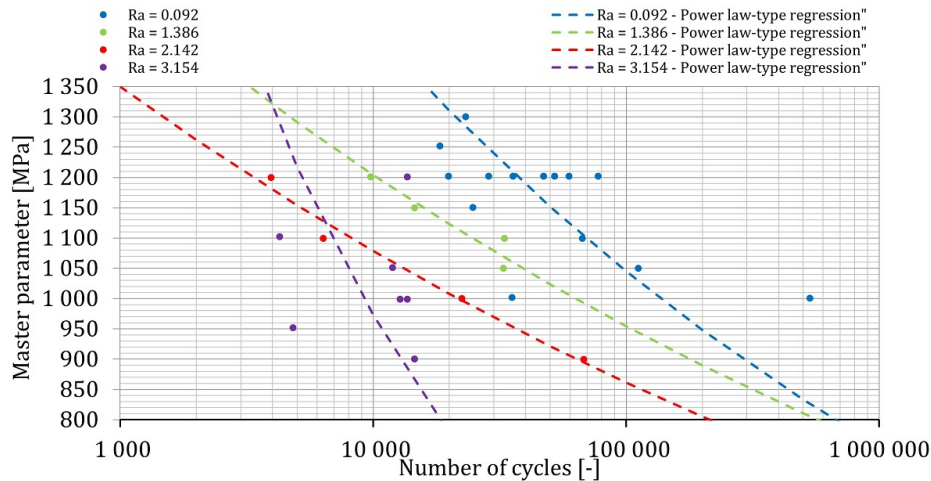


Figure 39: ITN data set.

LAL [54]

In this paper, the results of the fatigue tests for tensile loading are presented as graphs. The data set is made up of three S-N curves with different roughness values. However, the S-N curve of the shot-peened specimens was omitted from the evaluation because this surface treatment achieves high compressive residual stresses and significantly improves fatigue life despite higher roughness values. The material used for these tests was 34CrNiMo6 steel. The reference S-N curve was obtained from polished samples where the value of R_a was $0.03 \mu\text{m}$. The remaining series had a roughness value of $R_a = 0.81 \mu\text{m}$, where the final surface quality was achieved by turning.

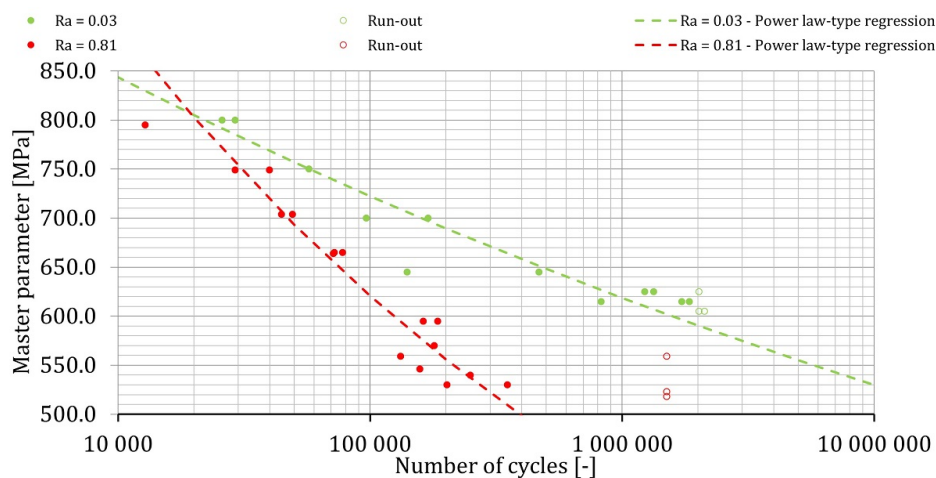


Figure 40: LAL data set.

LDD [55]

The results of the rotational bending load testing are presented in a graph in this paper. The data set is made up of three S-N curves with different roughness values. The material used for these tests was medium carbon steel. The reference S-N curve was obtained from machined samples where the value of R_a was $0.4\ \mu\text{m}$. The remaining series had the roughness level $R_a = 0.8\ \mu\text{m}$, and $R_a = 1.6\ \mu\text{m}$, respectively, where the final surface quality for both sets was achieved by machining.

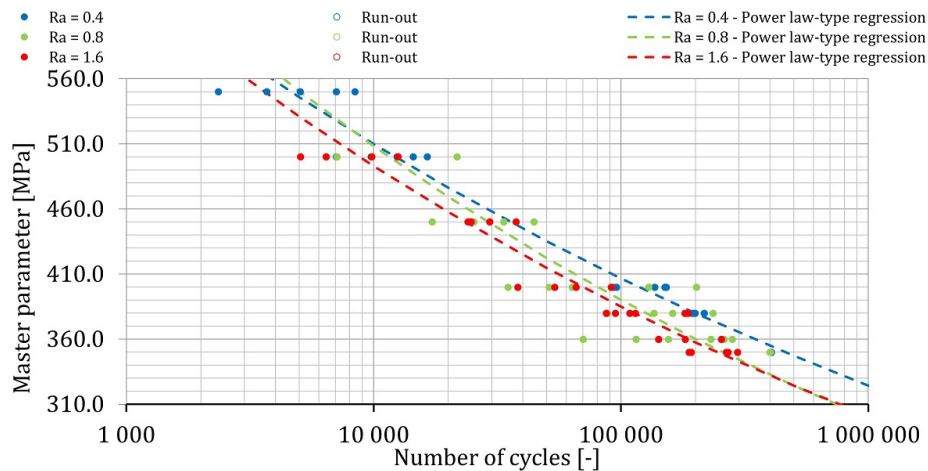


Figure 41: LDD data set.

LHB [53]

In this paper, three different data sets on two types of steel are presented. All of them were subjected to rotating bending fatigue tests. The reference samples were polished in a longitudinal direction and had the roughness value of $R_a = 0.07\ \mu\text{m}$. For the other series, the different surface qualities were achieved by further polishing with emery paper. The first data set was tested on 100CrMnMniSi8 steel with bainitic structure and is made up of three different groups of rough samples and is denoted as LHA and all roughness values are shown in Figure 42. The second data set was tested on 100CrMnMniSi8 steel with martensitic structure and contains only one group of samples that were further polished and had $R_a = 0.085\ \mu\text{m}$ and is denoted as LHB data set. The last data set was tested on 50CrMo4 steel and also contains only one rough set of rough samples with $R_a = 2.1\ \mu\text{m}$ and is denoted as LHC.

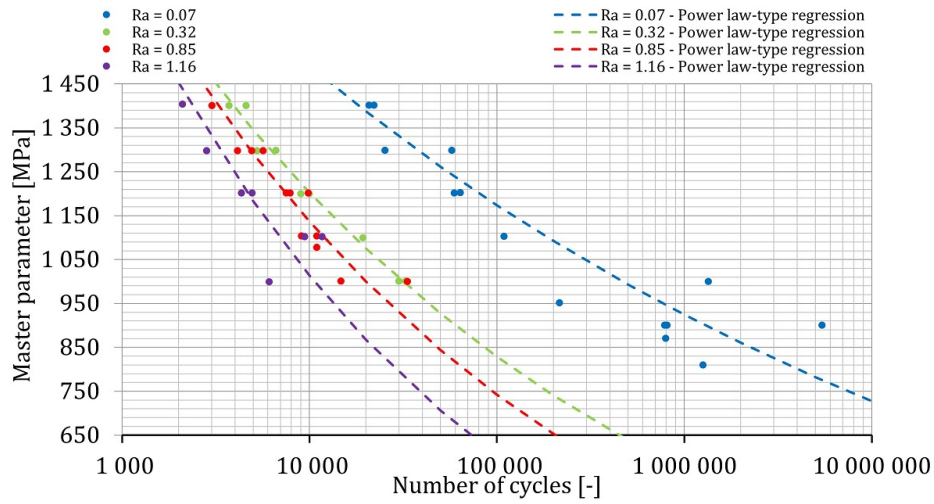


Figure 42: LHA data set.

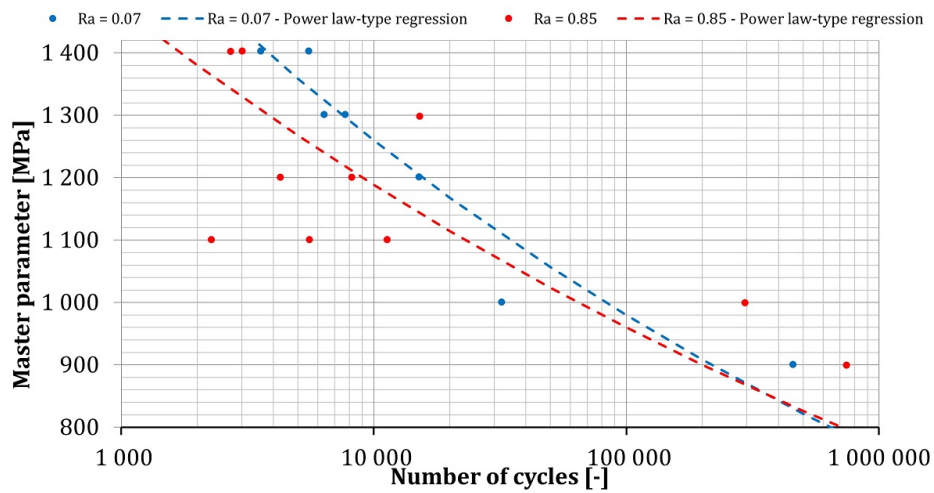


Figure 43: LHB data set.

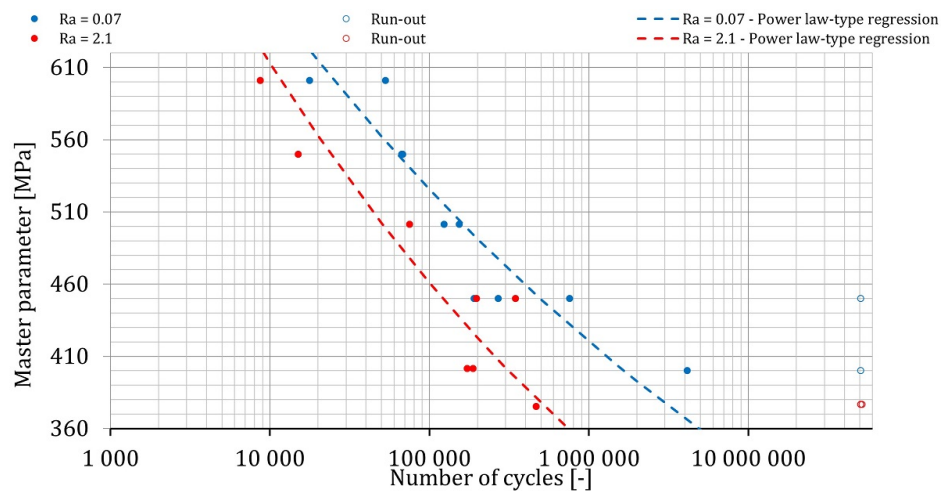


Figure 44: LHC data set.

SCC [69]

The results of the rotating bending type load fatigue test are presented in the graph in this article. The data set is made up of two S-N curves with different roughness values. The material used for these tests was Al7010 aluminum alloy. The reference S-N curve was obtained from samples where the final surface quality was achieved by machining and the roughness value was $R_a = 0.6 \mu\text{m}$. The other series had the roughness value of $R_a = 3.2 \mu\text{m}$ and these are also machined samples.

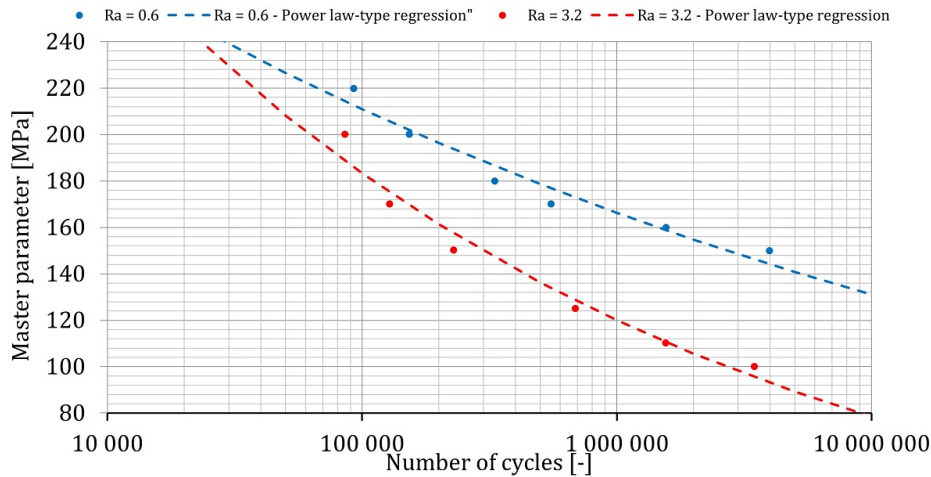


Figure 45: SCC data set.

SSC [71]

In this paper, the results of fatigue from the tensile loading are presented in a graph. The data set is made up of three S-N curves with different roughness values. The material used for these tests was AISI 4130 steel. The reference S-N curve was obtained from polished samples where the value of R_a was $0.1 \mu\text{m}$. The remaining series had a roughness level $R_a = 0.5 \mu\text{m}$, $R_a = 1.5 \mu\text{m}$, respectively. The final surface quality was achieved by milling, but for the latter, the surface was subsequently roughened by brushing with coarse grit sandpaper.

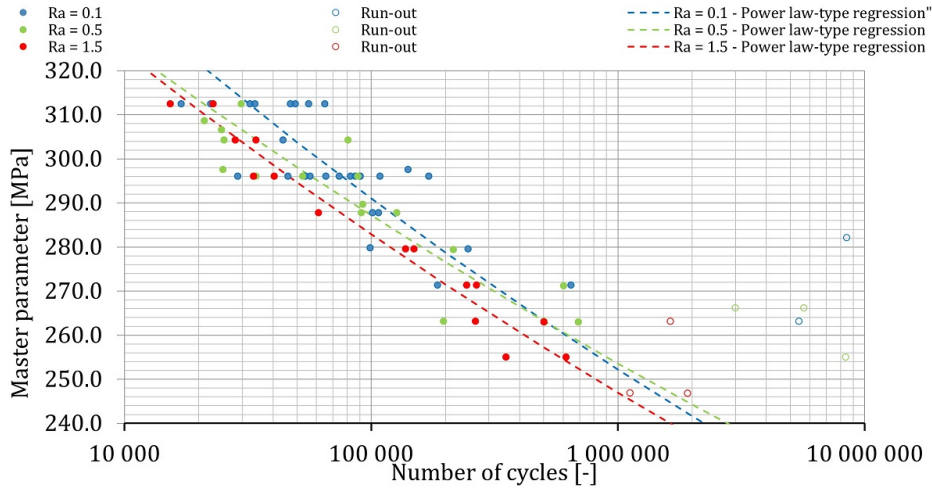


Figure 46: SSC data set.

ZWW [78]

In this paper, the results of the tensile loading fatigue testing are presented in a graph. The data set is made up of three S-N curves with different roughness values. The material used for these tests was FV520B-I steel (similar to 17-4PH steel). The reference S-N curve was obtained from polished samples where the value of R_a was $0.05 \mu\text{m}$. The final surface quality of the remaining series was also achieved by polishing, and their roughness values were: $R_a = 0.2 \mu\text{m}$, $R_a = 0.6 \mu\text{m}$. In the fatigue testing results, the position of crack initiation was distinguished into surface and subsurface, and only those specimens in which the crack started on the surface of the specimen were selected for the calculation of the S-N curves.

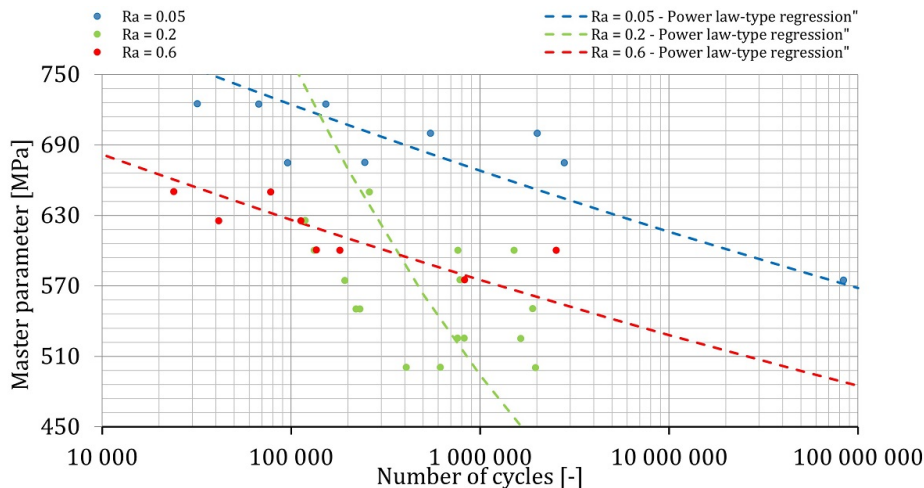


Figure 47: ZWW data set.

5.2 Results

For the calculation of the surface finish factor and the corresponding fatigue strength, the simplified and logarithmic models described in the methodology were used. The use

of c_{sf} shifted the fatigue strength, corresponding to the highest fatigue life, against the direction of the vertical axis of the S-N diagram, and the rest of the S-N curve changed depending on the model used. The evaluation of the results is divided into several units. The results of the simplified model are presented first, followed by the results of the logarithmic model, and finally their comparison with each other. A summary of the data sets and basic parameters is shown in Table 5.

Table 5: Overview of selected data sets. "T" = tensile loading, "RB" = rotating bending loading.

Set	Load	Material	Mat. type	R_m [MPa]	σ_F [MPa]	N_F
APG	B	AA7050	Al Alloy	635	179.5	$5 \cdot 10^5$
ITN	RB	JIS SNCM439	Steel	1863	1045	$1 \cdot 10^5$
LAL	T	34CrNiMo6	Steel	1209	618.5	$1 \cdot 10^6$
LDD	RB	Medium carbon	Steel	710	380	$2 \cdot 10^5$
LHA	RB	100CrMnMniSi8	Steel	2200	860	$2 \cdot 10^6$
LHB	RB	100CrMnMniSi8	Steel	2200	908	$2 \cdot 10^5$
LHC	RB	50CrMo4	Steel	1000	404	$1.5 \cdot 10^6$
SCC	RB	Al7010	Al alloy	525	155	$2 \cdot 10^6$
SSC	T	AISI4130	Steel	530	263	$5 \cdot 10^5$
ZWW	T	FV520B-I	Steel	1170	568	$1 \cdot 10^8$

5.2.1 Simplified model

The results of the simplified model are shown in Table 6, where the bottom part shows the average relative errors of the individual fatigue life estimation methods and the right part shows the average errors for each data set. The most accurate method was the Shigley method, in which the size of the surface finish factor is calculated based on the surface finish technique. It is followed by the Schijve method with a -2 % average relative error. On the other hand, the ASME BPVC method had the largest relative error as it estimated a fatigue strength at least 10 % higher than the actual one for half of the data sets.

The most accurate estimates were for the LDD data set where all series, including the reference one, were turned. It was followed by the APG data set, which also had the smallest standard deviation, even though the series with the highest roughness had a higher fatigue limit than the one with lower roughness. On the other hand, the estimates were the least accurate for the SCC data set, by almost a quarter on average. All methods estimated a fatigue strength higher than the actual value. For such large errors, further measurements should be made to validate the results. For SCC, all specimens were turned as well as for the LDD data set. It was followed by the LHB data set, which had the two highest relative errors of the entire simplified method. In terms of the effect of ultimate tensile strength on the estimation results, it can be

seen from the table that the largest standard deviations were for the datasets with the largest UTS value i.e. for materials with high UTS the estimates of the different methods differ more than for lower strengths.

Table 6: Average errors of each method and of each series for the simplified model.

Data set	Average error						\bar{x}_r	StDev
	Uni.	Juv.	RCJ.	Sch.	Shi.	ASM.		
APG	-0.06	0.02	-0.04	0.01	-0.03	-0.02	-0.02	0.03
ITN	-0.11	0.27	0.20	0.01	-0.07	-0.14	0.03	0.16
LAL	-0.10	-0.08	-0.02	-0.06	0.17	-0.16	-0.04	0.10
LDD	-0.01	-0.04	0.00	0.04	0.06	0.03	0.01	0.03
LHA	-0.21	0.24	0.10	-0.16	-0.07	-0.27	-0.06	0.18
LHB	0.05	0.39	0.34	0.11	0.15	0.00	0.17	0.14
LHC	0.06	0.01	0.07	0.15	0.02	0.00	0.05	0.05
SCC	-0.20	-0.31	-0.24	-0.20	-0.31	-0.14	-0.23	0.06
SSC	0.03	0.05	0.01	0.05	0.09	0.03	0.04	0.03
ZWW	-0.16	-0.02	-0.12	-0.14	-0.02	-0.19	-0.11	0.06
\bar{x}_r	-0.07	0.05	0.03	-0.02	0.00	-0.09	-	-
Max x_r	-0.21	0.39	0.34	-0.20	-0.31	-0.27	-	-
Min x_r	-0.01	0.01	0.00	0.01	0.02	0.00	-	-
StDev	0.10	0.20	0.16	0.12	0.14	0.11	-	-

* Uni. = UNI 7670, Juv. = Juvinall, RCJ. = RcJohnson, Sch. = Schijve, Shi. = Shigley, ASM. = ASME BPVC, StD = standard deviation, \bar{x}_r = Average error [-].

5.2.2 Logarithmic model

The results of the logarithmic model are shown in Table 7, where the bottom part shows the average errors of the individual fatigue life estimation methods and the right part shows the average errors for each data set. Overall, it can be seen that most of the relative errors are in the negative values, which means that the estimated fatigue limits were higher than the experimentally measured values, thus the model is more non-conservative. The Juvinall method was the most accurate, with an average error of 2 %, but had the highest standard deviation. It was followed by the Johnson method, in which the value of the surface finish factor is determined from the graph. In contrast, the least accurate method and the one with the highest error for a single data set was the ASME BPVC method, where the average relative error was -11 %. In this method, the surface finish factor is calculated according to the equation. The UNI 7670 method was the second least accurate method, where the average relative error was -10%.

In terms of individual data sets, the lowest average error was for the LDD and LHC data sets, where the error was only 1 %, but for the former it was. As with the simplified model, the lowest accuracy estimate was for the SCC data set, where the estimated fatigue limit was again almost a quarter higher.

Table 7: Average errors of each method and each series for the logarithmic model.

Data set	Average error						\bar{x}_r	StD.
	Uni.	Juv.	RCJ.	Sch.	Shi.	ASM.		
APG	-0.08	-0.01	-0.07	-0.02	-0.06	-0.05	-0.05	0.02
ITN	-0.19	0.03	-0.02	-0.13	-0.17	-0.21	-0.12	0.1
LAL	-0.12	-0.10	-0.06	-0.09	-0.07	-0.16	-0.10	0.04
LDD	-0.02	-0.04	-0.01	0.02	-0.04	0.01	-0.01	0.02
LHA	-0.26	-0.05	-0.12	-0.25	-0.20	-0.32	-0.20	0.1
LHB	0.03	0.31	0.26	0.07	0.11	-0.01	0.13	0.13
LHC	0.00	-0.04	0.01	0.06	-0.03	-0.04	-0.01	0.04
SCC	-0.21	-0.31	-0.25	-0.21	-0.31	-0.16	-0.24	0.06
SSC	0.03	0.04	0.01	0.04	0.09	0.02	0.04	0.03
ZWW	-0.16	-0.06	-0.13	-0.15	-0.06	-0.19	-0.13	0.05
\bar{x}_r	-0.10	-0.02	-0.04	-0.07	-0.07	-0.11	-	-
Max x_r	-0.26	-0.31	0.26	-0.25	-0.31	-0.32	-	-
Min x_r	0.00	-0.01	0.01	0.02	-0.03	0.01	-	-
StD.	0.11	0.15	0.13	0.11	0.13	0.12	-	-

* Uni. = UNI 7670, Juv. = Juvinall, RCJ. = RcJohnson, Sch. = Schijve, Shi. = Shigley, ASM. = ASME BPVC, StD = standard deviation, \bar{x}_r = Average error [-].

5.2.3 Comparison of models

Finally, the two models were compared to see how accurate they were to each other and to analyze their advantages and disadvantages.

The results of how the two models performed for each method are shown in Figure 48. For most methods, the average error achieved by the simplified model was lower. For the Shigley method, the average error for the simplified model was 0% and, in contrast, for the logarithmic model, -7%. The estimates of the logarithmic model were more non-conservative and tended more towards negative values. In terms of standard deviations, the logarithmic model is more accurate for all methods except Shigley, with differences ranging from 1 to 5 %.

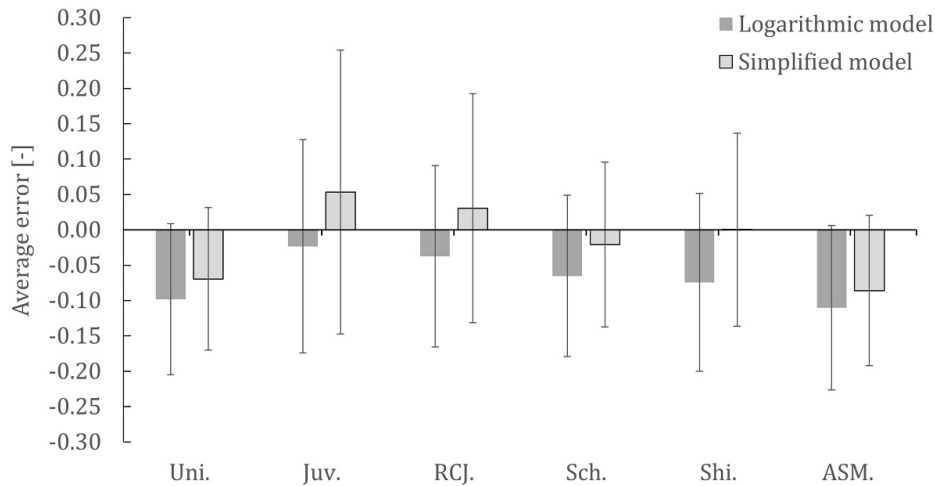


Figure 48: Model comparison in terms of accuracy of methods.

The results of how the two models performed for each data set are shown in Figure 49. No visible relationship can be observed between where the simplified model is more accurate and where the logarithmic model is more accurate. As an example, the LHA and LHB data sets used the same material and the same surface treatment for each series. Therefore, from this perspective, they are very similar. However, in terms of the accuracy of the two models, the results are very different, where for LHA the simplified model was more accurate and for LHB the opposite. However, as already mentioned when comparing the two models in terms of their respective methods, the standard deviations of the logarithmic model are smaller, thus giving more comprehensive estimates.

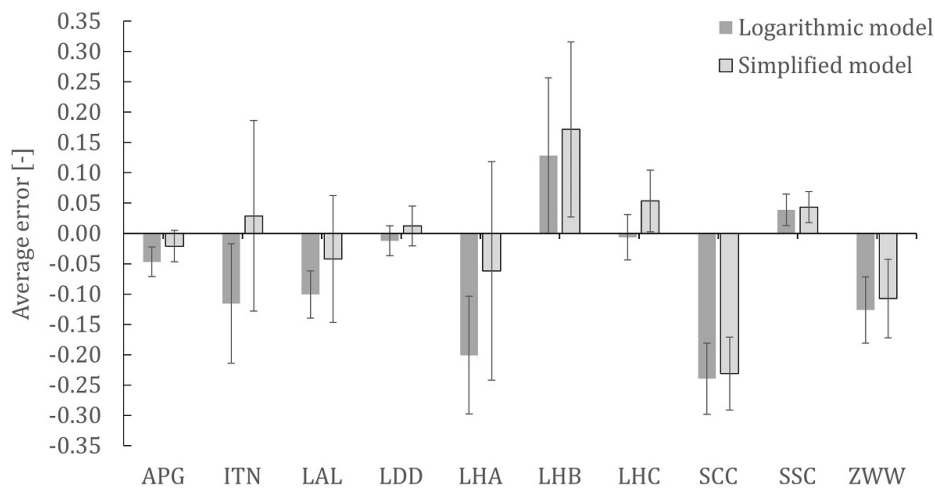


Figure 49: Comparison of the model in terms of accuracy of estimation of methods for data set.

5.3 Conclusion

The aim of this section was to investigate the precision of different methods of estimating the reduced fatigue life based on specific surface roughness. The analysis was performed on external data sets from the literature. From the results for the simplified model, the Shigley method was found to be the most accurate, where the calculation depends on the surface finish technique used. It was followed by ASME BPVC and Juvinal methods. However, it should be noted that the Juvinal method had the largest standard deviation of 20 %. The least accurate method was the UNI 7670 method. When evaluating individual data sets, the SCC was the worst, with an average relative error of -23 %. For such a large error, further measurements would be needed to validate the results or to try to evaluate other fatigue limit reducing factors such as residual stresses. Very high tensile residual stresses may have been introduced during the turning of the specimens.

The results for the logarithmic model showed that the average relative errors of all methods were negative, which means all methods estimated a higher fatigue strength than the actual one. The Juvinal method was found to be the most accurate, where the calculation depends on the specific value of surface roughness, but it had the biggest standard deviation. For this model, the ASME BPVC method was the least accurate.

The comparison between the models showed that the logarithmic model was more non-conservative and also gave more consistent results for most methods, i.e. smaller standard deviation. This is because the entire S-N curve is not shifted in the logarithmic model but is only tilted. The same results are seen when comparing the estimates of the individual data sets, where all the results of the logarithmic model were less conservative. Furthermore, again, they had a lower standard deviation and thus gave more comprehensive results.

These results indicate that the simplified model is preferable for two reasons. The first reason is that it gives more conservative estimates, that is, on the safety side, which is very important in practice. Secondly, it is computationally simpler and therefore faster.

6 Experimental Testing

6.1 Material and Methods

6.1.1 Material and sample geometry

Material properties

Samples of all series were manufactured from medium carbon 42CrMo4+QT high-strength steel. The semi-finished product was a hot rolled quenched and tempered bar with a diameter of 35 mm. The material properties are shown in Table 8 and its chemical composition is shown in Table 9.

Table 8: Material properties.

Ultimate tensile strength Rm	Yield strength Re	Elongation A5	Contraction Z	Grain size	Reduction ratio
1097 MPa	1001.5 MPa	16.50%	62.50%	8	25

Table 9: Chemical composition (wt. %).

C	Mn	Si	P	S	Cu	Cr
0.42	0.64	0.21	0.013	0.009	0.02	1.04
Ni	Al	Mo	V	Ti	Sn	
0.06	0.026	0.185	0.006	0.001	0.003	

Sample geometry

A total of 8 series of samples with the same geometry were produced and ordered to have the same surface roughness $Ra = 0.8 \mu\text{m}$ prescribed on the surface near critical volume. It was required that this roughness be achieved for each batch by different machining variables settings. The drawing of the specimen is shown in Figure 50.

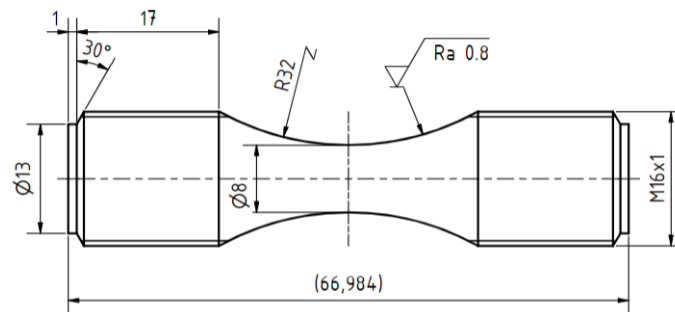


Figure 50: Specimen drawing.

6.1.2 Manufacturing setup

For a series of experiments, it was chosen that the final surface quality would be achieved by turning. The machining was carried out at VŠB Ostrava workshop. A group of machining parameters was chosen, the values of which were varied for different series of samples. The cutting speed, feed rate, tool nose radius, and cut depth were chosen as variable parameters. Tables 1 and 2 show the settings for each series. The series A25-A29 were manufactured in January 2022 and the remaining three series were produced later, in July 2022, with modified machining parameters requirements, where the same turning speed value was chosen.

Table 10: Machining setup for series A25-A29 ; *(Decocut 1040 during roughing).

Machining Parameters		A25	A26	A27	A28	A29
Spindle speed	[rot/min]	2984	3000	3979	2500	3000
Cutting speed	V_c [m/min]	75	75.4	100	62.8	75.4
Feed rate	F [mm/rev]	0.05	0.05	0.1	0.1	0.1
Process fluid*	Y/N	Y	Y	Y	Y	Y
Cooling fluid during last cuts	Y/N	Y	N	Y	N	N
Cutter nose radius	R_n [mm]	0.4	0.4	0.4	0.4	0.4
Last cut height	a_p [mm]	0.05	0.1	0.1	0.05	0.1
Second-last cut height	[mm]	0.1	0.1	0.1	0.1	0.1
Third-last cut height	[mm]	0.15	0.1	0.1	0.15	0.1

Table 11: Machining setup for series A35-A37 ; *(Decocut 1040 during roughing).

Machining Parameters		A35	A36	A37
Spindle speed	[rot/min]	3979	3979	3979
Cutting speed	V_c [m/min]	100.0	100	100.0
Feed rate	F [mm/rev]	0.05	0.05	0.05
Process fluid*	Y/N	Y	Y	Y
Cooling fluid during last cuts	Y/N	Y	Y	Y
Cutter nose radius	R_n [mm]	0.8	0.4	0.4
Last cut height	a_p [mm]	0.1	0.05	0.1
Second-last cut height	[mm]	0.2	0.15	0.2
Third-last cut height	[mm]	0.2	0.3	0.2

6.1.3 Roughness characterization

As mentioned above, different series were produced at different times and the method and location of measurement of their roughness depend on this. The A25-A29 series, which were first produced, were measured in 3 different laboratories, at the University of Ostrava, where they were also produced, at the Czech Technical University in Prague, and at the University of Mondragon, Spain. The later A35-A37 series

were also measured at the University of Ostrava and in Prague and then measured by the author at the University of Mondragon.

External measurement

External measurements are referred to those that were measured by other entities, and it was not possible to control the entire measurement process.

VSB Ostrava The first measurement was carried out in laboratories of the Technical University of Ostrava, shortly after its production. Alicona 3D Areal profilometer featuring focus variation technology was used to obtain surface topography. Depending on the series, 2 to 4 samples were measured from which the 2D parameters (R_a , R_z , R_q , R_t , R_p , R_v , R_c , R_{sk} , R_{ku} , R_{dq}) were calculated in Alicona - Measuresuite software.

CTU Prague Further measurements were performed at the Czech Technical University in Prague in the Department of Machining, Process planning and Metrology, which is equipped with a Mahr contact stylus profilometer. 2 to 3 samples of each series were measured in the central part according to the ISO 4287 standard [45] and parameters R_a , R_z and R_{sm} were calculated.

Mondragon University As part of the FABER project, three samples from series A25-A29 were sent to Mondragon University to be measured using the 2D contact stylus method under the supervision of Dr. Alaitz Zabala. Three measurements were performed according to the ISO 4287 standard [45] in the central part of each sample and the mean values of three different 2D parameters (R_a , R_z and R_{sm}) were calculated for each series.

Measurements conducted in the current project

The last roughness measurement of the A35-A37 series was carried out in the laboratory of the University of Mondragon. Three samples from each series were selected for measurement.

First, a visual inspection was carried out to detect defects visible to the naked eye, which could have been caused both during production and by non-careful handling, and it was also checked whether the surface was marked where previous measurements of roughness or residual stresses had been made.

3D areal measurement were made on the SensoFar NeoX optical profilometer, on which sensitivity analysis measurements were also performed (4.2). The white light interferometry method was selected for this set of measurements. The objective with 20x magnification was used.

Three surface scans were performed on each specimen in the central part. After each scan, the sample was rotated by 90 ° around the axis.

First, the sample was placed in a holder that was attached to the sliding platform of the microscope to prevent it from moving during the measurement. The measurement setup is shown in Figure 51. The center of the sample was then found using the profilometer control software, which was chosen as the center of the scanned area. Its size was chosen to be 2x1 of the FOV (field of view of the objective), which is equal to 1534.8 x 635 μm . The size of the measured area was chosen as a compromise between the acquisition time, which increases significantly due to the geometry of the specimen, and the amount of surface data acquired, which is sufficient for measured surface topography due to the periodicity of the machining surface and the geometry of the surface, where the critical cross section is in the smallest diameter of the specimen under uniaxial push-pull loading.

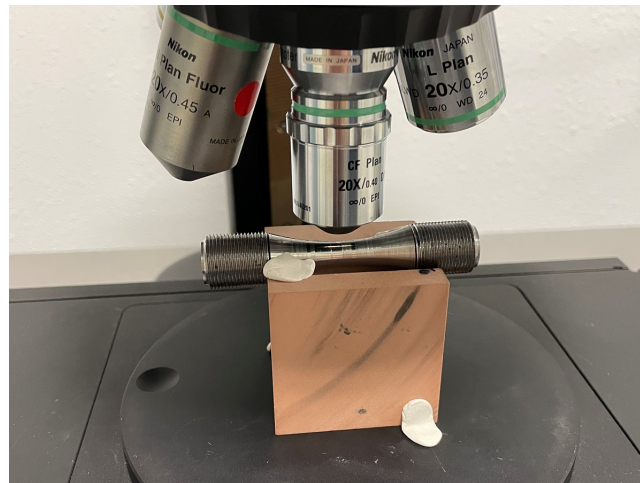


Figure 51: Areal measurement setup.

The following post-processing of the acquired data was performed in SensoMap Premium software. At first, the form removal operator was used, where the form was defined as a second-degree polynomial function. The noise was then removed, followed by spike management. Subsequently, the final roughness topography of the surface was obtained. The areal parameters were calculated according to the standard ISO 25178 [44]. From these, the mean value and standard deviation of three measurements were calculated for each sample. The final surface topography is shown in Figure 52.

Due to the occurrence of the step in most samples, it was decided to analyze how much it affects the final roughness values. For comparison, a raw topographic scan from the 3D areal measurement was chosen, which was cropped from one side in front of the step so that it did not appear in the evaluation area, and the subsequent procedure was applied as for the evaluation of the uncropped area.

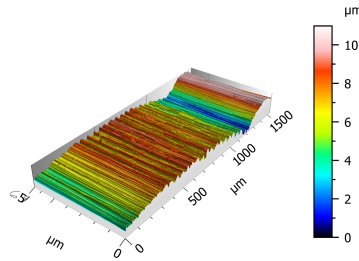


Figure 52: The final surface topography after post-processing.

Linear measurement were made using the contact stylus method using a portable surface roughness tester Mitutoyo SURFTTEST SJ-210 with a deep groove detector tip. In total, the profile was recorded at six locations in the central part of each sample, three of which were at the same location as the areal scan. The remaining were recorded at 45° , 240° and 300° angles relative to the first. The sample was always inserted into the fixture so that its position relative to the stylus tip was identical in all cases. The setup of the linear measurement is shown in Figure 53.



Figure 53: Linear measurement setup.

Measurements were carried out according to the ISO 4287 standard [45]. The default cut-off λ_c value was set to 0.8 mm and then kept or changed according to the R_{sm} value as an indicator of the λ_c value for the periodic profile.

The profilometer operation and data export were performed using SurfTest SJ USB communication tool software. In total 23 different 2D roughness parameters and the profile were exported. The mean value and standard deviation of six measurements were calculated for each sample from the recorded parameters. However, only the parameters that were selected as possible indicators of the effect of roughness on material fatigue were retained (see 4.2).

6.1.4 Residual stresses testing

The residual stress measurements were performed to measure residual stresses after machining. The samples were subjected to X-ray diffraction measurement, which is based on the principle of determining lattice deformations by measuring the distances of the lattice planes. These deformations are then converted into stresses using the relations of linear elasticity theory [36]. The X'pert PRO MPD (PANalytical) was used for measurements. The measurements were taken in the central part where the critical cross-section is located. The residual stresses in the axial and tangential directions were calculated from the measurements.

6.1.5 Fatigue setup

The fatigue testing was performed on an Amsler HFP422 resonator with a load range of 100 kN with load-controlled push-pull load and controlled by Texpert software. The samples were subjected to uniaxial compression-tension cyclic loading with constant stress amplitude and zero mean stress. The test frequency was 152 Hz, which was equal to the natural frequency of the sample. The end criterion was defined by the drop in frequency by 10 % or the change in static or dynamic force by 0.5 kN, or the test was terminated manually after 10^6 cycles and was considered to be run-out. Before fatigue testing, the samples were painted with black paint of known reflectivity to measure the temperature response of the sample during testing using a thermal imaging camera. After testing, the samples were visually inspected for cracks and, when no cracks were found, a capillary test was performed. The results of the fatigue tests were processed in FinLivQ software, where the measured data were approximated and the S-N curves were calculated and described using the power-law model.

6.2 Results and discussion

6.2.1 Roughness results

Measurements conducted in the current project

Two types of surface defects were discovered during the visual inspection. The first defect is a step defect in the central part of the sample, located around the perimeter. Figure 54(a) shows the circled position of this defect in sample A35_2 and indicates its approximate shape.

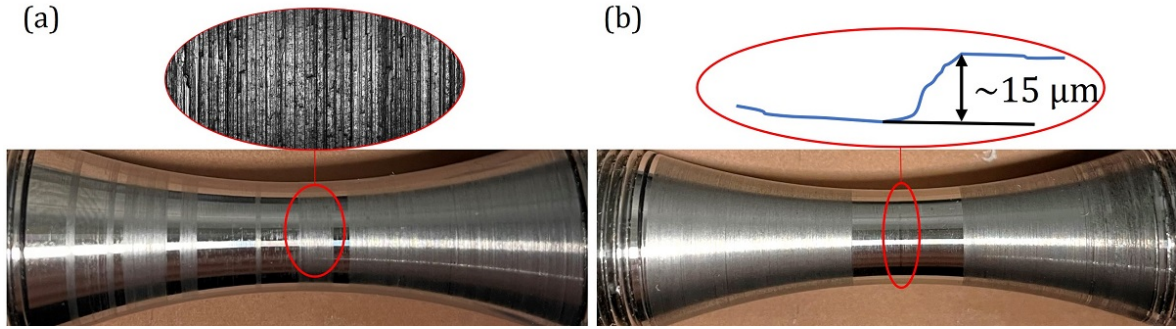


Figure 54: Surface defect observed by visual inspection. (a) Step defect on A35_2 (b) Inhomogeneous defect on A36_3.

The second defect is inhomogeneous surface quality and is probably caused by an inappropriate choice of turning parameters, which leads to poor chip debonding. The position of this defect on sample A36_3 is circled in Figure 54(b) and a close-up microscope view is shown in detail. All these defects have been recorded in a summary table Table 12. Some of the samples had a mark in the center by a marker, indicating the point at which a previous measurement of roughness or residual stress had been made.

Table 12: Visual inspection of measured samples.

Sample	Marking		Defects		
	Number	Dot	Central step	No homogeneous roughness	
A35_1	I	Y	N		Y
A35_2	I	N	Y		N
A35_3	I	N	N		Y
A36_1	II	Y	N		Y
A36_3	II	N	N		Y
A36_5	II	N	N		Y
A37_1	III	Y	Y		Y
A37_10	III	N	Y		Y
A37_11	III	Y	Y		Y

The results of the contact measurement are shown in Figure 55 (the remaining parameters are attached in Appendix A). The A35 series showed the best roughness characteristics. The A35 series showed the lowest roughness values in all variables studied except R_{sm} , where it had the highest value and the largest standard deviation. The value of R_a for this series was more than a quarter lower than for the other series. Similar trends were also observed for other parameters such as R_z , R_q , and R_c . A35 had an almost symmetrical profile against the mean line, as expressed by R_{sk} . The lowest values compared to the remaining series were probably achieved as a result of the lowest occurrence of defects in the central part. For two samples of A35, the inhomogeneous defects were located in the central part, but their size was smaller compared to the other series. The values of the roughness parameters of the A36 series were higher

compared to those of the A35 but lower than those of the A37. The graph shows that in most parameters, the values were closer to A37. The A37 achieved the worst surface roughness values and this result was consistent with a visual inspection, where the worst surface was observed on samples from this series.

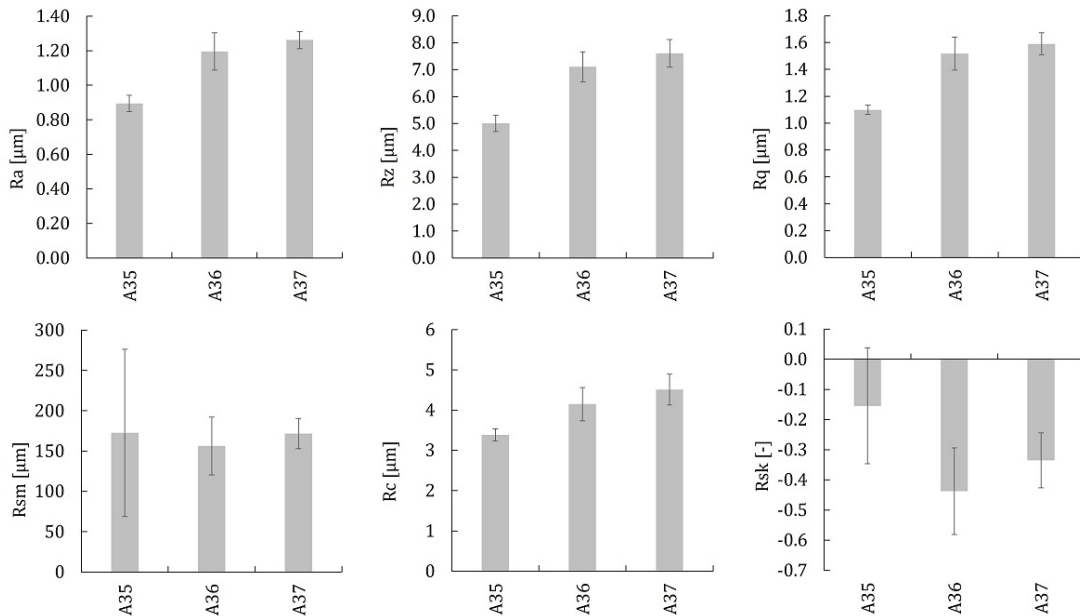


Figure 55: 2D roughness parameters obtained by contact stylus profilometer.

The results of the 3D areal measurement are shown in Figure 56 (the remaining parameters are attached in Appendix A). For parameters, except for S_{sk} , which are, by definition, equivalent to 2D parameters, trends can be observed where the smoothest roughness is again achieved by the A35 series. However, no similar trend is observed for S_{sk} , where the values for A36 and A37 are positive.

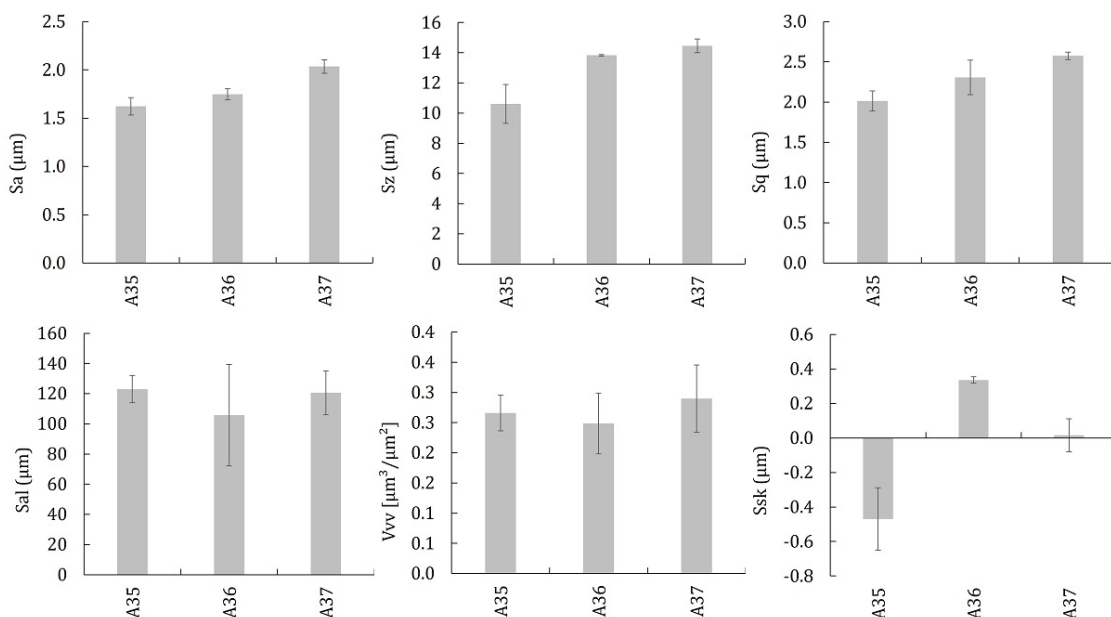


Figure 56: Areal roughness parameters obtained by non-contact 3D areal profilometer.

S_a ranged from 1.6 μm to 2.0 μm compared to R_a , where the values ranged from 0.9 μm to 1.25 μm , which is a difference of more than 50%. A similar difference occurred also for S_z/R_z and S_q/R_q . The best values of autocorrelation length (S_{al}) and void volume (V_{vv}) were measured for A36, followed by A35, and were the worst for A37. For A35, the height distribution, expressed by S_{Sk} , deviated above the mean surface, for A36 the opposite deviation occurred and the surface of A37 was almost symmetric against the mean surface.

Finally, the effect of the center step on the surface roughness values was analyzed. The results are shown in Figure 57, where two average parameters, one void parameter and one extreme parameter are displayed. As can be seen in the plots, the step significantly affected the roughness values, up to several times. It can be concluded that this defect is a significant topographic aspect of the surface that cannot be filtered out and must be treated as a potential factor affecting fatigue life.

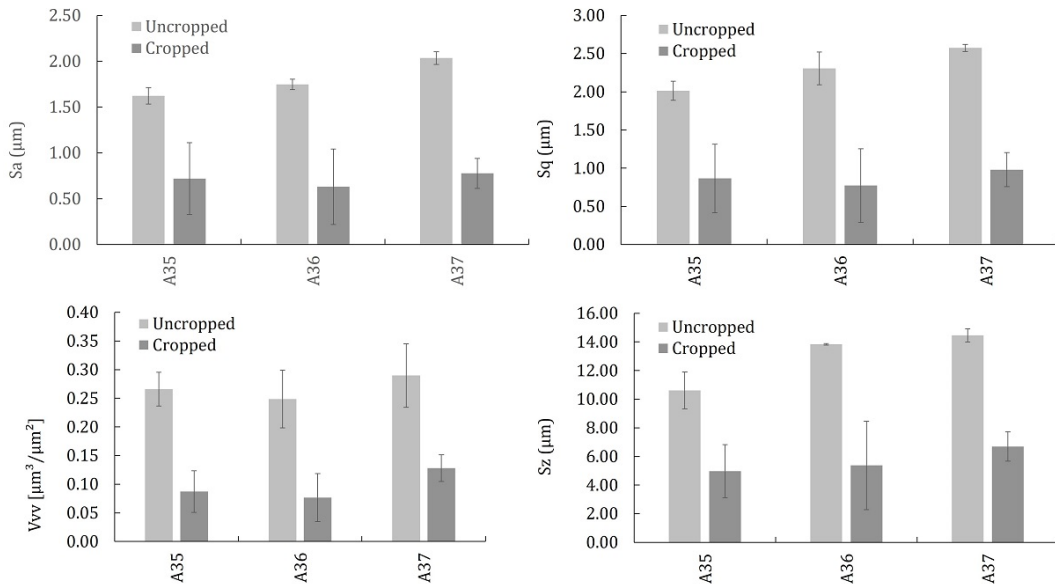


Figure 57: The effect of the central step on areal parameters. Uncropped = step is located within the evaluation area, cropped = step is not located in the evaluation area.

External measurement

The results of different laboratories were put together and the average value and standard deviation were calculated. Only three parameters, R_a , R_z , and R_{sm} , could be calculated in this way because no other parameters were measured in Prague and Mondragon. Other parameters were calculated only in Ostrava. The average values and standard deviations are presented in Figure 58.

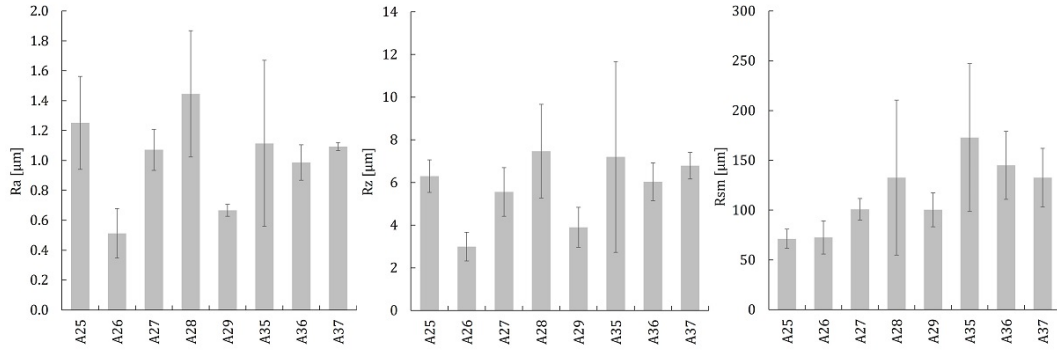


Figure 58: Average values of 2D parameters calculated from external measurements.

A26 had the lowest value of R_a and R_z followed by A29, the lowest value of R_{sm} was recorded for A25, followed by A26. On the other hand, A28 had the highest value of R_a and R_z . The highest standard deviations were calculated for series A28 and A35.

6.2.2 Residual stresses results

The results of the residual stress measurement are shown in Table 13. It shows that series A25-A29 + A36 had the tensile residual stresses in the axial direction, for the A35 series, only one sample had the tensile residual, and for A37, both samples had the compressive residual stresses in the axial direction.

Table 13: Results of residual stresses measurement. The table is taken from my colleague Bc. Petr Kolovratník.

Identification		Evaluation position	Axial		Tangential	
Series	Specimen No.		σ [Mpa]	$\Delta\sigma$ [Mpa]	σ [Mpa]	$\Delta\sigma$ [Mpa]
A25	I	center	75	13	-58	16
	II		128	18	24	21
A26	I	center	7	6	9	17
	II		103	19	195	28
A27	I	center	443	35	113	22
	II		440	13	112	40
A28	I	center	199	15	-31	24
	II		244	23	-92	21
A29	I	center	216	10	97	16
	II		198	18	271	27
A35	I	center	59	19	-96	9
	II		-143	7	-80	17
A36	I	center	25	18	-14	18
	II		99	25	92	30
A37	I	center	-63	18	-12	15
	II		-359	22	-148	19

Series A37 had the lowest tensile residual stresses and series A27 had the highest tensile residual stresses. The difference between the lowest and highest value of residual

stresses in the axial direction for all series was 802 MPa. It is more complex in the tangential direction, where series A26, A27, and A29 had only the tensile residual stresses. Series A28, A35, and A37 had only the compressive residual stresses and the remaining series had a mix of both, the tensile and compressive residual stresses.

From the table it can be seen that there were significant differences between specimens from the same series, for example, for A35, the first specimen had residual stresses of 59 MPa in the axial direction and the second specimen had -143 MPa. In fracture mechanics, tensile residual stresses are associated with a tendency for fatigue cracks to open and with a higher rate of propagation. In contrast, compressive residual stresses act oppositely on the initiation of fatigue cracks and prevent them from opening and propagating.

6.2.3 Fatigue results

The results of fatigue tests are shown in Figure 59, where the graph on the left shows the S-N curves of the series A25-A29 obtained by Kohout & Vechet-type regressions and on the right the S-N curves of the series A35-A37 and the two reference curves of the graph on the left. The results showed that the lowest fatigue life was achieved by series A28, followed by series A26. In contrast, the longest fatigue life was achieved by series A35, followed by series A36. The difference between the best and worst series at $5 \cdot 10^5$ cycles was more than 100 MPa, which is almost a quarter higher stress level.

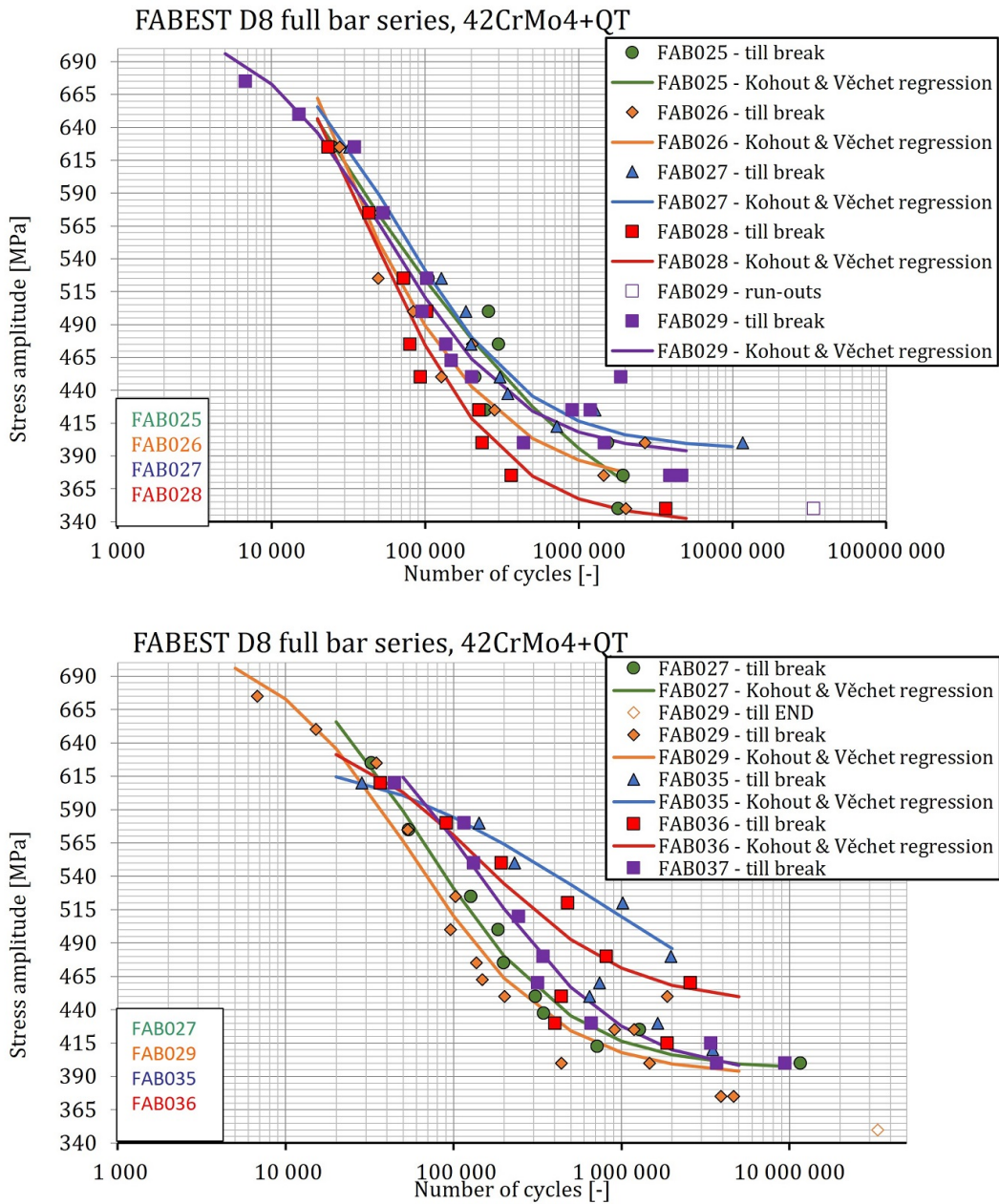


Figure 59: S-N curves obtained from measured data.

7 Effect of machining on surface roughness

In this section, the relationship between the manufacturing parameters and the roughness is analyzed in experimental data sets from section 6. The first part focuses on determining the direct dependence between the change in the value of the roughness parameter when changing the values of the machining parameters, for example, whether the value of R_q increases as the cutting speed increases. The second part deals with calculating the roughness from the machining variables using the relations given in 2.4.3, where the equations are divided into analytical and empirical.

7.1 Methodology

The input values of the 2D roughness parameters were taken from all measurements, and only the values of the measurement conducted in the current project were also used. For series A35-A37, the correlation between the machining variables and the areal parameters was also examined.

First, the series were sorted according to the magnitude of the machining variable being evaluated, and then the values of both input and output parameters were normalized by the value (of the parameter) of the series that was ranked first (in some cases the series were sorted from the smallest value to the largest and in others vice versa). With this normalization, it was then possible to observe the trend between the series for each roughness parameter and determine if they had a similar trend to the machining variable trend. For series A35-A37, only the effects of the nose radius of the cutting tool and the last depth of cut were analyzed, since the other variables remained unchanged throughout the series. When comparing all series, the influence of feed rate and cutting speed was also analyzed, as they varied between different series. When the trends were analyzed for all series, the values of the roughness parameters averaged from the values obtained from all the measurement sites were used. For this reason, only R_a , R_z , and R_{sm} were used because the remaining parameters were calculated only at VSB of Ostrava.

7.2 Results

Correlation between manufacturing variables and roughness parameters

First, it was analyzed whether there is a trend between the machining parameters and the surface roughness parameters. The values of all parameters were normalized to make it easier to observe a possible trend. The machining variables were also normalized and sorted in an increasing trend of their normalized values.

The first comparison was made for the 2D and areal parameters of surface roughness measured in the current project. The results for the change in the radius of the cutting

tool nose (0.8 to 0.4 mm) are shown in Figure 60(a), where the shadow bars are normalized values of the radius of the cutting tool nose.

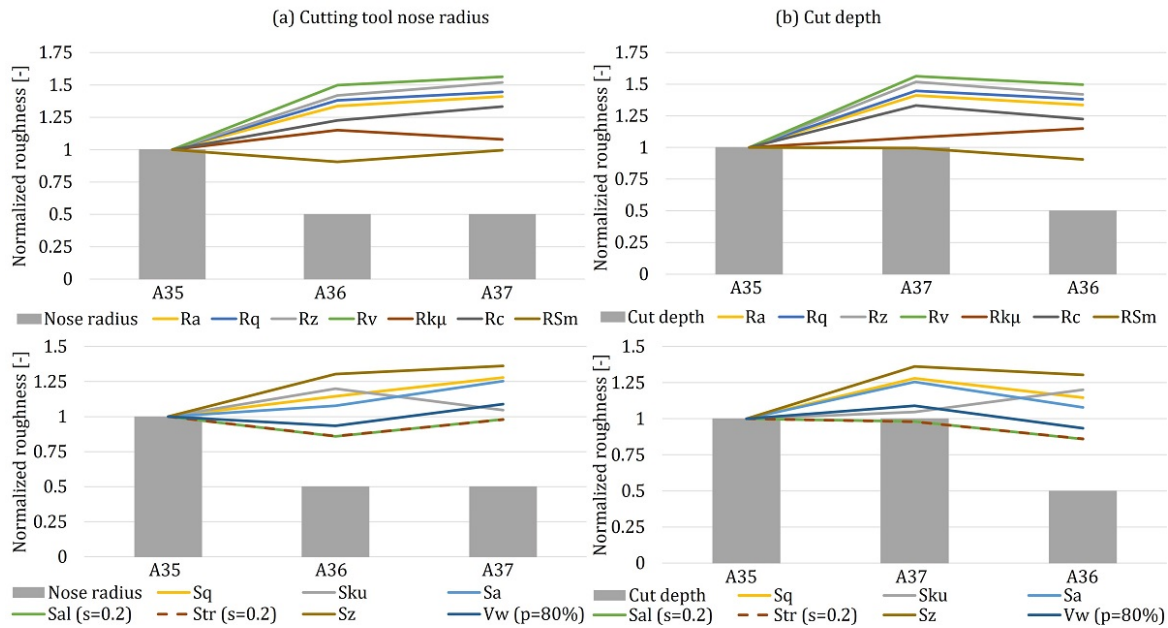


Figure 60: Comparison of trends for series A35-A37 from the measurement conducted in the current project

For the 2D parameters, as the radius of the cutting tool nose changed between A35 and A36, so did the normalized values of all parameters, with a decrease in the value for R_{sm} and an increase for the rest. Between A36 and A37, the radius of the cutting tool nose remained unchanged, but the values of the roughness parameters continued to increase but at a slower rate, except for the values of R_{sm} and R_{ku} where they returned almost to their original values. The best correlation was for the parameters R_v and R_q , where, at first, there was an increase of 50 % and 40 %, respectively, in their value, and then there was only a slight increase of approximately 6 % for both parameters. A similar trend but not as pronounced was observed for R_a . From this, it can be concluded that when the radius was reduced from 0.8 to 0.4 mm, the values of the roughness parameters increased.

For areal parameters, S_z had the most similar pattern of values for each series, where there was a 30 % increase in the value when the radius of the cutting tool nose was changed. Next, between the A36 and A37 series, where the radius remained the same, there was only about a 5 % increase in the value of S_z . No similar trend was observed for the remaining parameters as their values changed independently of the change in the machining variable.

The results for the change in the depth of cut (0.1 to 0.05 mm) are shown in Figure 60(b), where the shadow bars are normalized values of the depth of cut. The correlation between the change in depth of cut and the change in the 2D roughness parameters was only observed for R_{sm} as its value remained almost the same for the

unchanged value of a_p between A35-A6 and then its value decreased as the size of a_p changed between A36-A37. No similar trend was observed for the remaining parameters as their values changed independently of the change in the machining variable.

For the areal parameters, the most similar trend can be observed for S_{al} and S_{tr} , as their values changed approximately 2% between A35 and A36, where the depth of cut was unchanged, and then their values decreased by 10 % with the change of a_p . Furthermore, S_{ku} and V_{vv} also had similar trends, as their values changed slightly between A35 and A36, and then their values changed more significantly. This may indicate that the change in the machining variable had an effect on the above parameters. The values of S_{al} , S_{tr} , and V_{vv} decreased with decreasing depth of cut and the value of S_{ku} increased.

The trend results for all series can be seen in Figure 61, where it can be seen that there was no observable relationship between the trends of the individual machining variables and the roughness parameters. The values of R_a , R_z , and R_{sm} changed independently of the value of the machining variables.

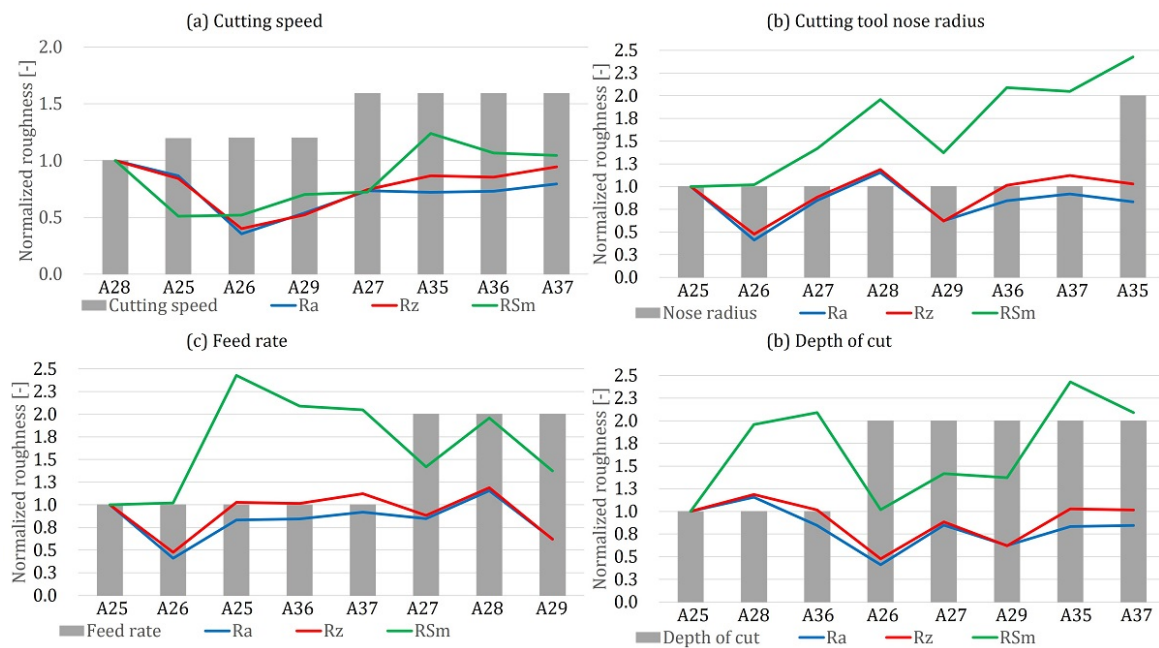


Figure 61: Comparison of trends for all series from data from all measurements.

Formulas

The results of the roughness estimates calculated using the equations from 2.4.3 were calculated as a relative error of the measured values. A dual evaluation of these methods was chosen, namely, by series and by mathematical relationships. For the former, the errors of each method were first calculated and, from these values, the average error and standard deviation were then calculated and compared between the series. For the latter, a similar procedure was chosen, where the error of each series was first calculated and then the average error and standard deviation of the whole

method were calculated, and these values were then compared with the results of the other methods.

As shown in Figure 62 (a), the series errors range from 2 % to 107 %, where the smallest error was achieved by A28, followed by A27, and the largest was achieved by A29, followed by A26. A29 and A26 had the two lowest measured values of R_a of all series, while A28 had the highest measured value of R_a . However, no correlation was observed between the relative error and the roughness values for all series. For the A26 and A29 series, the methods estimated higher roughness values than the measured values, and the highest relative errors were also obtained for these series using empirical formulas, where for some methods the errors exceeded 150 %.

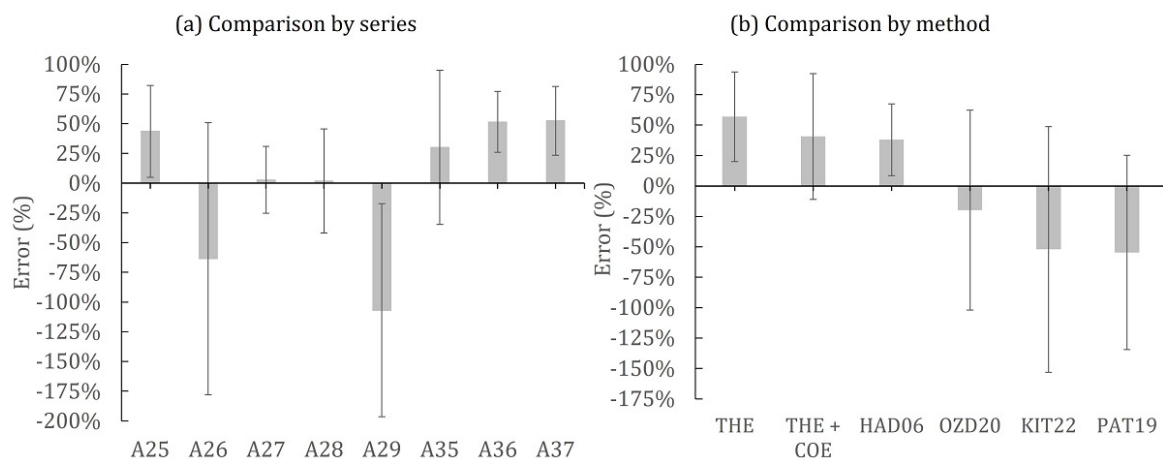


Figure 62: Comparison of roughness estimation errors from machining parameters according to (a) series, (b) method. THE = ideal roughness, COE = correction factor between ideal and actual roughness.

Figure 62 (b) shows a comparison of the average errors of each method. These ranged from 20 % (OZD20) to 53 % (THE), with three of the four empirical methods achieving the three largest standard deviations and the fourth method achieving the smallest standard deviation. Both analytical methods estimated lower roughness values than were measured. In addition, the methods with the highest standard deviations estimated roughness values lower than the measured ones.

7.3 Discussion

When evaluating the effect of the machining variables on the roughness parameters, only correlation was observed for the data obtained in the current project, where R_q , R_v , R_a , and S_z increased with decreasing radius of the cutting tool nose. Furthermore, the change in the values of R_{sm} , S_{al} , S_{tr} , V_{vv} and S_{ku} was observed in the case of a change in the depth of cut. In addition, in the case of changing the depth of cut, a change in the values of R_{sm} , S_{al} , S_{tr} , V_{vv} and S_{ku} was observed, where for the first four parameters their values decreased as the depth of cut decreased, while the opposite

effect was observed for V_{vv} .

For the results of all series where only three parameters were available, it was not possible to observe any connection between the input and output parameters at all. Even no correlation is visible for the feed rate, although according to the equation for ideal roughness, the value of R_a should change with the square of the feed rate. One of the reasons could be the inaccuracy of the roughness parameter measurements, but this effect should be minimal since results from multiple measurements were used. The most likely reason that no correlation was observed is the insufficient number of series for this type of analysis. Although eight different series were produced, four different machining parameters were investigated. Therefore, for most of the series, the values of multiple machining parameters were varied. For this reason, it was probably not possible to discover the effect of individual machining parameters on surface roughness.

When such large percentage errors occur for calculation methods, it should be considered whether these roughness estimation equations can be used in practice and also to discuss the reasons for such large deviations. Mostly for the case of analytical methods, where some part of these errors could be due to observed defects. The central defect significantly affected the roughness values, as was demonstrated in the previous section for the areal parameters. However, these estimates gave very low roughness values anyway. For example, for the A35 series, the calculated ideal roughness was $0.1 \mu\text{m}$, which is below the lower end of the roughness range obtained by machining. The equation for calculating the ideal roughness takes into account only the feed rate and nose radius, which are only two machining parameters. If the cutting speed or depth of cut were changed, the value would remain the same. Hence, a correction factor has been introduced. The one given in [41], depends on the cutting speed and on the type of material. However, it is no longer possible to know whether other effects have been considered in addition to the cutting speed and material properties. The problem with empirical relationships obtained from various papers is that these equations were determined by regression analysis from measured data. All empirical regressions are subjected to the experimental data used for this fitting and linked to the machining processes used to generate these data. If the equipment used is changed, other non-measured parameters, such as vibrations, may change and affect the results.

To summarize, in the case of using the above equations for the estimation of surface roughness in the experimental data of section 6, no clear conclusions can be drawn from the results because the measured samples had defects affecting the roughness values. Therefore, affected the results of this chapter. Further experiments would be needed to prove the reliability and accuracy of these methods. Even so, the use of empirical regression models appears to be problematic because only certain machining variables enter the regression analysis but others that may affect the result are not included in these models.

8 Correlation between roughness and fatigue

In this section, the relationship between surface roughness and fatigue endurance is analyzed on the experimental data from section 6. The first part focuses on the analysis of the direct relationship between the change in fatigue life and the change in the values of the roughness parameters between series, for example, whether fatigue life increases as R_a decreases. The second part deals with the calculation of the fatigue life of individual series from the reference curve using various surface finish factors, which are given in 2.5.

8.1 Methodology

Direct correlation between roughness parameters and fatigue

The average values of all measurements (CTU, VSB, and Mondragon) were taken as input values for the 2D parameters to use the most representative values, but only the parameters R_a , R_z , and R_{sm} were used because they were the only ones measured in all laboratories. Additionally, for the A35-A37 series, the values of the 2D and areal parameters measured in the current project were used. The evaluation was performed for stress values at $2 \cdot 10^5$ cycles because for this lifetime the S-N curves of all series obtained by regression were well-defined. The power-law model was chosen to describe the curves (Eq. 4).

The roughness values were plotted against the stress values, a trend curve was fitted through the values, and R-squared (R^2) was checked to indicate how the regression model describes the observed data. However, for the A35-A37 series, where the correlation was analyzed on the roughness values measured in the current project, many more roughness parameters were calculated. Therefore, it was decided to use a different approach. First, all series were ordered by the stress magnitudes from largest to smallest, then all values were divided by the corresponding value of the parameter from the series with the highest stress, and then, for the case of roughness parameters, the inverse values were calculated. This normalized the values so that trends could be examined more easily. Parameters that showed a pure decreasing or pure increasing trend were further examined by fitting a trend curve through the values and calculating its R^2 value.

Surface finish factor

The procedure to calculate the factors of surface finish and corresponding stresses was the same as in Section 5.

The A22 series, which was also measured in the FABER project but was measured at Opole University of Technology by Prof. Aleksander Karolczuk, was chosen as the

reference curve for which the lowest possible roughness, ideally achieved by polishing, was required. This option was chosen because the fatigue life calculation using the surface finish factor is based on a reference curve that was measured on a smooth test specimen, on which most of the resulting surface quality is achieved by polishing. Although no experimental value for the A22 series exceeded 10^5 cycles, it was decided to approximate the stress value at a lifetime of $2 \cdot 10^5$ cycles. This approximation was possible based on previous experiments on the same material, which confirmed that the approximated value at a given number of cycles was equal to the experimental value.

The stress values in the $5 \cdot 10^4$, 10^5 , and $2 \cdot 10^5$ cycles were selected for evaluation. Higher values of cycles were not used because the experimental data for the reference curve are only up to 10^5 and the approximation beyond $2 \cdot 10^5$ cycles cannot be considered accurate. Secondly, the experimental data for certain series did not exist beyond $2 \cdot 10^5$. It was not meaningful to evaluate the effect of surface roughness on fatigue life for a lower number of cycles due to the high stress values at which plastic deformation is more likely to occur.

8.2 Results

Direct correlation between roughness parameters and fatigue

First, the direct dependence between the roughness value and the fatigue life was analyzed using data from all series. For this comparison, the parameter R_a , which is most commonly used in practice and also showed the best correlation among the available parameters, and the stress at $2 \cdot 10^5$ cycles were selected. The results are shown in Figure 63.

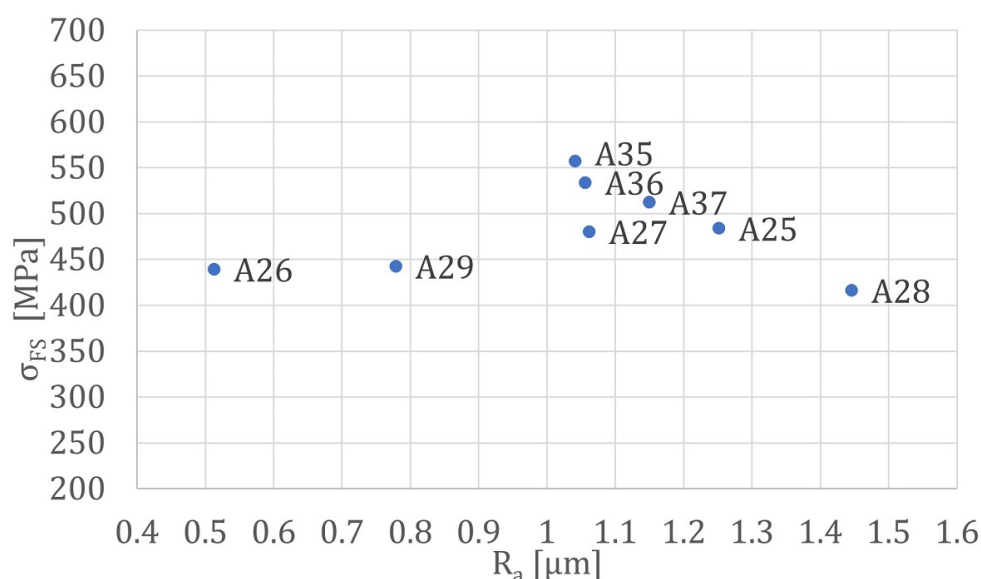


Figure 63: Scatter graph showing the dependence of the fatigue strength on the roughness parameter R_a .

When all values were analyzed, there was no obvious trend between roughness and fatigue strength. When the values were fitted with a linear trend, it appeared that fatigue life increased with increasing roughness values, which is contrary to any expectation. This was caused by the A26 and A29 series, which had the lowest measured roughness, but the second and third-lowest fatigue life. However, when these two series were omitted from the evaluation, the remaining values showed a trend where fatigue life decreases with increasing roughness, which is consistent with the theory presented in 2.5. The R^2 for this case was approximately 0.75, where the precision of this regression was reduced by the value of the A27 series, which achieved a lower fatigue strength for a given roughness. When even this series was omitted, $R^2 = 0.98$, which can already be considered a very good result. This was done on the assumption that the surface roughness was not correctly measured for the A27 series as well, but it must be stressed that this is only a theoretical idea that is not supported by data.

For the A35-A37 series, the trends were first analyzed to determine the parameters that followed the trend of fatigue strength. The results are shown in Figure 64, where (a) shows the results of the 2D parameters and (b) shows the results for the areal parameters. For 2D parameters, R_c had the most similar trend to the trend of fatigue strength, followed by R_a , R_q , and R_z . In contrast, no trend was observed for R_{sm} and R_{sk} . For the areal parameters, S_a and S_q trends were the most similar to the fatigue strength trend, followed by S_z which also had a steadily decreasing pattern.

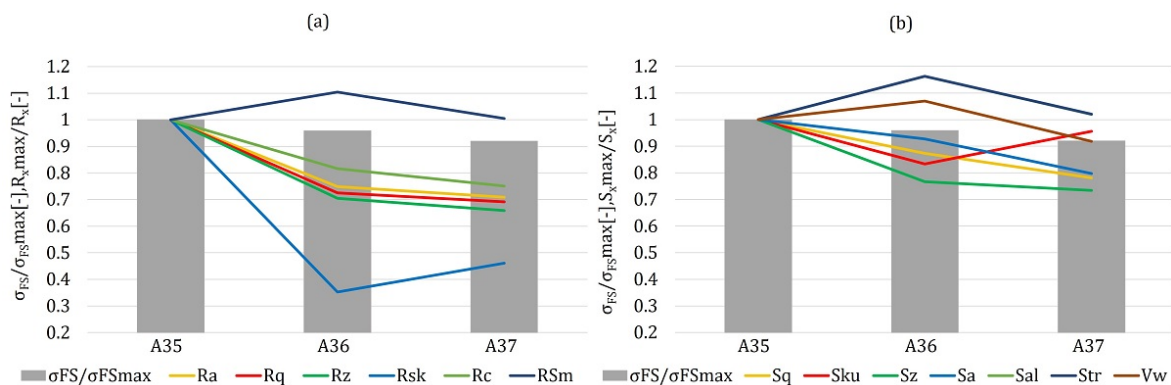


Figure 64: Comparison of trends of roughness parameters and fatigue strength for series A35-A37 from the measurement conducted in the current project. (a) 2D parameters (b) areal parameters.

The most promising parameters were then taken and their values were plotted in a scatter plot against the fatigue strength values. The results for the 2D parameters are shown in Figure 65. The parameter R_c showed the best correlation between its values and the fatigue strength values; when a linear regression curve was fitted, the value of R^2 was equal to 0.967 which can be considered a very good regression. R_c was followed by R_z , R_a , and R_q . When the regression curves were fitted to the values of R_z , R_a and R_q , the values of R^2 were 0.9, 0.89, and 0.87, respectively.

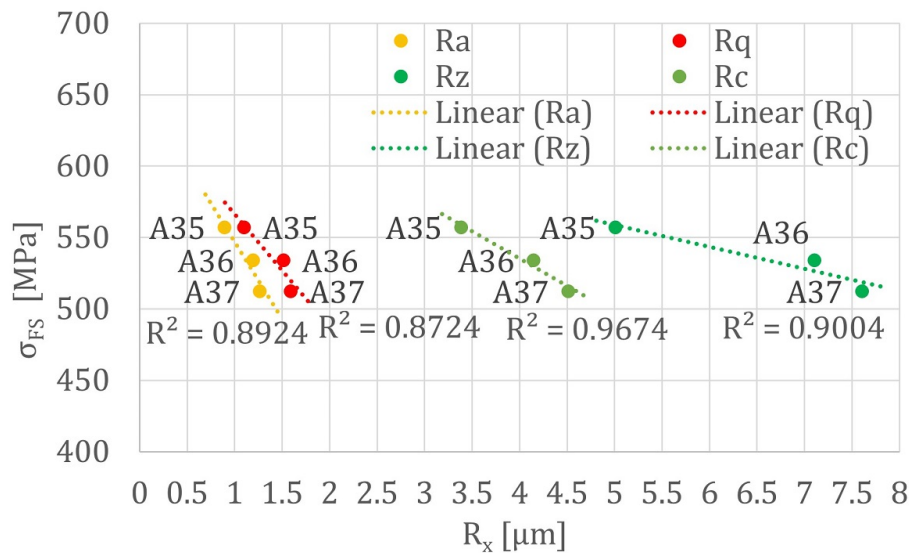


Figure 65: Scatter graph showing the dependence of the fatigue strength on the 2D roughness parameters.

The results for the areal parameters are shown in Figure 66. The parameter S_q showed the best correlation between its values and fatigue strength values, when a linear regression curve was fitted to the measured data, the value of R^2 was equal to 1, which means that the regression curve approximates the measured data by 100 %. S_q was followed by S_a , where $R^2 = 0.94$ for the linear regression curve.

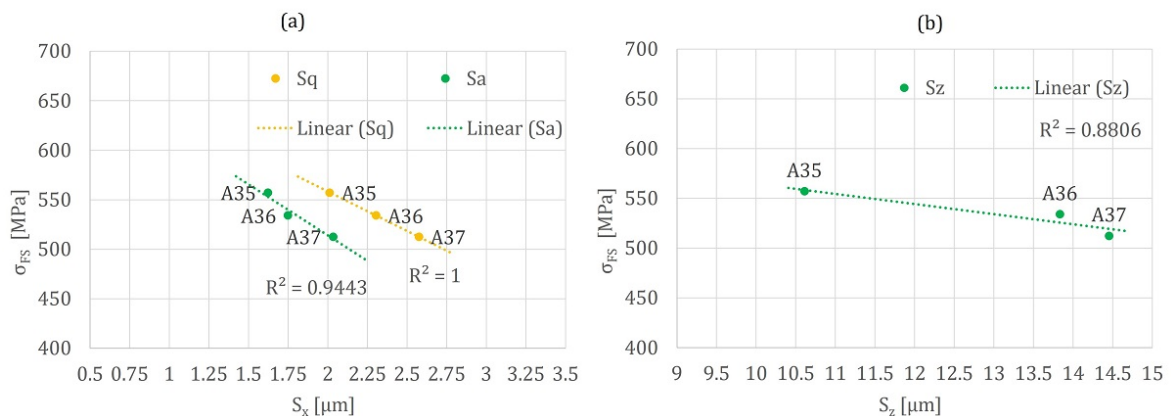


Figure 66: Scatter graph showing the dependence of the fatigue strength on the 2D roughness parameters. (a) S_a and S_q parameters, (b) S_z parameter

Among the selected parameters, S_z had the worst correlation with fatigue strength, but since it is an extreme parameter that is determined by the lowest and highest point in the evaluation area, its correlation is questionable because its value is very easily influenced by any defect that was not filtered during post-processing and at the same time it may not affect the fatigue strength of the component.

Surface finish factor

Results are displayed as average errors of the calculated values compared to the measured values. A different evaluation had to be done for the Murakami method, where it was only possible, according to Eq. 39, to estimate the fatigue limit of each curve. Its results are not included in the average relative error of each series. Furthermore, given only the fatigue limit estimation, its results are the same for both models. The model according to EN 13445-2009 was not evaluated for the logarithmic model, because according to Eq 31, the value of the surface finish factor is given by the number of cycles.

The results showing the average error of each method for the simplified model (the model was described in 5.1) are shown in Table 14 (the values are at the bottom of the table). The largest average error was achieved by the method using Juvinall's graph, where the value of the surface finish factor was determined by UTS and the finishing method, in this case, machining. It was followed by Shigley's method, where the same procedure was used to calculate the surface finish factor. Both methods estimated a fatigue strength that was higher than the measured one. The biggest errors were for the A35-A37 series, where the errors were more than 25 %.

On the other hand, the lowest average error was achieved by using the Schijve graph, where the value depended on UTS and R_a . It was followed by the method using the graph from Johnson, which is based on the same principle. All four methods, which are based on a direct calculation from the roughness value, estimated a fatigue strength higher than those actually measured. When evaluating the Murakami method, the error for the A26 series is more than one-third, but for the last three series, the estimation was very accurate.

Table 14: Average errors of each method and of each series for the simplified model.

Series	Uni.	Juv.	RCJ.	Sch.	Shi.	Mur.	ASM.	KHS.	EN1	FKM	\bar{x}_r^*	StD
A25	-0.06	0.21	0.00	0.02	0.18	-0.07	-0.08	-0.09	-0.01	-0.01	0.02	0.11
A26	-0.18	0.16	-0.14	-0.15	0.13	-0.37	-0.23	-0.24	-0.14	-0.14	-0.11	0.15
A27	-0.06	0.22	0.00	0.01	0.19	-0.11	-0.09	-0.10	-0.02	-0.01	0.02	0.11
A28	-0.18	0.12	-0.10	-0.07	0.09	-0.21	-0.18	-0.19	-0.11	-0.10	-0.08	0.12
A29	-0.11	0.18	-0.07	-0.08	0.15	-0.27	-0.17	-0.19	-0.09	-0.09	-0.05	0.13
A35	0.03	0.28	0.08	0.09	0.25	0.04	0.00	0.01	0.08	0.08	0.10	0.10
A36	0.02	0.28	0.07	0.09	0.25	0.00	0.00	0.00	0.07	0.08	0.10	0.10
A37	0.01	0.27	0.06	0.09	0.24	-0.02	-0.01	-0.01	0.07	0.07	0.09	0.10
\bar{x}_r	-0.07	0.21	-0.01	0.00	0.18	-0.13	-0.09	-0.10	-0.02	-0.02	-	-
Max x_r	-0.18	0.28	-0.14	-0.15	0.25	-0.37	-0.23	-0.24	-0.14	-0.14	-	-
Min x_r	0.01	0.12	0.00	0.01	0.09	0.00	0.00	0.00	-0.01	-0.01	-	-
StD.	0.09	0.06	0.08	0.09	0.06	0.14	0.09	0.10	0.09	0.09	-	-

Uni. = UNI 7670, Juv. = Juvinall, RCJ. = RcJohnson, Sch. = Schijve, Shi. = Shigley, ASM. = ASME BPVC, KHS = KHKS0220, EN1 = EN 13445-2009, StD = standard deviation, \bar{x}_r = Average relative error, * average relative error without Murakami method.

The results of the average errors for each series are shown in Table 14 (the values are at the bottom of the table). As mentioned earlier, for the series A26, A28, and

A29 the actual fatigue strengths were lower than the calculated one; the average error of these series was not so large because of Juvinall's and Shingley's methods, which are extremely conservative and even for these series they estimated a lower fatigue strength. On the other hand, the A35-A37 series had the highest positive average error, which means that their fatigue strength was higher than the estimated one, which is a desirable fact, unlike the previous case, i.e. the result is on the side of safety. The remaining 2 series had the smallest average error, but their standard deviation is still quite high, thus for some cases the series underperformed, and for others the opposite.

Comparison of models

A comparison between the simplified and logarithmic models is shown in Figure 67. The table with data for the logarithmic model is attached in Appendix A. The smaller average error of the logarithmic method compared to the simplified model is achieved with the Juvinall and Shingley method, which uses only the surface finish technique but not the roughness value.

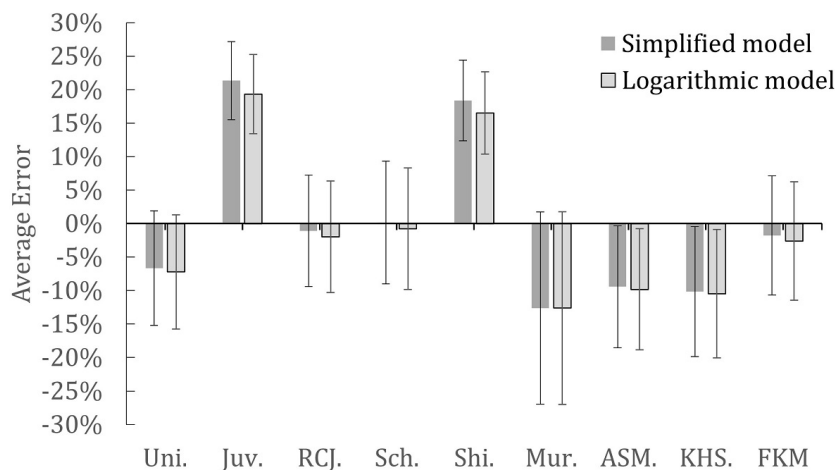


Figure 67: Comparison of average errors for the simplified and logarithmic models for each method.

For the other methods, the average error for the logarithmic model was larger than for the simplified model. For the logarithmic model, the standard deviation was approximately one percent smaller, which is statistically insignificant.

Further comparison of the simplified and logarithmic models in terms of individual series is given in Figure 68. Higher average errors for the logarithmic model were obtained for the A26, A28, and A29 series, i.e. those that underperformed compared to the estimated fatigue strengths. For the remaining series, the estimates for the logarithmic model were more precise compared to the simplified model by approximately 1 %.

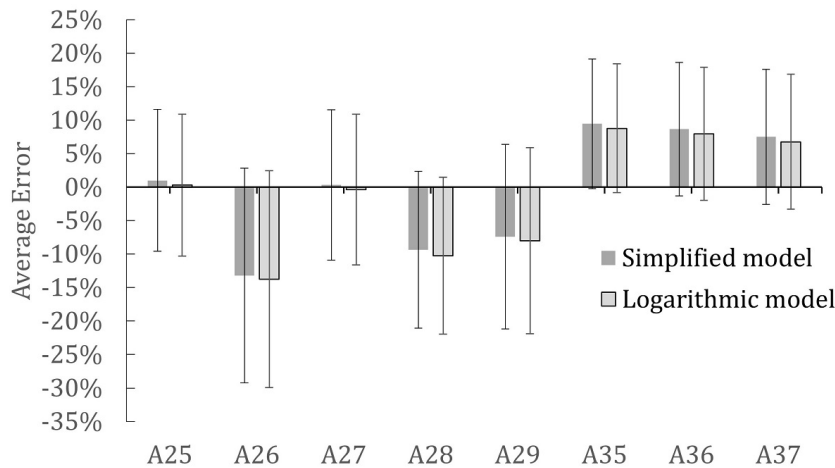


Figure 68: Comparison of average errors for the simplified and logarithmic models for each series.

8.2.1 Comparison of results with results from Section 5

In the end, the results of this chapter were compared with the results of Section 5, where the same methods for fatigue life estimation based on specific surface roughness were used. The comparison of the results is divided according to the simplified and logarithmic models.

The comparison of the simplified models are shown in Figure 69. Methods, where the surface factor value was subtracted from the graph for a particular roughness value, were more accurate for FABEST data, for the remaining methods it was the other way around. Overall, the methods had larger standard deviations for the external data. The biggest difference can be seen for the Juvinall and Shigley methods, where for the FABEST data these methods estimated on average almost 20 % lower fatigue strength, while for the external data, the relative errors were much smaller, even zero for the first method, but had a very high standard deviation, so their range of estimation was very large. In contrast, the most similar estimates were for the UNI 7670 method.

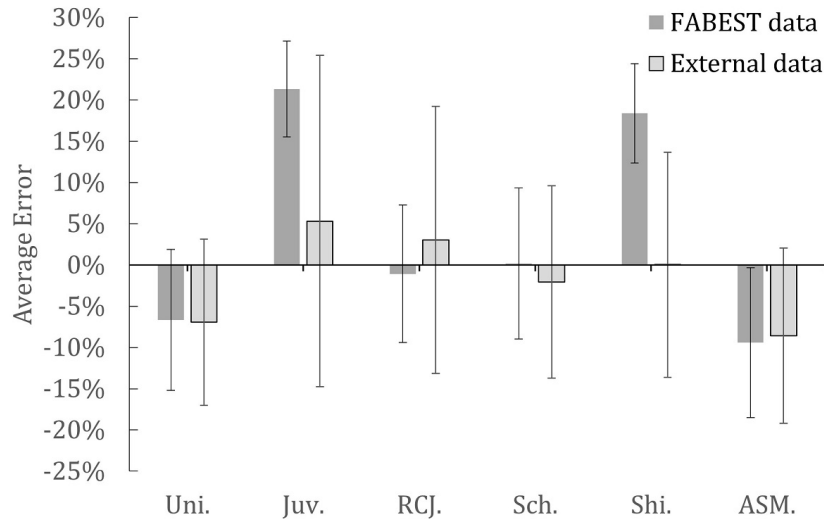


Figure 69: Comparison of the simplified model when applied to FABEST and external data.

The comparison of the logarithmic models are shown in Figure 70. Different results were observed for the logarithmic model, where most estimation methods were more accurate for FABEST data and only the Juvinall and Shigley methods were more accurate for external data. Higher standard deviations were again found for the external data

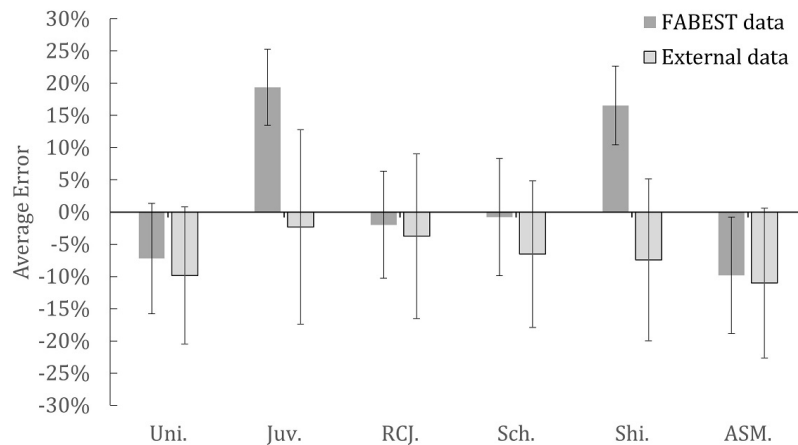


Figure 70: Comparison of the simplified model when applied to FABEST and external data.

8.3 Conclusion

In this part, the effect of surface roughness on fatigue was analyzed using experimental data from section 6. In the first part, different roughness parameters were analyzed as potential indicators of fatigue performance. When the values of the parameter R_a of all series were plotted against the fatigue strengths, a trend was visible for the series A25, A27, A28, A35, A36, and A37, where the fatigue strength decreased almost linearly with increasing roughness. The values for the A26 and A29 series

were completely out of trend, where a much longer fatigue life was expected for their roughness value. A different fatigue factor must have dominated these two series. One possibility could be the effect of residual stresses. This is supported by the fact that A29 had the highest residual tensile stress and A26 had the third highest residual tensile stress. A more detailed analysis would be required to prove this effect, but that would be beyond the scope of this thesis. Furthermore, other roughness parameters were analyzed on the A35-A37 series as potential identifiers of the effect of roughness on fatigue. For the areal parameters, a linear dependence was found between S_q and fatigue strength where the three experimental values lay on the linear regression curve. A slightly worse dependence was obtained for the parameter S_a . However, further experimental tests are necessary to verify this correlation. For the 2D parameters, R_c showed the best correlation between the roughness value and the fatigue strength. It was followed by R_z , since this is an amplitude (extreme) parameter that is calculated using 10 extreme values, it is not an ideal quantifier of surface roughness. However, in the case of actual experimental data, it may be a good parameter characterizing the central defect (step), which acted as a stress concentration, especially when located in the critical cross-section.

In the second part, different methods of fatigue life estimation based on specific surface roughness were analyzed. The least accurate methods were those that did not use the roughness value to calculate the surface finish factor, but they only utilized the surface finishing technique, machining in this case. It must be emphasized that their estimates were on the side of safety, i.e., the estimated fatigue life was lower than the actual one. The most accurate methods were those that subtracted the factor value from the graph, where it was given by the UTS value and the R_a value. They were followed by two methods in which the factor value is calculated by an equation in which a specific value of R_z and UTS is used. However, these methods estimated a higher fatigue life than the experimental one, which is not desired in practice. When comparing the series, for the series A26, A28, and A29, the estimated fatigue life was higher than the experimentally measured. From this, it can be concluded that these series underperformed and their fatigue life was probably influenced by another fatigue factor. The most accurate estimates were for the A25 and A27 series, where the estimate differed by less than 2 %. For the remaining three series, the fatigue life was underestimated, and the estimate was on the safe side. The magnitude of the average error for these series was mainly due to the Juvinall and Shigley methods, where the error was around 25 %.

When comparing the precision of the simplified and logarithmic models, their difference was only around 1 %, therefore, the use of the simplified method appears to be more practical as it is much simpler and faster to calculate. The logarithmic model for all methods was non-conservative compared to the simplified model, so it had lower positive values in the region of positive relative errors and higher negative values in

the region of negative relative errors.

When comparing the results from this Section with the results of Section 5, the largest differences were for estimation methods based on the surface finish technique, where the data were very conservative for FABEST. For the logarithmic model, all methods were non-conservative for external data. Standard deviations were lower for the FABEST data for almost all methods and for both models.

9 Conclusion

The aim of this thesis was to analyze surface roughness and its impact on fatigue life. The area of concern is restricted to the samples that were produced by conventional processes (not additively manufactured) and mainly by machining, strictly metal materials (aluminum alloys, steels, and cast irons).

First, a State of the Art was conducted to determine how the scientific community approaches surface roughness measurement in terms of measuring technologies and the roughness parameters used during material fatigue testing. The most interesting result was that almost 50 % of all measurements were made by 3D areal measurement technology, but only 13 % of the articles reported roughness in the areal parameters. Thus, many authors performed 3D areal measurements but then calculated only 2D parameters from the obtained data. This procedure for calculating 2D parameters is not under any standard, and individual results may differ, for example, due to different filter usage or length of the evaluation length. It was also found that the most frequent 2D parameter was the R_a parameter, which is also the most used in the industry. Its undeniable advantage is its long application history and established standards. However, its use for characterizing surfaces in terms of fatigue can be complicated because it is a 2D parameter. Its definition is too general to describe surface topography and its attributes that have the greatest influence on fatigue strength, such as the tip radius of notches and their mutual distance. As an example, profiles with the same R_a value but various geometry were proposed, giving different values of the stress concentration factor.

The next chapter focused on the sensitivity analysis of the areal parameters that were suggested as potential indicators of fatigue performance. How their values differ when using various 3D areal measurement technologies, objectives with different magnification, different evaluation area sizes, and different post-processing procedures. The results of interferometry and confocal microscopy were found to be very similar, but this was not the case for focus variation, where the measurement was very noisy. In terms of magnification, the results for the 20x and 10x magnification lenses differed by several percentages, therefore using 10x magnification is preferable as it scans the same area in a shorter time. The results for 5x magnification were unusable because of the very poor quality of the resulting topography. From the results of the effect of the size of the evaluation area, it can be concluded that its size does not have a significant effect on the average parameters S_a and S_q , but the other parameters were more affected. It was also found that it is essential to remove the form correctly during post-processing, otherwise, the roughness values can be affected by hundreds of percent. Analysis of the effect of post-processing on 2D parameters did not give clear conclusions. For one surface, it was found that it is more accurate to apply the λ_c filter after the form removal operator, but for the other surface, it was found that its

application has a negative effect on the values of 2D parameters.

The fifth section focused on the investigation of the precision of different methods for estimating reduced fatigue life based on the specific roughness of the surface. Two models were used for comparison, the simplified and the logarithmic model. They differed in the way the reduced fatigue strength was calculated. The simplified model proved to be more conservative, giving results on the safe side. As far as the different estimation methods are concerned, their average relative error ranged from 4 to -11 %. Overall negative relative errors dominated, meaning that estimates, where the calculated fatigue strength was higher than the actual one, prevailed.

As part of this work, experimental tests on the effect of surface roughness on fatigue were performed. First, 2D and areal roughness parameters were measured on samples intended for fatigue testing in a laboratory in Mondragon, Spain. Two types of surface defects were found on the samples, and one of them was a step in a critical cross-section and therefore appeared to be a risk factor for fatigue strength. During the roughness measurements, its occurrence affected the roughness values up to three times. Fatigue tests on samples of different roughness showed that fatigue strengths varied by up to a quarter between series with different roughness. In a subsequent analysis of the correlation between the roughness parameters and the fatigue strength, a very good correlation was found between the fatigue strength and the change in the values of the roughness parameters R_a , R_c , R_q , S_a . The best correlation was for S_q , where a clear linear dependence occurred. However, more experiments are required to validate these results, because most of the indicated parameters were measured only on three different series; furthermore, to rule out the influence of defects on the results. Subsequently, different methods for fatigue life estimation based on the specific roughness value were verified on this set of experimental data. Some of these methods provided a conservative estimate of fatigue strength and predicted approximately 20 % lower fatigue strength. In contrast, methods based on subtracting the value of the surface roughness coefficient from empirically constructed graphs, where the value depends on the tensile strength and the roughness value, were found to be very accurate, with an error of approximately 1 % to the actual value. These methods showed, as well as a direct trend between roughness values and fatigue limit, that the series A26 and A29 had a much lower fatigue life than expected for their roughness value. One possible reason for this could be that the external roughness measurements were poorly performed, with the central defect not being evaluated, but this seems unlikely as the measurements were taken in three different laboratories and all gave similar roughness results. Another possible reason appeared to be the effect of residual stresses since these series had the second and third highest axial tensile residual stresses.

Finally, in Section 7, the effect of manufacturing parameters on surface roughness was analyzed using experimental data. For the A35-A37 series, a correlation was found between the size of the radius of the cutting tool nose and the parameters R_q , R_v , R_a ,

and S_z , where their value increased as the radius decreased. Furthermore, the decrease in the depth of the cut affected the parameters R_{sm} , S_{al} , S_{tr} , V_{vv} , and S_{ku} . For the first four parameters, their values decreased, while the opposite effect was observed for V_{vv} . Part of this section was to validate different methods of estimating surface roughness based on the manufacturing parameters. The inaccuracy of the analytical methods was partly due to surface defects on the samples that increased their roughness, but even so, the estimation values were very low. As for the regression analysis-based methods, their Achilles heel is the use of only some machining variables as input variables for regression analysis. The remaining variables, such as vibration, are omitted, and thus their influence is not evaluated. This can lead to the inaccuracy of these methods if they are used for roughness estimation where these variables differed during their manufacturing.

Potential topics for future research, based on the conclusions made in this thesis, will now be proposed:

- Estimation of the values of the areal parameters based on specific manufacturing variables.
- More extensive sensitivity analysis of the areal parameters to other acquisition variables.
- Validation of the correlation between the indicated areal parameters and fatigue life. Whether these parameters can be used as more reliable indicators of fatigue life in terms of surface quality than the R_a parameter.

Appendix A

Table A1: Table of computed areal parameters obtained by different technology for two measured samples with different surface roughness.

	(a) $R_a = 0.8 \mu\text{m}$			(b) $R_a = 1.6 \mu\text{m}$		
	Int.	Con.	FV	Int.	Con.	FV
Sq [μm]	0.88	0.86	0.81	1.82	1.77	1.62
Ssk [-]	-0.49	-0.46	0.02	0.41	0.43	0.41
Sku [-]	2.87	2.82	2.67	2.33	2.36	2.48
Sz [μm]	4.98	4.83	5.78	9.05	8.81	8.88
Sa [μm]	0.71	0.69	0.66	1.51	1.47	1.33
Sal [μm]	76.42	76.68	76.93	46.15	46.13	47.83
Str [-]	0.23	0.24	0.24	0.15	0.15	0.15
Vvv [*]	0.12	0.11	0.08	0.13	0.13	0.12

* $\mu\text{m}^3/\mu\text{m}^2$, Int. = interferometry, Con. = Confocal, FV = focus variation.

Table A2: Table of computed areal parameters obtained by objectives with different magnification for two measured samples with different surface roughness.

	(a) $R_a = 0.8 \mu\text{m}$			(b) $R_a = 1.6 \mu\text{m}$		
	20x	10x	5x	20x	10x	5x
Sq [μm]	0.84	0.85	1.90	1.74	1.71	3.86
Ssk [-]	-0.45	-0.49	-0.03	-0.30	-0.35	0.42
Sku [-]	2.99	3.15	3.47	2.18	2.25	3.46
Sz [μm]	4.94	5.45	14.32	8.71	9.21	25.92
Sa [μm]	0.66	0.67	1.49	1.47	1.44	3.08
Sal [μm]	66.13	65.64	13.29	43.35	44.22	31.46
Str [-]	0.20	0.19	0.04	0.13	0.13	0.09
Vvv [*]	0.12	0.12	0.23	0.19	0.19	0.34

* $\mu\text{m}^3/\mu\text{m}^2$.

Table A3: Table of computed areal parameters obtained by cropping the size of evaluation area for two measured samples with different surface roughness.

	(a) Ra = 0.8 μm					(b) Ra = 1.6 μm				
	Uc.	3/4	2/4	1/4	1/8	Uc.	3/4	2/4	1/4	1/8
Sq [μm]	0.83	0.79	0.78	0.80	0.77	2.01	1.94	1.95	1.95	2.01
Ssk [-]	-0.30	-0.37	-0.34	-0.29	-0.41	-0.31	-0.23	-0.22	-0.23	-0.38
Sku [-]	2.70	2.77	2.67	2.42	2.44	2.52	2.61	2.69	2.42	2.55
Sz [μm]	4.79	4.79	4.79	4.79	4.32	11.89	11.89	11.89	10.94	10.96
Sa [μm]	0.67	0.64	0.64	0.66	0.64	1.65	1.58	1.59	1.60	1.61
Sal [μm]	58.91	46.94	51.33	56.46	47.67	50.97	49.82	50.39	52.87	39.82
Str [-]	0.07	0.07	0.09	0.14	0.16	0.06	0.07	0.08	0.13	0.19
Vvv [*]	0.10	0.10	0.09	0.08	0.08	0.25	0.23	0.22	0.20	0.22

* $\mu\text{m}^3/\mu\text{m}^2$, UC. = Uncropped.

Table A4: Table of computed areal parameters obtained by different post-processing approaches for two measured samples with different surface roughness.

	(a) Ra = 0.8 μm				(b) Ra = 1.6 μm			
	Normal	A	B	C	Normal	A	B	C
Sq [μm]	0.83	0.72	4.03	0.83	2.01	1.88	8.82	2.01
Ssk [-]	-0.28	-0.40	-0.44	-0.28	-0.31	-0.32	-1.02	-0.31
Sku [-]	2.73	2.71	2.68	2.73	2.52	2.44	3.04	2.52
Sz [μm]	5.22	4.40	21.25	5.24	11.28	11.89	41.12	11.31
Sa [μm]	0.67	0.59	3.28	0.67	1.65	1.57	7.20	1.65
Sal [μm]	59.08	40.77	398.45	59.06	50.98	46.52	297.14	50.97
Str [-]	0.07	0.05	0.28	0.07	0.06	0.06	0.20	0.06
Vvv [*]	0.10	0.09	0.51	0.10	0.25	0.22	1.43	0.25

* $\mu\text{m}^3/\mu\text{m}^2$, Normal = λ_f and λ_s were applied + λ_c not applied; A = All filters applied; B = only λ_s applied; C = only λ_f applied

Table A5: Table of computed 2D parameters obtained by areal measurement for two measured samples with different surface roughness.

	(a) Ra = 0.8 μm				(b) Ra = 1.6 μm			
	Stylus	A	B	C	Stylus	A	B	C
Ra [μm]	0.65	0.64	0.84	0.61	1.59	1.44	1.60	1.54
Rq [μm]	0.79	0.84	1.10	0.75	1.90	1.70	1.92	1.79
Rz [μm]	3.49	5.69	7.49	3.47	7.62	7.61	9.30	7.33
Rt [μm]	4.63	5.69	7.49	3.47	9.22	7.61	9.30	7.33
Rsk [-]	-0.32	-0.66	-0.95	-0.58	-0.18	-0.15	-0.16	-0.34
Rku [-]	2.66	4.26	4.87	2.86	2.36	2.13	2.36	2.05
Rc [μm]	2.49	1.80	2.22	1.70	5.55	4.55	4.79	4.97
RSm [μm]	244.73	123.44	159.89	89.74	226.40	170.48	181.49	172.57

A = $\lambda_c = 0.8$ mm; B = $\lambda_c = -$ mm; C = $l_n = 2$ mm + $\lambda_c = 0.8$ mm

Table A6: 2D roughness parameters calculated from 2D measurement that was conducted in the current project.

2D parameters - 2D measurement							
Parameter		Average value			Standard deviation		
		A35	A36	A37	A35	A36	A37
Ra	[μm]	0.89	1.20	1.26	0.05	0.11	0.05
Rq	[μm]	1.10	1.52	1.59	0.03	0.12	0.08
Rz	[μm]	5.01	7.10	7.60	0.30	0.56	0.52
Rp	[μm]	2.45	3.28	3.49	0.09	0.37	0.38
Rv	[μm]	2.55	3.82	3.99	0.23	0.27	0.15
Rsk	[—]	-0.15	-0.44	-0.34	0.19	0.14	0.09
Rk μ	[—]	2.68	3.09	2.89	0.17	0.30	0.16
Rc	[μm]	3.39	4.15	4.51	0.15	0.42	0.38
RSm	[μm]	173	156	172	104	36	19
RDq	[—]	0.15	0.17	0.16	0.05	0.02	0.01
Rmr	[%]	0.16	0.11	0.10	0.08	0.06	0.03
Rmr(c)1	[%]	1.60	0.84	0.91	0.78	0.12	0.32
Rmr(c)2	[%]	3.15	1.49	1.39	1.88	0.17	0.21
Rdc	[μm]	0.70	0.88	0.93	0.02	0.09	0.10
Rt	[μm]	7.58	11.06	11.20	1.28	0.78	0.92
Rz1max	[μm]	7.42	10.31	10.85	1.26	0.59	0.99
Rk	[μm]	2.79	3.44	3.90	0.31	0.44	0.41
Rpk	[μm]	1.31	2.13	2.15	0.35	0.20	0.58
Rvk	[μm]	1.49	2.19	1.89	0.30	0.48	0.20
Mr1	[%]	10.29	10.27	9.41	0.74	0.42	1.86
Mr2	[%]	90.21	86.86	88.75	1.20	0.41	1.77
A1	[—]	6.80	10.63	10.44	2.15	0.80	4.89
A2	[—]	7.24	14.43	10.81	1.60	2.77	2.69

Table A7: Areal roughness parameters calculated from 3D areal measurement that was conducted in the current project.

Areal parameters - 3D areal measurement							
Parameter		Average value			Standard deviation		
		A35	A36	A37	A35	A36	A37
Sq	[μm]	2.01	2.31	2.57	0.12	0.21	0.05
Ssk	[$-$]	-0.47	0.34	0.02	0.18	0.02	0.10
Sku	[$-$]	2.85	3.42	2.98	0.20	0.12	0.29
Sp	[μm]	4.42	7.29	7.26	0.30	0.36	0.49
Sv	[μm]	6.18	6.54	7.19	1.08	0.41	0.10
Sz	[μm]	10.61	13.83	14.45	1.28	0.05	0.46
Sa	[μm]	1.62	1.75	2.03	0.09	0.06	0.07
Sal	[μm]	123.01	105.75	120.61	9.09	33.59	14.56
Str	[$-$]	0.35	0.30	0.34	0.02	0.09	0.04
Std	[$^{\circ}$]	90.47	89.71	90.28	0.84	0.40	1.55
Sdq	[$-$]	0.18	0.25	0.24	0.10	0.07	0.02
Sdr	[$\%$]	1.52	2.37	2.23	1.37	1.18	0.29
Vm	[$\mu\text{m}^3/\mu\text{m}^2$]	6.18	6.54	7.19	1.08	0.41	0.10
Vmp	[$\mu\text{m}^3/\mu\text{m}^2$]	0.07	0.11	0.15	0.01	0.02	0.01
Vmc	[$\mu\text{m}^3/\mu\text{m}^2$]	1.94	2.00	2.35	0.09	0.12	0.23
Vvc	[$\mu\text{m}^3/\mu\text{m}^2$]	2.22	3.23	3.04	0.20	0.85	0.18
Vw	[$\mu\text{m}^3/\mu\text{m}^2$]	0.27	0.25	0.29	0.03	0.05	0.06
Spk	[μm]	0.44	1.13	1.06	0.06	0.13	0.34
Sk	[μm]	2.26	2.34	1.95	1.44	1.42	0.27
Svk	[μm]	0.66	1.12	1.25	0.09	0.00	0.12

Table A8: Average errors of each method and of each series for the logarithmic model.

	Uni.	Juv.	RCJ.	Sch.	Shi.	Mur.	ASM.	KHS.	EN1	FKM	\bar{x}_r^*	StD.
A25	-0.07	0.19	-0.01	0.01	0.16	-0.07	-0.08	-0.09	-	-0.02	0.00	0.11
A26	-0.18	0.14	-0.14	-0.16	0.11	-0.37	-0.23	-0.24	-	-0.15	-0.14	0.16
A27	-0.06	0.20	-0.01	0.00	0.17	-0.11	-0.09	-0.10	-	-0.02	0.00	0.11
A28	-0.19	0.10	-0.11	-0.08	0.07	-0.21	-0.19	-0.20	-	-0.12	-0.10	0.12
A29	-0.12	0.16	-0.08	-0.08	0.13	-0.27	-0.17	-0.19	-	-0.10	-0.08	0.14
A35	0.02	0.26	0.07	0.08	0.24	0.04	0.00	0.00	-	0.07	0.09	0.10
A36	0.02	0.26	0.07	0.08	0.23	0.00	-0.01	0.00	-	0.07	0.08	0.10
A37	0.00	0.25	0.06	0.08	0.22	-0.02	-0.01	-0.01	-	0.06	0.07	0.10
\bar{x}_r	-0.07	0.19	-0.02	-0.01	0.17	-0.13	-0.10	-0.10	-	-0.03	-	-
Max x_r	-0.19	0.26	-0.14	-0.16	0.24	-0.37	-0.23	-0.24	-	-0.15	-	-
Min x_r	0.00	0.10	-0.01	0.00	0.07	0.00	0.00	0.00	-	-0.02	-	-
StD.	0.09	0.06	0.08	0.09	0.06	0.14	0.09	0.10	-	0.09	-	-

Uni. = UNI 7670, Juv. = Juvinal, RCJ. = RcJohnson, Sch. = Schijve, Shi. = Shigley, ASM. = ASME BPVC, KHS. = KHKS0220, EN1. = EN 13445-2009, StD = standard deviation, \bar{x}_r^* = Average error, * average relative error without Murakami method.

References

- [1] Arithmetical mean height (ra, pa, wa) — surface roughness parameters — introduction to roughness — keyence america [figure]. <https://www.keyence.com/ss/products/microscope/roughness/line/parameters.jsp>. (Accessed on 11/16/2022).
- [2] Confocal microscopy - introduction. <https://www.olympus-lifescience.com/en/microscope-resource/primer/techniques/confocal/confocalintro/>. (Accessed on 11/15/2022).
- [3] Confocal microscopy - introduction — olympus ls. <https://www.olympus-lifescience.com/en/microscope-resource/primer/techniques/confocal/confocalintro/>. (Accessed on 01/09/2023).
- [4] Contact-type surface roughness/profile measuring instruments — instruments used for roughness measurements — solving the questions about profile and surface roughness measurements! introduction to "roughness" — keyence international belgium. https://www.keyence.eu/ss/products/microscope/roughness/equipment/line_01.jsp. (Accessed on 01/09/2023).
- [5] Difference between feed rate and cutting speed — rapiddirect blog. <https://www.rapiddirect.com/blog/difference-between-feed-rate-and-cutting-speed/>. (Accessed on 11/23/2022).
- [6] Drsnosti povrchů a jejich značení a převodník - mikon tools s.r.o. <https://www.mikon-tools.cz/drsnosti-povrchu-a-jejich-znaceni-a-prevodnik/>. (Accessed on 11/16/2022).
- [7] Fatigue modifying factors - roy mech. https://roymech.org/Useful_Tables/Fatigue/FAT_Mod_factors.html. (Accessed on 01/06/2023).
- [8] How to measure surface roughness of medical needles using a laser scanning confocal microscope. <https://www.azom.com/article.aspx?ArticleID=18946>. (Accessed on 01/09/2023).
- [9] Interferometry: Measuring with light. https://www.photonics.com/Articles/Interferometry_Measuring_with_Light/a25128. (Accessed on 11/15/2022).
- [10] International journal of fatigue. <https://www.scimagojr.com/journalsearch.php?q=21105&tip=sid>. (Accessed on 01/23/2023).
- [11] Material fatigue definition. <https://www.comsol.com/multiphysics/material-fatigue>. (Accessed on 09/22/2022).

- [12] Nose radius in cutting tool - its function, value, advantage & disadvantage. <http://www.minaprem.com/machining/cutter/geometry/nose-radius-in-cutting-tool-its-function-value-advantage-disadvantage/>. (Accessed on 11/23/2022).
- [13] Principle of confocal microscope — lasertec corporation. https://www.lasertec.co.jp/en/products/microscope/optelics_hybrid/principle/microscope.html. (Accessed on 11/15/2022).
- [14] Surface roughness measurement—parameters — olympus. [https://www.olympus-ims.com/en/metrology/surface-roughness-measurement-portal/parameters/#!cms\[focus\]=004](https://www.olympus-ims.com/en/metrology/surface-roughness-measurement-portal/parameters/#!cms[focus]=004). (Accessed on 11/16/2022).
- [15] Surface roughness measurement—terms and standards — olympus. [https://www.olympus-ims.com/en/metrology/surface-roughness-measurement-portal/terms-and-standards/#!cms\[focus\]=002](https://www.olympus-ims.com/en/metrology/surface-roughness-measurement-portal/terms-and-standards/#!cms[focus]=002). (Accessed on 01/09/2023).
- [16] What is depth of cut in machining? its unit, value, effects and selection. <http://www.minaprem.com/machining/principle/parameter/what-is-depth-of-cut-in-machining-its-unit-value-effects-and-selection/>. (Accessed on 12/28/2022).
- [17] When rz isn't rz - michigan metrology. <https://michmet.com/when-rz-isnt-rz/>. (Accessed on 11/16/2022).
- [18] White light interferometers. <https://www.keyence.com/ss/products/microscope/roughness/equipment/interferometers.jsp>. (Accessed on 11/15/2022).
- [19] FKM-Guideline: Analytical Strength Assessment of Components in Mechanical Engineering . 5th revised edition, Forschungskuratorium Maschinenbau (FKM), Frankfurt/Main, 2003.
- [20] KHKS 0220:2008. Standard for superhigh-pressure gas equipment., Tokyo, Japan, 2008.
- [21] BS EN 13445-3:2009 Unfired Pressure Vessels, Part3: Design, British Standards Institution, 2009.
- [22] The ASME Boiler and Pressure Vessel Code, Sec. VIII, Div.3, The American Society of Mechanical Engineers, New York, 2010.
- [23] How to make the right choice between 2d vs. 3d in surface metrology, quality magazine. <https://www.qualitymag.com/articles/95593-how-to-make-the-right-choice-between-2d-vs-3d-in-surface-metrology>, 08 2019. (Accessed on 11/15/2022).

- [24] Meccanismi per apparecchi di sollevamento. Istruzioni per il calcolo. UNI 7670, 1988.
- [25] F. Abroug, E. Pessard, G. Germain, and F. Morel. A probabilistic approach to study the effect of machined surface states on hcf behavior of a aa7050 alloy. *International Journal of Fatigue*, 116:473–489, 2018.
- [26] H. Akkuş and H. Yaka. Experimental and statistical investigation of the effect of cutting parameters on surface roughness, vibration and energy consumption in machining of titanium 6al-4v eli (grade 5) alloy. *Measurement*, 167:108465, 2021.
- [27] D. Arola and M. Ramulu. An examination of the effects from surface texture on the strength of fiber reinforced plastics. *Journal of Composite Materials*, 33(2):102–123, 1999.
- [28] D. Arola and C. Williams. Estimating the fatigue stress concentration factor of machined surfaces. *International Journal of Fatigue*, 24(9):923–930, 2002.
- [29] V. P. Astakhov. Turning. In J. Paulo Davim, editor, *Modern Machining Technology*, pages 1–78. Woodhead Publishing, 2011.
- [30] R. K. Bhushan. Impact of nose radius and machining parameters on surface roughness, tool wear and tool life during turning of aa7075/sic composites for green manufacturing. *Mechanics of Advanced Materials and Modern Processes*, 6(1):1, Aug 2020.
- [31] E. Capello. Residual stresses in turning: Part i: Influence of process parameters. *Journal of Materials Processing Technology*, 160(2):221–228, 2005.
- [32] E. Capello. Residual stresses in turning: Part ii. influence of the machined material. *Journal of Materials Processing Technology*, 172(3):319–326, 2006.
- [33] H. Chen, Z. Liu, X. Wang, Y. Wang, and S. Liu. Effect of surface integrity on fatigue life of 2024 aluminum alloy subjected to turning. *Journal of Manufacturing Processes*, 83:650–666, 2022.
- [34] Z. Chen, R. Lin Peng, J. Zhou, R. M’Saoubi, D. Gustafsson, and J. Moverare. Effect of machining parameters on cutting force and surface integrity when high-speed turning ad 730TM with pcbn tools. *The International Journal of Advanced Manufacturing Technology*, 100(9):2601–2615, Feb 2019.
- [35] L. G. P. de Souza, J. E. M. Gomes, É. M. Arruda, G. Silva, A. P. de Paiva, and J. R. Ferreira. Evaluation of trade-off between cutting time and surface roughness robustness regarding tool wear in hard turning finishing. *The International Journal of Advanced Manufacturing Technology*, Nov 2022.

- [36] M. Fitzpatrick, A. Fry, P. Holdway, F. Kandil, J. Shackleton, and L. Suominen. Determination of residual stresses by x-ray diffraction. 52, 01 2002.
- [37] Y. Fukuta, H. Kanasaki, S. Asada, and T. Sera. Proposal of surface finish factor on fatigue strength in design fatigue curve. *American Society of Mechanical Engineers, Pressure Vessels and Piping Division (Publication) PVP*, 1, 07 2014.
- [38] E. Gadelmawla, M. Koura, T. Maksoud, I. Elewa, and H. Soliman. Roughness parameters. *Journal of Materials Processing Technology*, 123:133–145, 04 2002.
- [39] C. R. Gagg and P. R. Lewis. In-service fatigue failure of engineered products and structures – case study review. *Engineering Failure Analysis*, 16(6):1775–1793, 2009. Papers presented at the Third International Conference on Engineering Failure Analysis (Sitges, Spain, 13–16 July 2008) Part II.
- [40] G. Garcia, E. Vázquez, H. Siller, L. Ruiz-Huerta, and A. Caballero-Ruiz. Calibration of ball nose micro end milling operations for sculptured surfaces machining. *International Journal of Machining and Machinability of Materials*, 19:587 – 605, 12 2017.
- [41] M. P. Groover. *Fundamentals of modern manufacturing*. John Wiley & Sons, Chichester, England, 4 edition, Jan. 2010.
- [42] Y. Hadi and S. G. Ahmed. Assessment of surface roughness model for turning process. In K. Wang, G. L. Kovacs, M. Wozny, and M. Fang, editors, *Knowledge Enterprise: Intelligent Strategies in Product Design, Manufacturing, and Management*, pages 152–158, Boston, MA, 2006. Springer US.
- [43] Y. Hua and Z. Liu. Effects of cutting parameters and tool nose radius on surface roughness and work hardening during dry turning inconel 718. *The International Journal of Advanced Manufacturing Technology*, 96(5):2421–2430, May 2018.
- [44] Geometrical Product Specification (GPS)—Surface Texture: Areal – Part 2: Terms, definitions and surface texture parameters. Standard ISO 25178-2, International Organization for Standardization, Geneva, CH, 2012.
- [45] Geometrical product specifications (GPS) – Surface texture: Profile method – Terms, definitions and surface texture parameters. Standard ISO 4287:1997, International Organization for Standardization, Geneva, CH, 1997.
- [46] H. Itoga, K. Tokaji, M. Nakajima, and H.-N. Ko. Effect of surface roughness on step-wise s–n characteristics in high strength steel. *International Journal of Fatigue*, 25(5):379–385, 2003.

- [47] M. Jekle and T. Becker. Wheat dough microstructure: The relation between visual structure and mechanical behavior. *Critical Reviews in Food Science and Nutrition*, 55:369–382, 02 2015.
- [48] R. Johnson. Specifying a surface finish that won't fail in fatigue. *Machine Design*, 45(11):108, 1973.
- [49] R. C. Juvinall. *Engineering Considerations of Stress, Strain and Strength*. McGraw-Hill, New York, 1967.
- [50] P. Kittali, V. Kalwa, D. Athith, K. P. Prashanth, and B. K. Venkatesh. Optimization of machining parameters in turning operation to minimize the surface roughness using taguchi technique for en1a alloy steel. *Materials Today: Proceedings*, 54:463–467, 2022. 5th International Conference on Advanced Research in Mechanical, Materials and Manufacturing Engineering-2021.
- [51] A. Kumar Parida and K. Maity. Modeling of machining parameters affecting flank wear and surface roughness in hot turning of monel-400 using response surface methodology (rsm). *Measurement*, 137:375–381, 2019.
- [52] A. Kurek, M. Kurek, and T. Lagoda. Stress-life curve for high and low cycle fatigue. *Journal of Theoretical and Applied Mechanics*, 57(3):677–684, 2019.
- [53] J. Lai, H. Huang, and W. Busing. Effects of microstructure and surface roughness on the fatigue strength of high-strength steels. *Procedia Structural Integrity*, 2:1213–1220, 2016. 21st European Conference on Fracture, ECF21, 20-24 June 2016, Catania, Italy.
- [54] N. Leguinagoicoa, J. Albizuri, and A. Larrañaga. Fatigue improvement and residual stress relaxation of shot-peened alloy steel din 34crnimo6 under axial loading. *International Journal of Fatigue*, 162:107006, 2022.
- [55] C. Li, W. Dai, F. Duan, Y. Zhang, and D. He. Fatigue life estimation of medium-carbon steel with different surface roughness. *Applied Sciences*, 7(4), 2017.
- [56] K. Loshkarev. Fatigue analysis of a combustion engine block. Diplomová práce, České vysoké učení technické v Praze, Fakulta strojní, Ústav mechaniky, 2019.
- [57] W. Macek. Fracture areas quantitative investigating of bending-torsion fatigued low-alloy high-strength steel. *Metals*, 11(10), 2021.
- [58] Y. Murakami. *Metal Fatigue: Effects of Small Defects and Nonmetallic Inclusions*. Referex Engineering. Elsevier, 2002.

- [59] Y. Murakami, T. Takagi, K. Wada, and H. Matsunaga. Essential structure of s-n curve: Prediction of fatigue life and fatigue limit of defective materials and nature of scatter. *International Journal of Fatigue*, 146:106138, 2021.
- [60] J. MÁDL. *Technologie obrábění*. ČVUT, Praha, 2000.
- [61] M. Mžourek. Vliv středního napětí na dynamickou pevnost a životnost. Diplomová práce, České vysoké učení technické v Praze, Fakulta strojní, Ústav mechaniky, 2020.
- [62] K. Nabil, Z. Hessainia, M. Yallese, and N. Ouelaa. Statistical analysis of surface roughness by design of experiments in hard turning. *Mechanika*, 18(5):605–611, 11 2012.
- [63] V. D. Patel and A. H. Gandhi. Analysis and modeling of surface roughness based on cutting parameters and tool nose radius in turning of aisi d2 steel using cbn tool. *Measurement*, 138:34–38, 2019.
- [64] F. Quan, Z. Chen, H. Ye, C. Cui, and Y. Cui. Study of the effect of surface roughness on fatigue strength of gh4169 based on indirect evaluation of the notch root radius. *International Journal of Fatigue*, 152:106440, 2021.
- [65] M. Růžička, M. Hanke, and M. Rost. *Dynamická pevnost a životnost*. ČVUT, Praha, 2. přeprac. vyd edition, 1992.
- [66] S. Sarnobat and H. Raval. Experimental investigation and analysis of the influence of tool edge geometry and work piece hardness on surface residual stresses, surface roughness and work-hardening in hard turning of aisi d2 steel. *Measurement*, 131:235–260, 2019.
- [67] S. Scherer. Focus variation - a new technology for high resolution optical 3d surface metrology. 11:8457, 03 2009.
- [68] J. Schijve. *Fatigue of Structures and Materials*. Springer Dordrecht, 12 2008.
- [69] M. Shahzad, M. Chaussumier, R. Chieragatti, C. Mabru, and F. Rezai Aria. Influence of surface treatments on fatigue life of al 7010 alloy. *Journal of Materials Processing Technology*, 210(13):1821–1826, 2010.
- [70] J. Shigley, C. Mischke, and R. Budynas. *Mechanical Engineering Design*. McGraw-Hill series in mechanical engineering. McGraw-Hill, 2004.
- [71] K. Singh, F. Sadeghi, M. Correns, and T. Blass. A microstructure based approach to model effects of surface roughness on tensile fatigue. *International Journal of Fatigue*, 129:105229, 2019.

- [72] D. Stephenson and J. Agapiou. *Metal Cutting Theory and Practice*. CRC Press, 2016.
- [73] D. Yang, Z. Liu, X. Xiao, and F. Xie. The effects of machining-induced surface topography on fatigue performance of titanium alloy ti-6al-4v. *Procedia CIRP*, 71:27–30, 2018. 4th CIRP Conference on Surface Integrity (CSI 2018).
- [74] W. Yang and Y. Tarng. Design optimization of cutting parameters for turning operations based on the taguchi method. *Journal of Materials Processing Technology*, 84(1):122–129, 1998.
- [75] Zabala, Alaitz, Blunt, Liam, Tato, Wilson, Aginagalde, Andrea, Gomez, Xabier, and Llavori, Iñigo. The use of areal surface topography characterisation in relation to fatigue performance. *MATEC Web Conf.*, 165:14013, 2018.
- [76] A. Zabala Eguren. *The use of 3D surface topography analysis techniques to analyse and predict the alteration of endosseous titanium dental implants generated during the surgical insertion*. PhD thesis, Mondragon Unibertsitatea. Goi Eskola Politeknikoa, 2015.
- [77] Q. Zeng, Y. Qin, W. Chang, and X. Luo. Correlating and evaluating the functionality-related properties with surface texture parameters and specific characteristics of machined components. *International Journal of Mechanical Sciences*, 149, 09 2018.
- [78] M. Zhang, W. Wang, P. Wang, Y. Liu, and J. Li. The fatigue behavior and mechanism of fv520b-i with large surface roughness in a very high cycle regime. *Engineering Failure Analysis*, 66:432–444, 2016.
- [79] T. Zielinski, A. Vovk, O. Riemer, and B. Karpuschewski. Influence of local material loads on surface topography while machining steel 42crmo4 and inconel 718. *Procedia CIRP*, 108:412–417, 2022. 6th CIRP Conference on Surface Integrity.
- [80] M. Özdemir, M. Kaya, and H. Akyildiz. Analysis of surface roughness and cutting forces in hard turning of 42crmo4 steel using taguchi and rsm method. *Mechanics*, 26:231–241, 06 2020.